

Efficient Cross-Device Federated Learning Algorithms for Minimax Problems

Jiahao Xie,¹ Chao Zhang,¹ Zebang Shen,² Weijie Liu,¹ Hui Qian¹

¹College of Computer Science and Technology, Zhejiang University

²University of Pennsylvania

xiejh@zju.edu.cn, zczju@zju.edu.cn, zebang@seas.upenn.edu, westonhunter@zju.edu.cn, qianhui@zju.edu.cn

Abstract

In many machine learning applications where massive and privacy-sensitive data are generated on numerous mobile or IoT devices, collecting data in a centralized location may be prohibitive. Thus, it is increasingly attractive to estimate parameters over mobile or IoT devices while keeping data localized. Such learning setting is known as cross-device federated learning. In this paper, we propose the first theoretically guaranteed algorithms for general minimax problems in the cross-device federated learning setting. Our algorithms require only a fraction of devices in each round of training, which overcomes the difficulty introduced by the low availability of devices. The communication overhead is further reduced by performing multiple local update steps on clients before communication with the server, and global gradient estimates are leveraged to correct the bias in local update directions introduced by data heterogeneity. By developing analyses based on novel potential functions, we establish theoretical convergence guarantees for our algorithms. Experimental results on AUC maximization, robust adversarial network training, and GAN training tasks demonstrate the efficiency of our algorithms.

1 Introduction

During the last few years, minimax problems have found a surge of important applications in machine learning. Typical examples include AUC (area under the ROC curve) maximization (Ying, Wen, and Lyu 2016; Liu et al. 2020a), robust adversarial learning (Namkoong and Duchi 2016; Madry et al. 2018), and Generative Adversarial Network (GAN) training (Goodfellow et al. 2014). These applications have sparked a lot of interests in developing efficient algorithms for minimax problems (Rafique et al. 2018; Jin, Netrapalli, and Jordan 2020; Thekumparampil et al. 2019; Nouiehed et al. 2019; Liu et al. 2020b; Lin, Jin, and Jordan 2020; Luo et al. 2020; Qiu et al. 2020; Wang et al. 2020; Xu et al. 2020; Huang et al. 2020; Yang, Kiyavash, and He 2020).

While mainstream minimax algorithms are designed for the single-machine setting, there is a growing trend of minimax optimization in the Federated Learning (FL) paradigm (Mohri, Sivek, and Suresh 2019; Deng, Kamani, and Mahdavi 2020; Reisizadeh et al. 2020; Rasouli, Sun, and Rajagopal 2020; Beznosikov, Samokhin, and Gasnikov 2020; Hou et al. 2021; Guo et al. 2020; Yuan et al. 2021; Deng and Mahdavi 2021). In such regime, multiple clients collaborate to train a machine learning model under the coordination

of a central server without transferring any client’s private data (McMahan et al. 2017). Existing federated algorithms for general minimax problems require all clients to participate in each training round. Thus, they are restricted to the *cross-silo* setting of FL and do not apply to another important setting—the *cross-device* setting. The former involves a relatively small number of organizations or data centers with reliable network connections (Kairouz et al. 2019). By contrast, in the latter setting, the clients are numerous (up to 10^{10}) unreliable mobile/IoT devices with relatively slow network connections, and only a fraction of devices are eligible for training at any one time (Kairouz et al. 2019, Table 1).

As the volume of data generated by mobile and IoT devices grows rapidly and privacy concerns increase, gathering data in an aggregation center may be prohibitive (McMahan et al. 2017). Therefore, the cross-device FL becomes an increasingly popular distributed computing paradigm (Li et al. 2018). In order to develop an efficient algorithm for minimax problems in the cross-device setting, the following three difficulties need to be overcome.

- (i) *Low availability of clients.* Only a portion of devices are available at any one time. For example, a device is temporarily unavailable when it is offline or out of power. This precludes global synchronization (i.e., synchronization over all clients), which is required by mainstream distributed minimax algorithms.
- (ii) *The communication bottleneck.* The network connection between the server and a client may be slow due to the limit of bandwidth. Thus, frequently transferring large amount of information over the network may significantly deteriorate the training efficiency.
- (iii) *Data heterogeneity.* In general, clients’ data vary significantly and thus a client’s local data distribution may be substantially different from the global distribution. As global synchronization is prohibitive, the data heterogeneity makes it more challenging to train a global model.

Contribution. (i) In this paper, we develop two theoretically guaranteed cross-device minimax algorithms, CD-MAGE and CD-MAGE+, to address the above difficulties. In each round of our algorithms, only a small subset of clients are required for training, which provides robustness against the limited availability of clients. To reduce the communication overhead, our algorithms perform multiple local stochas-

tic gradient descent-ascent steps on clients before communication to the server in each round. Two global gradient estimators, the *minibatch* and *recursive momentum* based estimators, are adopted for CD-MAGE and CD-MAGE+ separately, to mitigate the bias of local updates introduced by data heterogeneity. (ii) We develop analyses of the proposed algorithms based on novel potential functions, which show that our algorithms converge to a stationary point if the loss function is non-convex w.r.t. to the primal variable and satisfies the Polyak-Łojasiewicz (PL) condition on the dual variable. Specifically, CD-MAGE (resp., CD-MAGE+) achieves an $\mathcal{O}(1/T + 1/\sqrt{ST})$ (resp., $\tilde{\mathcal{O}}(1/T + 1/T^{2/3}S^{1/3})$)¹ convergence rate, where T and S denote the number of communication rounds and the number of clients participating per round, respectively. Note that these rates are the first convergence rates for cross-device federated algorithms on general minimax problems.

Experimental results on AUC maximization, robust adversarial neural network training, and GAN training tasks demonstrate the efficiency of the proposed algorithms.

Notation. We use bold lowercase symbols (e.g., \mathbf{x}) to denote vectors. For a vector \mathbf{x} , we denote its j -th coordinate as $[\mathbf{x}]_j$. For a function $f(\cdot, \cdot) : \mathbb{R}^p \times \mathbb{R}^q \rightarrow \mathbb{R}$, $\nabla_{\mathbf{x}}f$ and $\nabla_{\mathbf{y}}f$ denote its partial derivatives with respect to the first and second variables, respectively. We also denote $(\nabla_{\mathbf{x}}f, \nabla_{\mathbf{y}}f)$ as ∇f . The Euclidean norm of a vector \mathbf{x} is denoted by $\|\mathbf{x}\|$.

2 Related Work

Minimax Optimization. Minimax optimization has a long history dating back to (Brown 1951). The vast majority of existing works on minimax problems focus on the convex-concave regime (Korpelevich 1976; Nemirovski 2004; Nedić and Ozdaglar 2009; Palaniappan and Bach 2016; Mokhtari, Ozdaglar, and Pattathil 2019; Chavdarova et al. 2019; Lin, Jin, and Jordan 2020). Recently, there has emerged a surge of studies of more general nonconvex-concave and nonconvex-nonconcave minimax problems (Sanjabi, Razaviyayn, and Lee 2018; Nouiehed et al. 2019; Lin, Jin, and Jordan 2020; Luo et al. 2020; Xu et al. 2020; Liu et al. 2020b; Huang et al. 2020; Qiu et al. 2020; Yang, Kiyavash, and He 2020).

There are generally two types of algorithms for minimax problems in nonconvex-concave and nonconvex-nonconcave regimes: (i) GDmax-type algorithms (Sanjabi, Razaviyayn, and Lee 2018; Nouiehed et al. 2019; Luo et al. 2020; Xu et al. 2020), and (ii) GDA-type algorithms (Lin, Jin, and Jordan 2020; Liu et al. 2020b; Huang et al. 2020; Qiu et al. 2020; Yang, Kiyavash, and He 2020). The former alternate between performing a single update on the primal variable \mathbf{x} and approximately solving a maximization subproblem w.r.t. the dual variable \mathbf{y} . By contrast, the latter algorithms only perform both a gradient descent step on \mathbf{x} and a gradient ascent step on \mathbf{y} per iteration. Hence, the GDA-type methods are usually more computationally practical for real-world problems with complex structures (Qiu et al. 2020).

Federated learning. The principal cross-device federated learning algorithm for minimization problems is Fe-

dAvg (McMahan et al. 2017). While FedAvg has succeeded in a few applications, it suffers from the *client drift* issue (i.e., on heterogeneous data, the local variables move towards the individual client optima instead of a global optimum).

Recently, several minimax algorithms for cross-silo federated learning have been proposed (Reisizadeh et al. 2020; Beznosikov, Samokhin, and Gasnikov 2020; Hou et al. 2021; Guo et al. 2020; Yuan et al. 2021; Deng and Mahdavi 2021). However, these algorithms require *all* clients to participate in each round of training, and thus do not apply to the cross-device setting. Though these algorithms can be forcibly extended to the cross-device setting by involving only a subset of clients in each round, there are no theoretical guarantees for their cross-device versions.

Actually there are two algorithms for tackling a specific minimax problem in the cross-device setting (Mohri, Sivek, and Suresh 2019; Deng, Kamani, and Mahdavi 2020). Indeed, they are both specialized for a distributionally robust problem of the form $\min_{\mathbf{x}} \max_{\mathbf{y} \in \mathbb{R}_+^N, \|\mathbf{y}\|_1=1} \sum_{i=1}^N [\mathbf{y}]_i f_i(\mathbf{x})$, where N denotes the total number of clients and f_i is the local loss function of client i . As these two algorithms heavily depend on the special problem structure, they do not apply to many other popular minimax problems, e.g., AUC maximization, robust adversarial learning, and generative adversarial network training.

3 Problem Setting and Algorithms

We consider the following general minimax optimization problem in the cross-device federated learning setting:

$$\min_{\mathbf{x} \in \mathbb{R}^p} \max_{\mathbf{y} \in \mathbb{R}^q} \{f(\mathbf{x}, \mathbf{y}) := \mathbb{E}_{i \sim \mathcal{D}} [f_i(\mathbf{x}, \mathbf{y})]\}, \quad (1)$$

where $f_i(\mathbf{x}, \mathbf{y}) := \frac{1}{n_i} \sum_{j=1}^{n_i} F_i(\mathbf{x}, \mathbf{y}; \zeta_{i,j})$ is the local loss function of client i , $\{\zeta_{i,1}, \dots, \zeta_{i,n_i}\}$ denotes the local data points on client i , and \mathcal{D} represents the client distribution. A typical example of \mathcal{D} is the uniform distribution over N clients, which corresponds to the loss function $f = \frac{1}{N} \sum_{i=1}^N f_i$. Generally, \mathcal{D} can be any (nonuniform) distribution over N clients, even with infinite N . We note that we do not need access to all clients during the whole optimization procedure as the number of clients may be extremely large in the cross-device setting.

To solve problem (1), we propose two algorithms: (i) CD-MAGE, and (ii) CD-MAGE+. These two algorithms are detailed in Algorithms 1-3. In each round, CD-MAGE and CD-MAGE+ proceed in the following two phases.

- (i) **Gradient collection phase.** The server sends $(\mathbf{x}_t, \mathbf{y}_t)$ (and $(\mathbf{x}_{t-1}, \mathbf{y}_{t-1})$ in CD-MAGE+) to a subset of clients, and then proceeds once it receives local gradients from S clients. We denote these S clients as \mathcal{S}'_t . The server then computes the global gradient estimate $(\mathbf{u}_t, \mathbf{v}_t)$ by aggregating the received local gradients. CD-MAGE and CD-MAGE+ utilize different global gradient estimators. The former incorporates the minibatch gradient estimator which simply averages the local gradients of the clients in \mathcal{S}'_t . This estimator is the most widely used and the simplest estimator in the optimization literature, but it

¹The symbol $\tilde{\mathcal{O}}()$ suppresses a logarithmic factor in T .

Algorithm 1: CD-MAGE/CD-MAGE+ on the server.

Input: initial point $(\mathbf{x}_{-1}, \mathbf{y}_{-1})$, the number of rounds T , and the batch size of clients S .

- 1: $\mathbf{x}_0 \leftarrow \mathbf{x}_{-1}, \mathbf{y}_0 \leftarrow \mathbf{y}_{-1}$;
- 2: **for** $t = 0, 1, \dots, T-1$ **do**
- 3: **Gradient collection phase:**
 Send $\{\mathbf{x}_t, \mathbf{y}_t\}$ or $\{\mathbf{x}_t, \mathbf{y}_t, \mathbf{x}_{t-1}, \mathbf{y}_{t-1}\}$ \triangleright CD-MAGE
 \triangleright CD-MAGE+
 to a subset of clients;
- 4: Once local gradient information from S clients is received, proceed;
 Compute \mathbf{u}_t and \mathbf{v}_t by Eq. (2) or Eq. (3); \triangleright CD-MAGE
 \triangleright CD-MAGE+
- 5: **Parameter update phase:**
- 6: Send $(\mathbf{u}_t, \mathbf{v}_t)$ and $(\mathbf{x}_t, \mathbf{y}_t)$ to a subset of clients;
- 7: Once local iterates $(\mathbf{x}_{t,i}^{(K)}, \mathbf{y}_{t,i}^{(K)})$ from S clients are received, proceed;
- 8: $\mathbf{x}_{t+1} \leftarrow \frac{1}{|\mathcal{S}_t|} \sum_{i \in \mathcal{S}_t} \mathbf{x}_{t,i}^{(K)}, \mathbf{y}_{t+1} \leftarrow \frac{1}{|\mathcal{S}_t|} \sum_{i \in \mathcal{S}_t} \mathbf{y}_{t,i}^{(K)}$,
 where \mathcal{S}_t is the S clients in the above step;
- 9: **end for**

Algorithm 2: CD-MAGE/CD-MAGE+ on client i in the gradient collection phase of the t -th round.

Input: $(\mathbf{x}_t, \mathbf{y}_t)$ (and $(\mathbf{x}_{t-1}, \mathbf{y}_{t-1})$ for CD-MAGE+).

- 1: Compute $\nabla f_i(\mathbf{x}_t, \mathbf{y}_t)$ or $\nabla f_i(\mathbf{x}_t, \mathbf{y}_t) - (1 - \alpha_t) \nabla f_i(\mathbf{x}_{t-1}, \mathbf{y}_{t-1})$ \triangleright CD-MAGE
 \triangleright CD-MAGE+
 and send it to the server;

usually has a large variance (Johnson and Zhang 2013). It is constructed as

$$\begin{cases} \mathbf{u}_t = \frac{1}{|\mathcal{S}'_t|} \sum_{i \in \mathcal{S}'_t} \nabla_{\mathbf{x}} f_i(\mathbf{x}_t, \mathbf{y}_t), \\ \mathbf{v}_t = \frac{1}{|\mathcal{S}'_t|} \sum_{i \in \mathcal{S}'_t} \nabla_{\mathbf{y}} f_i(\mathbf{x}_t, \mathbf{y}_t). \end{cases} \quad (2)$$

Inspired by (Cutkosky and Orabona 2019), the CD-MAGE+ algorithm further utilizes a lightweight estimator that aggregates historical gradients to reduce variance. It is constructed in the following recursive manner

$$\begin{cases} \mathbf{u}_t = (1 - \alpha_t) \mathbf{u}_{t-1} + \frac{1}{|\mathcal{S}'_t|} \sum_{i \in \mathcal{S}'_t} (\nabla_{\mathbf{x}} f_i(\mathbf{x}_t, \mathbf{y}_t) - (1 - \alpha_t) \nabla_{\mathbf{x}} f_i(\mathbf{x}_{t-1}, \mathbf{y}_{t-1})), \\ \mathbf{v}_t = (1 - \alpha_t) \mathbf{v}_{t-1} + \frac{1}{|\mathcal{S}'_t|} \sum_{i \in \mathcal{S}'_t} (\nabla_{\mathbf{y}} f_i(\mathbf{x}_t, \mathbf{y}_t) - (1 - \alpha_t) \nabla_{\mathbf{y}} f_i(\mathbf{x}_{t-1}, \mathbf{y}_{t-1})), \end{cases} \quad (3)$$

where α_t is a real number in $[0, 1]$, and \mathbf{u}_0 and \mathbf{v}_0 are initialized as $\frac{1}{|\mathcal{S}'_0|} \sum_{i \in \mathcal{S}'_0} \nabla_{\mathbf{x}} f_i(\mathbf{x}_0, \mathbf{y}_0)$ and $\frac{1}{|\mathcal{S}'_0|} \sum_{i \in \mathcal{S}'_0} \nabla_{\mathbf{y}} f_i(\mathbf{x}_0, \mathbf{y}_0)$, respectively.

- (ii) **Parameter update phase.** The server sends $(\mathbf{u}_t, \mathbf{v}_t)$ and $(\mathbf{x}_t, \mathbf{y}_t)$ to a subset of clients that is potentially different from the subset in the previous phase. Each client in this subset performs K local steps and sends its last iterate to the server. Upon receiving the local iterates from S clients, the server updates the global parameter by averaging the received local iterates. We denote these S clients as \mathcal{S}_t .

Note that, to ensure at least S clients successfully respond to the server in the two phases of each round t , the server can

Algorithm 3: CD-MAGE/CD-MAGE+ on client i in the parameter update phase of the t -th round.

Input: the number of local steps K , step sizes η_t and γ_t , $(\mathbf{x}_t, \mathbf{y}_t)$, and $(\mathbf{u}_t, \mathbf{v}_t)$.

- 1: Initialize local model $\mathbf{x}_{t,i}^{(0)} \leftarrow \mathbf{x}_t, \mathbf{y}_{t,i}^{(0)} \leftarrow \mathbf{y}_t$;
- 2: **for** $k = 0, 1, \dots, K-1$ **do**
- 3: Sample a minibatch $\mathcal{B}_{t,i}^{(k)}$ from local data;
- 4: Compute $\mathbf{d}_{\mathbf{x},t,i}^{(k)}$ and $\mathbf{d}_{\mathbf{y},t,i}^{(k)}$ by (4);
- 5: $\mathbf{x}_{t,i}^{(k+1)} \leftarrow \mathbf{x}_{t,i}^{(k)} - \eta_t \mathbf{d}_{\mathbf{x},t,i}^{(k)}$;
- 6: $\mathbf{y}_{t,i}^{(k+1)} \leftarrow \mathbf{y}_{t,i}^{(k)} + \gamma_t \mathbf{d}_{\mathbf{y},t,i}^{(k)}$;
- 7: **end for**
- 8: Send $(\mathbf{x}_{t,i}^{(K)}, \mathbf{y}_{t,i}^{(K)})$ to the server;

simply communicate to a large enough subset of clients and proceed once it receives information from S clients.

In each local iteration (line 3 to 6 in Algorithm 3) of our algorithms, we simultaneously take a descent step on the local primal variable and an ascent step on the dual one. Due to the data heterogeneity, simply using local gradients as local update directions may bias the local iterates towards individual local optima. To tackle this issue, we leverage global gradient estimates to correct local update directions, similar to the techniques in (Johnson and Zhang 2013; Karimireddy et al. 2020a). Specifically, the local primal and dual update directions are computed as

$$\begin{cases} \mathbf{d}_{\mathbf{x},t,i}^{(k)} = \nabla_{\mathbf{x}} F_i(\mathbf{x}_{t,i}^{(k)}, \mathbf{y}_{t,i}^{(k)}; \mathcal{B}_{t,i}^{(k)}) - \nabla_{\mathbf{x}} F_i(\mathbf{x}_t, \mathbf{y}_t; \mathcal{B}_{t,i}^{(k)}) + \mathbf{u}_t, \\ \mathbf{d}_{\mathbf{y},t,i}^{(k)} = \nabla_{\mathbf{y}} F_i(\mathbf{x}_{t,i}^{(k)}, \mathbf{y}_{t,i}^{(k)}; \mathcal{B}_{t,i}^{(k)}) - \nabla_{\mathbf{y}} F_i(\mathbf{x}_t, \mathbf{y}_t; \mathcal{B}_{t,i}^{(k)}) + \mathbf{v}_t, \end{cases} \quad (4)$$

where $F_i(\cdot, \cdot; \mathcal{B}_{t,i}^{(k)})$ is the average of local losses over the minibatch $\mathcal{B}_{t,i}^{(k)}$ of data samples, i.e.,

$$F_i(\mathbf{x}, \mathbf{y}, \mathcal{B}) := |\mathcal{B}|^{-1} \sum_{\zeta \in \mathcal{B}} F_i(\mathbf{x}, \mathbf{y}; \zeta).$$

The update strategy (4) drives the local update directions to be close to global gradients when $(\mathbf{x}_{t,i}^{(k)}, \mathbf{y}_{t,i}^{(k)})$ is close to $(\mathbf{x}_t, \mathbf{y}_t)$ and F_i is smooth. This mitigates the bias of local updates and thus provides robustness to the data heterogeneity. Besides, since only a subset of clients are involved in each round and multiple local steps are performed before communication, our algorithms are resilient to the limited availability of clients and have relatively low communication overhead.

If we simply use the local stochastic gradient $\nabla_{\mathbf{x}} F_i(\mathbf{x}_{t,i}^{(k)}, \mathbf{y}_{t,i}^{(k)}; \mathcal{B}_{t,i}^{(k)})$ (resp., $\nabla_{\mathbf{y}} F_i(\mathbf{x}_{t,i}^{(k)}, \mathbf{y}_{t,i}^{(k)}; \mathcal{B}_{t,i}^{(k)})$) as the local primal (resp., dual) update direction, we obtain a simpler algorithm. We refer to such algorithm as Cross-device Minimax Averaging (CD-MA), which is detailed in Algorithm 4 in Appendix A. CD-MA can be viewed as a cross-device variant of the Local SGDA algorithm (Deng and Mahdavi 2021), where the latter only applies to the cross-silo setting as it requires the participation of all clients in each round. As we shall see in Section 4, the convergence rates of CD-MAGE and CD-MAGE+ are superior to CD-MA, which demonstrates the advantage of utilizing global gradient estimates in local updates.

4 Convergence Analysis

In this section, we establish convergence guarantees for the proposed algorithms. We note that the key of our analyses is to bound the following three terms: the global gradient estimation error, the bias of local updates, and the gap between $f(\mathbf{x}_t, \mathbf{y}_t)$ and $\max_{\mathbf{y}} f(\mathbf{x}_t, \mathbf{y})$. However, these terms twist together as the algorithm proceeds and thus are difficult to control, which makes our convergence analyses particularly challenging. To address this, we construct delicate potential functions that properly handle these terms. Note that all missing proofs are deferred to the Appendix due to the limit of space. We also make the following common assumptions throughout.

Assumption 1 (Bounded gradient dissimilarity). *There exist two positive constants $\sigma_1 > 0$ and $\sigma_2 > 0$ such that $\forall \mathbf{x} \in \mathbb{R}^p, \forall \mathbf{y} \in \mathbb{R}^q$,*

$$\begin{cases} \mathbb{E}_{i \sim \mathcal{D}} [\|\nabla_{\mathbf{x}} f_i(\mathbf{x}, \mathbf{y}) - \nabla_{\mathbf{x}} f(\mathbf{x}, \mathbf{y})\|^2] \leq \sigma_1^2, \\ \mathbb{E}_{i \sim \mathcal{D}} [\|\nabla_{\mathbf{y}} f_i(\mathbf{x}, \mathbf{y}) - \nabla_{\mathbf{y}} f(\mathbf{x}, \mathbf{y})\|^2] \leq \sigma_2^2. \end{cases}$$

Assumption 2 (Lipschitz continuous gradient). *There exist four positive constants $L_1, L_2, L_{12}, L_{21} > 0$ such that for any $\zeta \in \{\zeta_{i,1}, \dots, \zeta_{i,n_i}\}$, $\mathbf{x}, \mathbf{x}_1, \mathbf{x}_2 \in \mathbb{R}^p$ and $\mathbf{y}, \mathbf{y}_1, \mathbf{y}_2 \in \mathbb{R}^q$, the following inequalities hold*

$$\begin{cases} \|\nabla_{\mathbf{x}} F_i(\mathbf{x}_1, \mathbf{y}; \zeta) - \nabla_{\mathbf{x}} F_i(\mathbf{x}_2, \mathbf{y}; \zeta)\| \leq L_1 \|\mathbf{x}_1 - \mathbf{x}_2\|, \\ \|\nabla_{\mathbf{x}} F_i(\mathbf{x}, \mathbf{y}_1; \zeta) - \nabla_{\mathbf{x}} F_i(\mathbf{x}, \mathbf{y}_2; \zeta)\| \leq L_{12} \|\mathbf{y}_1 - \mathbf{y}_2\|, \\ \|\nabla_{\mathbf{y}} F_i(\mathbf{x}_1, \mathbf{y}; \zeta) - \nabla_{\mathbf{y}} F_i(\mathbf{x}_2, \mathbf{y}; \zeta)\| \leq L_{21} \|\mathbf{x}_1 - \mathbf{x}_2\|, \\ \|\nabla_{\mathbf{y}} F_i(\mathbf{x}, \mathbf{y}_1; \zeta) - \nabla_{\mathbf{y}} F_i(\mathbf{x}, \mathbf{y}_2; \zeta)\| \leq L_2 \|\mathbf{y}_1 - \mathbf{y}_2\|. \end{cases}$$

Assumption 3 (Polyak-Łojasiewicz (PL) condition). *There exists a constant $\mu > 0$ such that $\forall \mathbf{x} \in \mathbb{R}^p, \mathbf{y} \in \mathbb{R}^q$,*

$$\|\nabla_{\mathbf{y}} f(\mathbf{x}, \mathbf{y})\|^2 \geq 2\mu \left(\max_{\mathbf{y}' \in \mathbb{R}^q} f(\mathbf{x}, \mathbf{y}') - f(\mathbf{x}, \mathbf{y}) \right).$$

The PL condition is a well-studied and common condition in the optimization literature and many practical problems satisfy this assumption. Actually, it holds for any strongly concave functions (e.g., the minimax formulation of the AUC maximization problem (Liu et al. 2020a)), and many non-concave functions arising in over-parameterized deep networks, deep networks with linear activations, one-hidden-layer networks with Leaky ReLU activation (Du et al. 2019; Allen-Zhu, Li, and Song 2019; Charles and Papailiopoulos 2018), to name a few.

Besides, we also assume that each client in \mathcal{S}'_t or \mathcal{S}_t is randomly drawn from the underlying distribution \mathcal{D} , which is a common assumption in the federated learning literature (Li et al. 2018, 2020; Karimireddy et al. 2020a). For ease of notation, we denote $\mathbf{z} := (\mathbf{x}, \mathbf{y})$ for any $(\mathbf{x}, \mathbf{y}) \in \mathbb{R}^p \times \mathbb{R}^q$. The notation $\mathbf{y}^*(\mathbf{x})$ denotes the projection of \mathbf{y} onto the solution set of $\max_{\mathbf{y}} f(\mathbf{x}, \mathbf{y})$. We also denote $\Phi(\mathbf{x}) := \max_{\mathbf{y} \in \mathbb{R}^q} f(\mathbf{x}, \mathbf{y})$. As stated in Section 3, for simplicity we assume $|\mathcal{S}'_t| = |\mathcal{S}_t| = S$ in our algorithms.

Under Assumptions 2 and 3, both f and Φ have Lipschitz continuous gradients, as shown in the two lemmas below.

Lemma 1. *Under Assumption 2, $\forall \zeta \in \{\zeta_{i,1}, \dots, \zeta_{i,n_i}\}$, $F_i(\mathbf{x}, \mathbf{y}; \zeta)$ is L_f -smooth with respect to (\mathbf{x}, \mathbf{y}) , i.e., $\forall \mathbf{x}_1, \mathbf{x}_2 \in \mathbb{R}^p$ and $\forall \mathbf{y}_1, \mathbf{y}_2 \in \mathbb{R}^q$,*

$$\left\| \begin{bmatrix} \nabla_{\mathbf{x}} F_i(\mathbf{x}_1, \mathbf{y}_1; \zeta) - \nabla_{\mathbf{x}} F_i(\mathbf{x}_2, \mathbf{y}_2; \zeta) \\ \nabla_{\mathbf{y}} F_i(\mathbf{x}_1, \mathbf{y}_1; \zeta) - \nabla_{\mathbf{y}} F_i(\mathbf{x}_2, \mathbf{y}_2; \zeta) \end{bmatrix} \right\| \leq L_f \left\| \begin{bmatrix} \mathbf{x}_1 - \mathbf{x}_2 \\ \mathbf{y}_1 - \mathbf{y}_2 \end{bmatrix} \right\|,$$

where $L_f := \max\{\sqrt{2(L_1^2 + L_{21}^2)}, \sqrt{2(L_2^2 + L_{12}^2)}\}$. Furthermore, both f_i and f are also L_f -smooth.

Lemma 2. (Nouiehed et al. 2019, Lemma 22) *Under Assumption 2 and 3, the function $\Phi(\mathbf{x})$ is differentiable, and its gradient is given by*

$$\nabla \Phi(\mathbf{x}) = \nabla_{\mathbf{x}} f(\mathbf{x}, \mathbf{y}^*), \quad (5)$$

where $\mathbf{y}^* \in \arg\max_{\mathbf{y} \in \mathbb{R}^q} f(\mathbf{x}, \mathbf{y})$. Moreover, Φ has L_Φ -Lipschitz continuous gradients with $L_\Phi := L_1 + \frac{L_{12}L_{21}}{2\mu}$.

Having established that $\Phi(\cdot)$ is a smooth function, a natural metric for measuring the performance of an algorithm on problem (1) is the squared gradient norm of Φ , i.e., $\|\nabla \Phi(\mathbf{x})\|^2$. This metric is commonly used in analyzing algorithms for nonconvex-PL or nonconvex-strongly-concave min-max problems (Reisizadeh et al. 2020; Deng and Mahdavi 2021; Lin, Jin, and Jordan 2020; Luo et al. 2020). Note that $\Phi(\mathbf{x})$ only measures the performance of \mathbf{x} . Once an approximate primal solution \mathbf{x}_T is obtained, one can efficiently approximate $\max_{\mathbf{y}} f(\mathbf{x}_T, \mathbf{y})$. Such approach is common in non-convex minimax optimization.

4.1 Analysis of CD-MAGE

To establish the convergence of CD-MAGE, we first provide several key lemmas. The lemma below reveals the relationship between two consecutive global iterates in CD-MAGE.

Lemma 3. *The global iterates of CD-MAGE satisfy*

$$\begin{cases} \mathbf{x}_{t+1} = \mathbf{x}_t - \eta_t K(\mathbf{u}_t + \mathbf{e}_{\mathbf{x},t}), \\ \mathbf{y}_{t+1} = \mathbf{y}_t + \gamma_t K(\mathbf{v}_t + \mathbf{e}_{\mathbf{y},t}), \end{cases}$$

where $\mathbf{e}_{\mathbf{x},t}$ and $\mathbf{e}_{\mathbf{y},t}$ are defined as $\mathbf{e}_{\mathbf{x},t} := \frac{1}{SK} \sum_{i \in \mathcal{S}_t} \sum_{k=0}^{K-1} (\nabla_{\mathbf{x}} F_i(\mathbf{z}_{t,i}^{(k)}; \mathcal{B}_{t,i}^{(k)}) - \nabla_{\mathbf{x}} F_i(\mathbf{z}_t; \mathcal{B}_{t,i}^{(k)}))$ and $\mathbf{e}_{\mathbf{y},t} := \frac{1}{SK} \sum_{i \in \mathcal{S}_t} \sum_{k=0}^{K-1} (\nabla_{\mathbf{y}} F_i(\mathbf{z}_{t,i}^{(k)}; \mathcal{B}_{t,i}^{(k)}) - \nabla_{\mathbf{y}} F_i(\mathbf{z}_t; \mathcal{B}_{t,i}^{(k)}))$, respectively.

The next lemma shows that the expected loss value $\mathbb{E}[\Phi(\mathbf{x}_t)]$ decreases in each round as long as the primal variable update error $\mathbb{E}[\|\mathbf{e}_{\mathbf{x},t}\|^2]$ and the dual variable update error $\mathbb{E}[\Phi(\mathbf{x}_t) - f(\mathbf{z}_t)]$ are controlled in a desired level.

Lemma 4. *Suppose that $\eta_t \leq \frac{1}{4L_\Phi K}$ in CD-MAGE. Then,*

$$\begin{aligned} & \mathbb{E}[\Phi(\mathbf{x}_{t+1}) - \Phi(\mathbf{x}_t)] \\ & \leq \frac{5\eta_t K}{4} \mathbb{E}[\|\mathbf{e}_{\mathbf{x},t}\|^2] + \frac{\eta_t K L_{12}^2}{2\mu} \mathbb{E}[\Phi(\mathbf{x}_t) - f(\mathbf{z}_t)] + \frac{L_\Phi \eta_t^2 K^2}{S} \sigma_1^2 \\ & \quad - \frac{\eta_t K}{2} \mathbb{E}[\|\nabla \Phi(\mathbf{x}_t)\|^2] - \frac{\eta_t K}{8} \mathbb{E}[\|\nabla_{\mathbf{x}} f(\mathbf{z}_t)\|^2], \end{aligned}$$

where $\mathbf{e}_{\mathbf{x},t}$ is defined in Lemma 3.

However, these two errors are coupled as the algorithm proceeds, which makes it difficult to directly control these error terms. To circumvent this difficulty, we define a new potential function

$$\mathcal{L}_t = \mathbb{E}[\Phi(\mathbf{x}_t) - \Phi(\mathbf{x}^*) + \frac{1}{20} (\Phi(\mathbf{x}_t) - f(\mathbf{x}_t, \mathbf{y}_t))],$$

where $\mathbf{x}^* \in \arg\min_{\mathbf{x} \in \mathbb{R}^p} \Phi(\mathbf{x})$. Note that $\mathcal{L}_t \geq 0$ since $\Phi(\mathbf{x}_t) \geq \Phi(\mathbf{x}^*)$ and $\Phi(\mathbf{x}_t) \geq f(\mathbf{x}_t, \mathbf{y}_t)$. If $\mathcal{L}_t = 0$, then \mathbf{x}_t is a minimizer of Φ and $\mathbf{y}_t \in \arg\max_{\mathbf{y} \in \mathbb{R}^q} f(\mathbf{x}_t, \mathbf{y})$. The following lemma provides an upper bound of \mathcal{L}_{t+1} .

Lemma 5. Suppose that the step sizes η_t, γ_t of CD-MAGE satisfy $\eta_t \leq \min \left\{ \frac{1}{36L_f K}, \frac{1}{4L_\Phi K}, \frac{\mu^2 \gamma_t}{21L_{12}^2} \right\}$ and $\gamma_t \leq \frac{1}{87L_f K}$. Then, we have

$$\mathcal{L}_{t+1} \leq \mathcal{L}_t - \frac{21\eta_t K}{40} \mathbb{E}[\|\nabla \Phi(\mathbf{x}_t)\|^2] + \frac{\eta_t^2 K^2}{S} (1.05L_\Phi + 0.81L_f) \sigma_1^2 + \frac{3\gamma_t^2 K^2 L_f}{4S} \sigma_2^2.$$

By recursively applying Lemma 5 and selecting appropriate step sizes, we derive the convergence rate of CD-MAGE as stated in the following theorem.

Theorem 1. Define the step sizes η_t and γ_t of CD-MAGE as $\eta_t = \min \left\{ \frac{1}{36L_f K}, \frac{1}{4L_\Phi K}, \frac{\mu^2 \gamma_t}{21L_{12}^2}, \sqrt{\frac{40\mathcal{L}_0 S}{21(L_\Phi + L_f)TK^2\sigma_1^2}} \right\}$ and $\gamma_t = \min \left\{ \frac{1}{87L_f K}, \sqrt{\frac{4\mathcal{L}_0 S}{3L_f TK^2\sigma_2^2}} \right\}$, where $\mathcal{L}_0 := \Phi(\mathbf{x}_0) - \Phi(\mathbf{x}^*) + \frac{1}{20}(\Phi(\mathbf{x}_0) - f(\mathbf{z}_0))$. Then

$$\begin{aligned} & \frac{1}{T} \sum_{t=0}^{T-1} \mathbb{E}[\|\nabla \Phi(\mathbf{x}_t)\|^2] \\ & \leq 4\sqrt{\frac{40\mathcal{L}_0(L_\Phi + L_f)\sigma_1^2}{21ST}} + \left(\frac{20}{7} + \frac{60L_{12}^2}{\mu^2} \right) \sqrt{\frac{\mathcal{L}_0 L_f \sigma_2^2}{3ST}} \\ & \quad + \left(8L_\Phi + \left(\frac{1827L_{12}^2}{\mu^2} + 72 \right) L_f \right) \frac{40\mathcal{L}_0}{21T}. \end{aligned}$$

Remark 1. The rate in Theorem 1 can be simplified as $\mathcal{O}(1/T + 1/\sqrt{ST})$, if we treat $L_\Phi, L_{12}, L_f, \mu, \mathcal{L}_0, \sigma_1$, and σ_2 as constants. In comparison, the non-local counterpart of CD-MAGE, i.e., Parallel SGDA, which directly parallelizes the single-machine SGDA algorithm (Lin, Jin, and Jordan 2020) over the clients, has an $\mathcal{O}(1/T + 1/S)$ (with constant step sizes independent of T) or $\mathcal{O}(1/T + 1/S^{1/3}T^{2/3} + 1/S^{2/3}T^{1/3})$ convergence rate (with step sizes depending on T)² under similar assumptions. Both of these two rates are inferior to that of CD-MAGE when $S < T$, and all of them are equal to $\mathcal{O}(1/T)$ when $S \geq T$. Thus, the communication cost of CD-MAGE with any $K \geq 1$ is comparable to or better than that of its non-local counterpart Parallel SGDA. In contrast, most existing rates of FL algorithms at best match those of their non-local counterparts only at certain values of K , given the same number of gradient evaluations.

4.2 Analysis of CD-MAGE+

The analysis of CD-MAGE+ is more sophisticated than that of CD-MAGE. Due to the limit of space, we defer the detailed analysis to the Appendix and summarize the main result in the following theorem.

Theorem 2. Define the parameters η_t, γ_t , and α_t of CD-MAGE+ as $\eta_t = \min \left\{ \frac{1}{2L_f}, \frac{1}{2L_\Phi}, \frac{2\mu^2 \gamma_t}{33L_{12}^2} \right\}$, $\gamma_t = \min \left\{ \frac{1}{100L_f K}, \frac{S^{1/3}}{L_f K(t+1)^{1/3}} \right\}$, and $\alpha_t = \frac{8192L_f^2 K^2 \gamma_t^2}{S}$. Then, $\frac{1}{SKT} \sum_{t=0}^{T-1} \sum_{k=0}^{K-1} \sum_{i \in \mathcal{S}_t} \mathbb{E}[\|\nabla \Phi(\mathbf{x}_{t,i}^{(k)})\|^2] =$

²Note that Lin, Jin, and Jordan (2020) only proves the $\mathcal{O}(1/T + 1/S)$ rate. Nevertheless, the other rate can be easily derived using similar arguments as in (Lin, Jin, and Jordan 2020, Section C).

$$\mathcal{O} \left(\left(\frac{L_\Phi}{TK} + \frac{L_{12}^2 L_f}{\mu^2} \left(\frac{1}{T} + \frac{1}{S^{1/3}T^{2/3}} \right) \right) (\tilde{\mathcal{L}}_0 + (\sigma_1^2 + \sigma_2^2) \frac{\log(T+1)}{L_f}) \right),$$

where $\tilde{\mathcal{L}}_0 := \Phi(\mathbf{x}_0) - \Phi(\mathbf{x}^*) + \frac{1}{10}(\Phi(\mathbf{x}_0) - f(\mathbf{z}_0))$.

Remark 2. The communication cost of CD-MAGE+ to reach an ϵ -stationary point is $\tilde{\mathcal{O}}((\tilde{\mathcal{L}}_0 + L_f^{-1}(\sigma_1^2 + \sigma_2^2))(L_\Phi/K\epsilon + L_{12}^2/\mu^2\epsilon) + (\tilde{\mathcal{L}}_0 + L_f^{-1}(\sigma_1^2 + \sigma_2^2))^{1.5}(L_{12}^3 L_f^{1.5}/\mu^3 S^{0.5}\epsilon^{1.5}))$. Increasing K reduces the first term of the cost. When K reaches certain threshold, other terms independent of K dominate the cost.

Remark 3. The convergence rate of CD-MAGE+ in Theorem 2 can be simplified as $\tilde{\mathcal{O}}(1/T + 1/S^{1/3}T^{2/3})$ if we treat $L_\Phi, L_{12}, L_f, \mu, \tilde{\mathcal{L}}_0, \sigma_1$, and σ_2 as constants. This rate is better than the $\mathcal{O}(1/T + 1/\sqrt{ST})$ rate of CD-MAGE when $S < T$, otherwise they are of the same order. Therefore, when the number of clients participate per round is relatively small compared to the number of communication rounds, CD-MAGE+ converges faster than CD-MAGE.

4.3 Analysis of CD-MA

In addition to CD-MAGE and CD-MAGE+, we also provide the theoretical analysis for CD-MA detailed in Algorithm 4 in Appendix A, which is the direct extension of the Local SGDA algorithm (Deng and Mahdavi 2021) to the cross-device setting. Besides Assumptions 1-3, the assumption below is also required.

Assumption 4. For any $(\mathbf{x}, \mathbf{y}) \in \mathbb{R}^{p \times q}$, and any client i ,

$$\begin{cases} \frac{1}{n_i} \sum_{j=1}^{n_i} \|\nabla_{\mathbf{x}} F_i(\mathbf{x}, \mathbf{y}; \zeta) - \nabla_{\mathbf{x}} f_i(\mathbf{x}, \mathbf{y})\|^2 \leq G_1^2, \\ \frac{1}{n_i} \sum_{j=1}^{n_i} \|\nabla_{\mathbf{y}} f_i(\mathbf{x}, \mathbf{y}; \zeta) - \nabla_{\mathbf{y}} f_i(\mathbf{x}, \mathbf{y})\|^2 \leq G_2^2. \end{cases}$$

The convergence rate of CD-MA is provided in the next theorem, whose proof is similar to that of Theorem 1 and is deferred to the Appendix.

Theorem 3. Define the step sizes of CD-MA as $\eta_t = \min \left\{ \sqrt{\frac{20\mathcal{L}_0 S}{7(L_\Phi + L_f)TK^2\sigma_1^2}}, \left(\frac{3\mathcal{L}_0}{L_f^2(\sigma_1^2 + G_1^2)TK^3} \right)^{1/3}, \frac{1}{36L_f K}, \frac{1}{4L_\Phi K}, \frac{\mu^2 \gamma_t}{21L_{12}^2} \right\}$ and $\gamma_t = \min \left\{ \sqrt{\frac{20\mathcal{L}_0 S}{L_f TK^2\sigma_2^2}}, \left(\frac{30\mathcal{L}_0}{L_f^2(\sigma_2^2 + G_2^2)TK^3} \right)^{1/3}, \frac{1}{87L_f K} \right\}$, where $\mathcal{L}_0 := \Phi(\mathbf{x}_0) - \Phi(\mathbf{x}^*) + \frac{1}{20}(\Phi(\mathbf{x}_0) - f(\mathbf{z}_0))$.

Further, suppose that the minibatches $\mathcal{B}_{t,i}^{(1)}, \dots, \mathcal{B}_{t,i}^{(K-1)}$ are drawn in a random reshuffling manner and K is an integral multiple of the epoch length. Then, we have

$$\begin{aligned} & \frac{1}{T} \sum_{t=0}^{T-1} \mathbb{E}[\|\nabla_{\mathbf{x}} \Phi(\mathbf{x}_t)\|^2] \\ & \leq \frac{160(9L_f + L_\Phi)\mathcal{L}_0}{7T} + 7\sigma_1 \sqrt{\frac{\mathcal{L}_0(L_f + L_\Phi)}{ST}} \\ & \quad + \frac{9L_{12}^2 \sigma_2^2}{\mu^2} \sqrt{\frac{\mathcal{L}_0 L_f}{ST}} + \left(8(\sigma_1^2 + G_1^2)^{1/3} + \frac{3(\sigma_1^2 + G_1^2)^{2/3}}{10(\sigma_2^2 + G_2^2)^{1/3}} \right. \\ & \quad \left. + (37 + \frac{13L_{12}^2}{\mu^2})(\sigma_1^2 + G_1^2)^{1/3} \right) \left(\frac{\mathcal{L}_0 L_f}{T} \right)^{2/3}. \end{aligned}$$

Remark 4. As shown in Theorem 3, CD-MA attains an $\mathcal{O}(1/T^{2/3} + 1/\sqrt{ST})$ convergence rate, which is inferior to that of CD-MAGE and CD-MAGE+. Our theory shows that

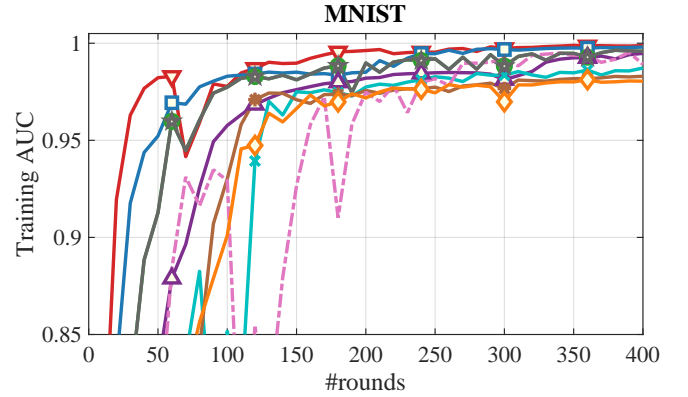
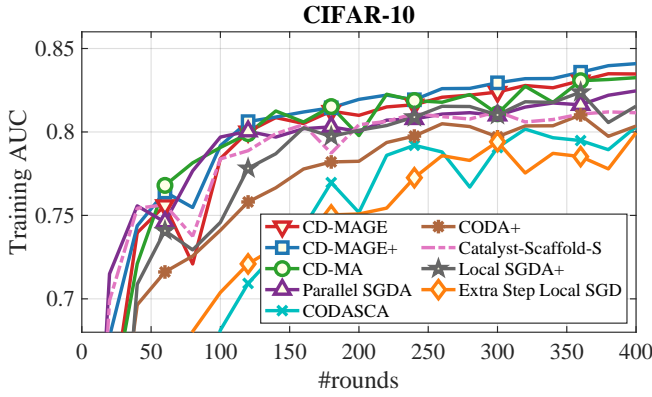


Figure 1: Results on the AUC maximization task (left: CIFAR-10, right: MNIST).

CD-MAGE and CD-MAGE+ are less affected by the data heterogeneity compared to CD-MA. Specifically, in the convergence rate of CD-MAGE (resp., CD-MAGE+), the terms depending on the gradient dissimilarity (σ_1 or σ_2) are of the order $\mathcal{O}(1/\sqrt{ST})$ (resp., $\tilde{\mathcal{O}}(1/T + 1/S^{1/3}T^{2/3})$), whereas CD-MA has a higher order of $\mathcal{O}(1/\sqrt{ST} + 1/T^{2/3})$. Note that the gradient dissimilarity is commonly used to quantify data heterogeneity in the FL literature (Kairouz et al. 2019; Rasouli, Sun, and Rajagopal 2020; Reiszadeh et al. 2020; Hou et al. 2021; Yuan et al. 2021; Deng and Mahdavi 2021). Actually most existing FL algorithms are affected by data heterogeneity. The Scaffold method (Karimireddy et al. 2020b) is an exception, but its convergence rate depends on N/S , where N is the total number of clients.

5 Experiments

To demonstrate the efficiency of the proposed algorithms, we conduct experiments on three tasks: (i) AUC maximization, (ii) robust adversarial neural network training, and (iii) generative adversarial network training. We compare the proposed algorithms with Parallel SGDA, which is the parallel version of the single-machine SGDA algorithm (Lin, Jin, and Jordan 2020), and the cross-device versions of Extra Step Local SGD (Beznosikov, Samokhin, and Gasnikov 2020), Local SGDA+ (Deng and Mahdavi 2021), Catalyst-Scaffold-S (Hou et al. 2021), CODA+, and CODASCA (Yuan et al. 2021). We note that Local SGDA+, Extra Step Local SGD, Catalyst-Scaffold-S, CODA+, and CODASCA are state-of-the-art federated minimax algorithms which are required to the participation of all clients in each round and thus only apply to the cross-silo setting. Here, we use their cross-device variants by only involving a subset of clients in each round, which are actually not theoretically guaranteed. We exclude the CODA algorithm (Guo et al. 2020) from our baselines as we have already included CODA+, which is an improved version of CODA (Yuan et al. 2021).

In our experimental setting, there are 500 clients in total and the client distribution \mathcal{D} is the uniform distribution (check the discussion below the problem formulation (1)). Since communication is often the major bottleneck in cross-device federated learning and clients generally have much slower

upload than download bandwidth (Kairouz et al. 2019), we compare the algorithms given the same amount of data transferred from clients to the server. Specifically, for CD-MA, Parallel SGDA, Local SGDA+, Extra Step Local SGD and CODA+, which are only required to send parameter updates from clients to the server in each round, we fix the number of clients participating at each time to $S = 10$. For the rest algorithms, we fix $S = 5$ because they require to send both parameter updates and gradient estimates to the server in each round. In this way, all algorithms have equal amount of client communication to the server in each round.

Throughout the experiments, we used the same random seed for all algorithms. We did a grid-search on hyperparameters for the algorithms and selected the best hyperparameters. The ranges of the tuning values are listed in Appendix B.1. All experiments were implemented in Pytorch and run on a workstation with 2 Intel E5-2680 v4 CPUs (28 cores and 56 threads) and 378GB memory, where each client is assigned to a single process.

5.1 AUC Maximization

In the first experiment, we consider the ℓ_2 -relaxed AUC maximization problem in the minimax formulation (Ying, Wen, and Lyu 2016; Liu et al. 2020a). AUC is a widely used metric for binary classification on imbalanced data. For completeness, we refer the reader to Appendix (?) for the ℓ_2 -relaxed AUC maximization problem and its minimax formulation.

We use two datasets: CIFAR-10 (Krizhevsky, Hinton et al. 2009) and MNIST (LeCun et al. 1998). To make the data imbalanced, we split the original CIFAR-10 dataset (resp., MNIST) into two classes by treating the original “airplane” (resp., 0) class as the positive class and the remaining as negative. In addition, we preprocess the data by rescaling each pixel value to the range $[-1, 1]$. To make the data heterogeneous, the training data is first sorted according to the original class label and then equally partitioned into 500 clients so that all data points on one client are from the same class. We use a convolutional neural network from (TensorFlow team 2021) as the classification model for CIFAR-10 following (McMahan et al. 2017) and LeNet5 (LeCun et al. 1998) for MNIST. The parameters of these networks are randomly initialized by default in Pytorch.

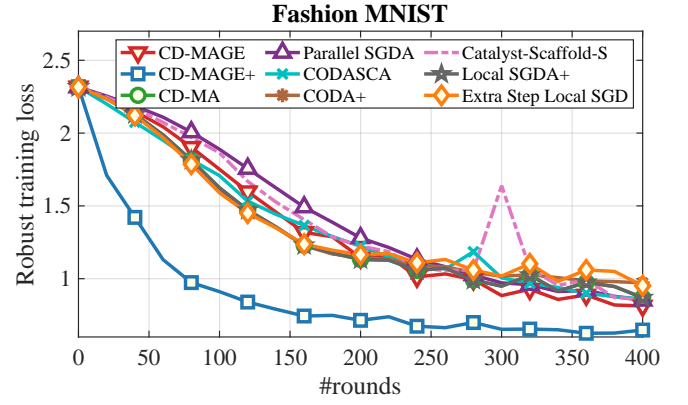
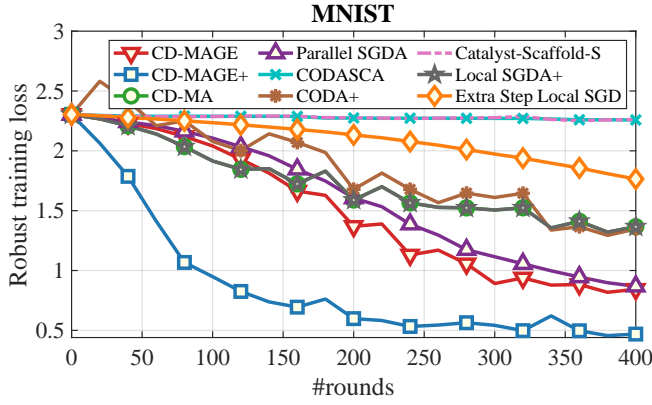


Figure 2: Results on the robust neural network training task (left: MNIST, right: Fashion MNIST).

We report the AUC value on the training dataset versus the number of rounds. Each algorithm runs exactly one epoch (10 local steps for CIFAR-10 and 12 for MNIST) on clients with the minibatch size $B = 10$. The results are shown in Figure 1. We observe that CD-MAGE+ and CD-MAGE are superior to other algorithms on both datasets. Besides, in the left plot, we see that CD-MAGE+ performs better than CD-MAGE on the CIFAR-10 dataset, which demonstrates the effectiveness of the variance-reduced technique used by CD-MAGE+. On the MNIST dataset which is much easier to classify, both CD-MAGE+ and CD-MAGE already attains a high AUC value of 0.998 in 240 rounds, and thus their performance is less distinguishable. It is reasonable to conjecture that the gradient dissimilarity is relatively small on MNIST and using the minibatch estimator to estimate the global gradient is accurate enough, which leads to the good performance of CD-MAGE.

5.2 Robust Adversarial Network Training

In the second experiment, we focus on training a classification model that is robust against adversarial noise (Deng and Mahdavi 2021). Let $h_{\mathbf{x}}$ be a neural network model parameterized by \mathbf{x} and denote the j -th data sample on client i as the feature-label pair $\zeta_{i,j} = (\mathbf{a}_{i,j}, b_{i,j})$. Our goal is to solve problem (1) with each f_i defined as

$$f_i(\mathbf{x}, \mathbf{y}) := \frac{1}{n_i} \sum_{j=1}^{n_i} \ell(h_{\mathbf{x}}(\mathbf{a}_{i,j} + \mathbf{y}), b_{i,j}),$$

where ℓ denotes the cross entropy function, and \mathbf{y} is the adversarial noise subject to the ℓ_2 -norm ball $\{\mathbf{y} : \|\mathbf{y}\|_2 \leq 1\}$. We relax this constrained minimax problem to an unconstrained one by replacing the constraint set with an ℓ_2 regularization term $-\frac{\lambda}{2} \|\mathbf{y}\|^2$, where λ is set to 0.001. We use MNIST and Fashion MNIST (Xiao, Rasul, and Vollgraf 2017) datasets in this experiment. The data partitioning scheme is the same as in Section 5.1 and each pixel value of the images is rescaled to $[-1, 1]$. Following the setting in (Deng and Mahdavi 2021), we use a 2-layer MLP with the ReLU activation, where each layer consists of 200 neurons. The performance measure is the robust training loss defined as $\max_{\mathbf{y}} \mathbb{E}_{i \sim \mathcal{D}} [\frac{1}{n_i} \sum_{j=1}^{n_i} \ell(h_{\mathbf{x}_t}(\mathbf{a}_{i,j} + \mathbf{y}), b_{i,j}) - \frac{\lambda}{2} \|\mathbf{y}\|^2]$. To

compute the robust training loss which involves solving a maximization problem, we run the gradient ascent algorithm for a few epochs following (Deng and Mahdavi 2021). Similar to the previous experiment, each algorithm runs with the minibatch size $B = 10$ for exactly one epoch (12 local steps) on clients. The results are shown in Figure 2. We can see that both CD-MAGE+ and CD-MAGE outperform other algorithms. In addition, CD-MAGE+ performs much better than CD-MAGE, which shows the effectiveness of variance reduction in global gradient estimates.

5.3 GAN Training

In the last experiment, we test the performance of our algorithms on training GANs (Goodfellow, Shlens, and Szegedy 2014). Denote the generator network parameterized by \mathbf{x} as $G_{\mathbf{x}}$ and the discriminator network parameterized by \mathbf{y} as $D_{\mathbf{y}}$. The local loss function is defined as

$$f_i(\mathbf{x}, \mathbf{y}) = \frac{1}{n_i} \sum_{j=1}^{n_i} \log D_{\mathbf{y}}(\mathbf{a}_{i,j}) + \mathbb{E}_{\mathbf{w} \sim \mathcal{P}} [\log(1 - D_{\mathbf{y}}(G_{\mathbf{x}}(\mathbf{w})))] ,$$

where $\mathbf{a}_{i,j}$ is the feature of the j -th data point on client i and \mathcal{P} is the prior distribution of the noise vector for generating samples. Following (Radford, Metz, and Chintala 2015), we use the Deep Convolutional GAN architecture and set \mathcal{P} to the uniform distribution over $[-1, 1]^{100}$. We use the MNIST and Fashion MNIST datasets and the same data partitioning and preprocessing schemes as in Section 5.2. The performance metric is the Inception score (Salimans et al. 2016), which is a common metric for evaluating GANs. Each algorithm runs with the minibatch size $B = 30$ for 5 local epochs (20 local steps). We run each algorithm for 400 (resp., 800) rounds on MNIST (resp., Fashion MNIST). Note that the number of rounds on Fashion MNIST is larger because the compared algorithms generally converge more slowly on Fashion MNIST. The experimental results are displayed in Figure 3. We observe that CD-MAGE and CD-MAGE+ achieve the best performance after 400 rounds of training. In addition, CD-MAGE slightly outperforms CD-MAGE+. We conjecture that this is due to DCGAN’s batch normalization layers, which already have the effect of reducing variance (Ioffe and Szegedy 2015). Figure 6 and 7 in Ap-

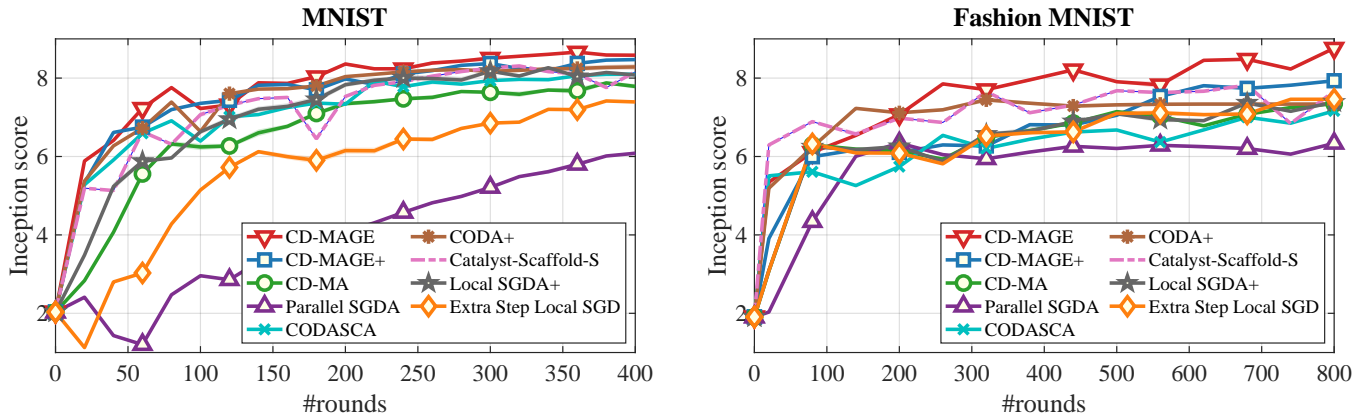


Figure 3: Results on the GAN training task (left: MNIST, right: Fashion MNIST). The horizontal axis stands for the number of rounds and the vertical axis represents the Inception score.

pendix B.4 depict samples generated by the compared algorithms after training, which also show that CD-MAGE and CD-MAGE+ generate high-quality images.

6 Conclusion

We present the first theoretically guaranteed algorithms for general minimax problems in the cross-device federated learning setting. Our algorithms have the advantages of being communication-efficient and being robust to the limited availability and the data heterogeneity of clients. Theoretical analyses and experimental results show the efficiency of our algorithms. Directions for future work include the development and analyses of variants with adaptive step sizes, and the study of lower bounds for minimax problems in the cross-device federated learning setting.

References

- Allen-Zhu, Z.; Li, Y.; and Song, Z. 2019. A convergence theory for deep learning via over-parameterization. In *International Conference on Machine Learning*, 242–252. PMLR.
- Beznosikov, A.; Samokhin, V.; and Gasnikov, A. 2020. Distributed Saddle-Point Problems: Lower Bounds, Optimal Algorithms and Federated GANs. *arXiv preprint arXiv:2010.13112*.
- Brown, G. W. 1951. Iterative solution of games by fictitious play. *Activity analysis of production and allocation*, 13(1): 374–376.
- Charles, Z.; and Papailiopoulos, D. 2018. Stability and generalization of learning algorithms that converge to global optima. In *International Conference on Machine Learning*, 745–754. PMLR.
- Chavdarova, T.; Gidel, G.; Fleuret, F.; and Lacoste-Julien, S. 2019. Reducing noise in GAN training with variance reduced extragradient. In *Advances in Neural Information Processing Systems*, 391–401.
- Cutkosky, A.; and Orabona, F. 2019. Momentum-based variance reduction in non-convex SGD. In *Advances in Neural Information Processing Systems*, 15236–15245.
- Deng, Y.; Kamani, M. M.; and Mahdavi, M. 2020. Distributionally Robust Federated Averaging. In Larochelle, H.; Ranzato, M.; Hadsell, R.; Balcan, M. F.; and Lin, H., eds., *Advances in Neural Information Processing Systems*, volume 33, 15111–15122. Curran Associates, Inc.
- Deng, Y.; and Mahdavi, M. 2021. Local Stochastic Gradient Descent Ascent: Convergence Analysis and Communication Efficiency. In Banerjee, A.; and Fukumizu, K., eds., *Proceedings of The 24th International Conference on Artificial Intelligence and Statistics*, volume 130 of *Proceedings of Machine Learning Research*, 1387–1395. PMLR.
- Du, S.; Lee, J.; Li, H.; Wang, L.; and Zhai, X. 2019. Gradient descent finds global minima of deep neural networks. In *International Conference on Machine Learning*, 1675–1685. PMLR.
- Goodfellow, I.; Pouget-Abadie, J.; Mirza, M.; Xu, B.; Warde-Farley, D.; Ozair, S.; Courville, A.; and Bengio, Y. 2014. Generative adversarial nets. In *Advances in neural information processing systems*, 2672–2680.
- Goodfellow, I. J.; Shlens, J.; and Szegedy, C. 2014. Explaining and harnessing adversarial examples. *arXiv preprint arXiv:1412.6572*.
- Guo, Z.; Liu, M.; Yuan, Z.; Shen, L.; Liu, W.; and Yang, T. 2020. Communication-Efficient Distributed Stochastic AUC Maximization with Deep Neural Networks. In *International Conference on Machine Learning*, 3864–3874. PMLR.
- Hou, C.; Thekumparampil, K. K.; Fanti, G.; and Oh, S. 2021. Efficient Algorithms for Federated Saddle Point Optimization. *arXiv preprint arXiv:2102.06333*.
- Huang, F.; Gao, S.; Pei, J.; and Huang, H. 2020. Accelerated zeroth-order momentum methods from mini to minimax optimization. *arXiv preprint arXiv:2008.08170*.
- Ioffe, S.; and Szegedy, C. 2015. Batch normalization: Accelerating deep network training by reducing internal covariate shift. In *International conference on machine learning*, 448–456. PMLR.
- Jin, C.; Netrapalli, P.; and Jordan, M. 2020. What is local optimality in nonconvex-nonconcave minimax optimization?

- In *International Conference on Machine Learning*, 4880–4889. PMLR.
- Johnson, R.; and Zhang, T. 2013. Accelerating stochastic gradient descent using predictive variance reduction. In *Advances in neural information processing systems*, 315–323.
- Kairouz, P.; McMahan, H. B.; Avent, B.; Bellet, A.; Bennis, M.; Bhagoji, A. N.; Bonawitz, K.; Charles, Z.; Cormode, G.; Cummings, R.; et al. 2019. Advances and open problems in federated learning. *arXiv preprint arXiv:1912.04977*.
- Karimi, H.; Nutini, J.; and Schmidt, M. 2016. Linear convergence of gradient and proximal-gradient methods under the polyak-lojasiewicz condition. In *Joint European Conference on Machine Learning and Knowledge Discovery in Databases*, 795–811. Springer.
- Karimireddy, S. P.; Jaggi, M.; Kale, S.; Mohri, M.; Reddi, S. J.; Stich, S. U.; and Suresh, A. T. 2020a. Mime: Mimicking Centralized Stochastic Algorithms in Federated Learning. *arXiv preprint arXiv:2008.03606*.
- Karimireddy, S. P.; Kale, S.; Mohri, M.; Reddi, S.; Stich, S.; and Suresh, A. T. 2020b. Scaffold: Stochastic controlled averaging for federated learning. In *International Conference on Machine Learning*, 5132–5143. PMLR.
- Korpelevich, G. 1976. The extragradient method for finding saddle points and other problems. *Matecon*, 12: 747–756.
- Krizhevsky, A.; Hinton, G.; et al. 2009. Learning multiple layers of features from tiny images. Citeseer.
- LeCun, Y.; Bottou, L.; Bengio, Y.; and Haffner, P. 1998. Gradient-based learning applied to document recognition. *Proceedings of the IEEE*, 86(11): 2278–2324.
- Li, T.; Sahu, A. K.; Zaheer, M.; Sanjabi, M.; Talwalkar, A.; and Smith, V. 2018. Federated optimization in heterogeneous networks. *arXiv preprint arXiv:1812.06127*.
- Li, X.; Huang, K.; Yang, W.; Wang, S.; and Zhang, Z. 2020. On the Convergence of FedAvg on Non-IID Data. In *International Conference on Learning Representations*.
- Lin, T.; Jin, C.; and Jordan, M. 2020. On Gradient Descent Ascent for Nonconvex-Concave Minimax Problems. In III, H. D.; and Singh, A., eds., *Proceedings of the 37th International Conference on Machine Learning*, volume 119 of *Proceedings of Machine Learning Research*, 6083–6093. PMLR.
- Liu, M.; Yuan, Z.; Ying, Y.; and Yang, T. 2020a. Stochastic AUC Maximization with Deep Neural Networks. In *International Conference on Learning Representations*.
- Liu, S.; Lu, S.; Chen, X.; Feng, Y.; Xu, K.; Al-Dujaili, A.; Hong, M.; and O’Reilly, U.-M. 2020b. Min-max optimization without gradients: Convergence and applications to black-box evasion and poisoning attacks. In *International Conference on Machine Learning*, 6282–6293. PMLR.
- Luo, L.; Ye, H.; Huang, Z.; and Zhang, T. 2020. Stochastic Recursive Gradient Descent Ascent for Stochastic Nonconvex-Strongly-Concave Minimax Problems. *Advances in Neural Information Processing Systems*, 33.
- Madry, A.; Makelov, A.; Schmidt, L.; Tsipras, D.; and Vladu, A. 2018. Towards Deep Learning Models Resistant to Adversarial Attacks. In *International Conference on Learning Representations*.
- McMahan, B.; Moore, E.; Ramage, D.; Hampson, S.; and y Arcas, B. A. 2017. Communication-efficient learning of deep networks from decentralized data. In *Artificial Intelligence and Statistics*, 1273–1282. PMLR.
- Mishchenko, K.; Khaled Ragab Bayoumi, A.; and Richtárik, P. 2020. Random reshuffling: Simple analysis with vast improvements. *Advances in Neural Information Processing Systems*, 33.
- Mohri, M.; Sivek, G.; and Suresh, A. T. 2019. Agnostic Federated Learning. In *International Conference on Machine Learning*, 4615–4625.
- Mokhtari, A.; Ozdaglar, A.; and Pattathil, S. 2019. A unified analysis of extra-gradient and optimistic gradient methods for saddle point problems: Proximal point approach. *arXiv preprint arXiv:1901.08511*.
- Namkoong, H.; and Duchi, J. C. 2016. Stochastic gradient methods for distributionally robust optimization with f-divergences. In *Advances in neural information processing systems*, 2208–2216.
- Nedić, A.; and Ozdaglar, A. 2009. Subgradient methods for saddle-point problems. *Journal of optimization theory and applications*, 142(1): 205–228.
- Nemirovski, A. 2004. Prox-method with rate of convergence $O(1/t)$ for variational inequalities with Lipschitz continuous monotone operators and smooth convex-concave saddle point problems. *SIAM Journal on Optimization*, 15(1): 229–251.
- Nouiehed, M.; Sanjabi, M.; Huang, T.; Lee, J. D.; and Razaviyayn, M. 2019. Solving a class of non-convex min-max games using iterative first order methods. In *Advances in Neural Information Processing Systems*, 14934–14942.
- Palaniappan, B.; and Bach, F. 2016. Stochastic variance reduction methods for saddle-point problems. In *Advances in Neural Information Processing Systems*, 1416–1424.
- Qiu, S.; Yang, Z.; Wei, X.; Ye, J.; and Wang, Z. 2020. Single-Timescale Stochastic Nonconvex-Concave Optimization for Smooth Nonlinear TD Learning. *arXiv preprint arXiv:2008.10103*.
- Radford, A.; Metz, L.; and Chintala, S. 2015. Unsupervised representation learning with deep convolutional generative adversarial networks. *arXiv preprint arXiv:1511.06434*.
- Rafique, H.; Liu, M.; Lin, Q.; and Yang, T. 2018. Non-convex min-max optimization: Provable algorithms and applications in machine learning. *arXiv preprint arXiv:1810.02060*.
- Rasouli, M.; Sun, T.; and Rajagopal, R. 2020. Fedgan: Federated generative adversarial networks for distributed data. *arXiv preprint arXiv:2006.07228*.
- Reisizadeh, A.; Farnia, F.; Pedarsani, R.; and Jadbabaie, A. 2020. Robust Federated Learning: The Case of Affine Distribution Shifts. In Larochelle, H.; Ranzato, M.; Hadsell, R.; Balcan, M. F.; and Lin, H., eds., *Advances in Neural Information Processing Systems*, volume 33, 21554–21565. Curran Associates, Inc.
- Salimans, T.; Goodfellow, I.; Zaremba, W.; Cheung, V.; Radford, A.; and Chen, X. 2016. Improved techniques for training gans. *Advances in neural information processing systems*, 29: 2234–2242.

- Sanjabi, M.; Razaviyayn, M.; and Lee, J. D. 2018. Solving non-convex non-concave min-max games under polyak-łojasiewicz condition. *arXiv preprint arXiv:1812.02878*.
- TensorFlow team. 2021. Convolutional neural network tutorial. <https://www.tensorflow.org/tutorials/images/cnn>. Accessed: 2021-09-04.
- Thekumparampil, K. K.; Jain, P.; Netrapalli, P.; and Oh, S. 2019. Efficient algorithms for smooth minimax optimization. In *Advances in Neural Information Processing Systems*, 12680–12691.
- Wang, Z.; Balasubramanian, K.; Ma, S.; and Razaviyayn, M. 2020. Zeroth-order algorithms for nonconvex minimax problems with improved complexities. *arXiv preprint arXiv:2001.07819*.
- Xiao, H.; Rasul, K.; and Vollgraf, R. 2017. Fashion-mnist: a novel image dataset for benchmarking machine learning algorithms. *arXiv preprint arXiv:1708.07747*.
- Xu, T.; Wang, Z.; Liang, Y.; and Poor, H. V. 2020. Enhanced first and zeroth order variance reduced algorithms for min-max optimization. *arXiv preprint arXiv:2006.09361*.
- Yang, J.; Kiyavash, N.; and He, N. 2020. Global convergence and variance-reduced optimization for a class of nonconvex-nonconcave minimax problems. *arXiv preprint arXiv:2002.09621*.
- Ying, Y.; Wen, L.; and Lyu, S. 2016. Stochastic online AUC maximization. In *Advances in neural information processing systems*, 451–459.
- Yuan, Z.; Guo, Z.; Xu, Y.; Ying, Y.; and Yang, T. 2021. Federated Deep AUC Maximization for Heterogeneous Data with a Constant Communication Complexity. In Meila, M.; and Zhang, T., eds., *Proceedings of the 38th International Conference on Machine Learning*, volume 139 of *Proceedings of Machine Learning Research*, 12219–12229. PMLR.

Appendix of Efficient Cross-Device Federated Learning Algorithms for Minimax Problems

A The CD-MA Algorithm

The CD-MA algorithm described in Section 3 is detailed in Algorithm 4.

Algorithm 4: Cross-device Minimax Averaging (CD-MA)

Input: initial point $(\mathbf{x}_0, \mathbf{y}_0)$, the number of rounds T , step sizes $\{\eta_t\}_{t=0}^{T-1}$, $\{\gamma_t\}_{t=0}^{T-1}$, and the batch size of clients S .

Server executes:

- 1: **for** $t = 0, 1, \dots, T - 1$ **do**
- 2: Send $(\mathbf{x}_t, \mathbf{y}_t)$ to a subset of clients;
- 3: Once local iterates $(\mathbf{x}_{t,i}^{(K)}, \mathbf{y}_{t,i}^{(K)})$ from S clients are received, proceed;
- 4: $\mathbf{x}_{t+1} \leftarrow \frac{1}{|S_t|} \sum_{i \in S_t} \mathbf{x}_{t,i}^{(K)}$, $\mathbf{y}_{t+1} \leftarrow \frac{1}{|S_t|} \sum_{i \in S_t} \mathbf{y}_{t,i}^{(K)}$, where S_t is the S clients in the above step;
- 5: **end for**

Client $i \in S_t$ executes:

- 6: Initialize local model $\mathbf{x}_{t,i}^{(0)} \leftarrow \mathbf{x}_t$, $\mathbf{y}_{t,i}^{(0)} \leftarrow \mathbf{y}_t$;
- 7: **for** $k = 0, 1, \dots, K - 1$ **do**
- 8: Sample a minibatch $\mathcal{B}_{t,i}^{(k)}$ from local data;
- 9: $\mathbf{x}_{t,i}^{(k+1)} \leftarrow \mathbf{x}_{t,i}^{(k)} - \eta_t \nabla_{\mathbf{x}} F_i(\mathbf{x}_{t,i}^{(k)}, \mathbf{y}_{t,i}^{(k)}; \mathcal{B}_{t,i}^{(k)})$;
- 10: $\mathbf{y}_{t,i}^{(k+1)} \leftarrow \mathbf{y}_{t,i}^{(k)} + \gamma_t \nabla_{\mathbf{y}} F_i(\mathbf{x}_{t,i}^{(k)}, \mathbf{y}_{t,i}^{(k)}; \mathcal{B}_{t,i}^{(k)})$;
- 11: **end for**
- 12: Send $(\mathbf{x}_{t,i}^{(K)}, \mathbf{y}_{t,i}^{(K)})$ to the server;

B Additional Details of Experiments

B.1 Specification of Hyper-parameters

The hyper-parameters of CD-MAGE, CD-MA, Parallel SGDA, and Local SGDA+ are the constant stepsizes η and γ . The Extra Step Local SGD algorithm has only one hyper-parameter, the local step size η_ℓ . CODA+ involves three hyper-parameters: the local step size η_ℓ , the weight coefficient θ of the proximal-point subproblem, and the interval K_0 (in terms of the number of local updates) between two proximal point updates. CODASCA and Catalyst-Scaffold-S have all the three hyper-parameters of CODA+ as well as an additional global step size η_g . Following Hou et al. (2021), we set $\eta_g = \eta_\ell$ for Catalyst-Scaffold-S. The hyper-parameters of CD-MAGE+ are η_t , γ_t and α_t . In our implementation, we set $\eta_t = \frac{c_\eta}{(t+1)^\rho}$, $\gamma_t = \frac{c_\gamma}{(t+1)^\rho}$, and $\alpha_t = \min\{1, \frac{c_\alpha}{(t+1)^{2\rho}}\}$, where c_η , c_γ , c_α , and ρ are tunable parameters. We note that Catalyst-Scaffold-S communicates with probability p at each local step, while other algorithms communicate after every K local steps. We set $p = 1/K$ so that the average number of local steps of Catalyst-Scaffold-S in each round is equal to K , where K has been defined in Section 5.1-5.3.

Hyper-parameters for AUC Maximization For the AUC maximization task, the hyper-parameters are chosen as follows.

- For CD-MAGE, CD-MA, Parallel SGDA, and Local SGDA+, η is chosen from $\{1, 3.162\text{e-}1, 1\text{e-}1\}^3$ and γ is chosen from $\{1, 3.162\text{e-}1, 1\text{e-}1, 3.162\text{e-}2, 1\text{e-}2, 3.162\text{e-}3, 1\text{e-}3\}$.
- The step size η_ℓ of Extra Step Local SGD is tuned from $\{1, 3.162\text{e-}1, 1\text{e-}1, 3.162\text{e-}2, 1\text{e-}2, 3.162\text{e-}3, 1\text{e-}3, 3.162\text{e-}4, 1\text{e-}4\}$.
- For CD-MAGE+, $c_\eta \in \{1, 3.162\text{e-}1, 1\text{e-}1\}$ and $c_\gamma \in \{1, 3.162\text{e-}1, 1\text{e-}1, 3.162\text{e-}2, 1\text{e-}2, 3.162\text{e-}3, 1\text{e-}3\}$, $c_\alpha \in \{5, 10\}$, and $\rho \in \{1/5, 1/3\}$. We note that while our theory suggests that $\rho = 1/3$, in practice CD-MAGE+ with $\rho = 1/5$ performs better in some cases.
- The hyper-parameters η_ℓ , θ , and K_0 of CODA+, and Catalyst-Scaffold-S are chosen from $\{1, 3.162\text{e-}1, 1\text{e-}1, 3.162\text{e-}2, 1\text{e-}2\}$, $\{0, 1\text{e-}1, 1\text{e}1\}$, and $\{2\text{e}3, 4\text{e}3\}$, respectively.
- For CODASCA, η_ℓ , θ , and K_0 are chosen in the same way as those of CODA+, and η_g is tuned from $\{1.1, 1.0, 0.99\}$ following Yuan et al. (2021).

Table 1 shows the best hyper-parameters for each algorithm on the AUC maximization experiment.

³Note that $3.162\text{e-}1 = 10^{-0.5}$.

Table 1: Best hyper-parameters on the AUC maximization experiment.

Algorithm	Best hyper-parameters on CIFAR-10	Best hyper-parameters on MNIST
CD-MAGE	$\eta = 1e-1, \gamma = 3.162e-1$	$\eta = 3.162e-1, \gamma = 3.162e-2$
CD-MA	$\eta = 3.162e-1, \gamma = 3.162e-2$	$\eta = 1, \gamma = 3.162e-1$
Parallel SGDA	$\eta = 1, \gamma = 3.162e-2$	$\eta = 1, \gamma = 1$
Local SGDA+	$\eta = 1e-1, \gamma = 1e-2$	$\eta = 1, \gamma = 3.162e-1$
Extra Step Local SGD	$\eta_\ell = 1e-1$	$\eta_\ell = 3.162e-1$
CD-MAGE+	$c_\eta = 3.162e-1, c_\gamma = 1, c_\alpha = 10, \rho = 1/5$	$c_\eta = 3.162e-1, c_\gamma = 1e-2, c_\alpha = 5, \rho = 1/5$
CODA+	$\eta_\ell = 1e-1, \theta = 0, K_0 = 2e3$	$\eta_\ell = 3.162e-1, \theta = 0, K_0 = 2e3$
Catalyst-Scaffold-S	$\eta_\ell = 1e-1, \theta = 0, K_0 = 2e3$	$\eta_\ell = 1e-1, \theta = 0, K_0 = 2e3$
CODASCA	$\eta_\ell = 3.162e-1, \eta_g = 1, \theta = 0, K_0 = 2e3$	$\eta_\ell = 1, \eta_g = 1.1, \theta = 0, K_0 = 2e3$

Hyper-parameters for Robust Adversarial Network Training For the robust adversarial network training task, the hyper-parameters are chosen as follows.

- For CD-MAGE, CD-MA, Parallel SGDA, and Local SGDA+, η is chosen from $\{3.162e-2, 1e-2, 3.162e-3, 1e-2\}$ and γ is chosen from $\{1, 3.162e-1, 1e-1, 3.162e-2, 1e-3\}$.
- The step size η_ℓ of Extra Step Local SGD is tuned from $\{1, 3.162e-1, 1e-1, 3.162e-2, 1e-2, 3.162e-3, 1e-3, 3.162e-4, 1e-4\}$.
- For CD-MAGE+, $c_\eta \in \{3.162e-2, 1e-2, 3.162e-3, 1e-2\}$ and $c_\gamma \in \{1, 3.162e-1, 1e-1, 3.162e-2, 1e-2\}$, $c_\alpha \in \{5, 10\}$, and $\rho \in \{1/5, 1/3\}$.
- The hyper-parameters η_ℓ , θ , and K_0 of CODA+, and Catalyst-Scaffold-S are chosen from $\{1e-1, 3.162e-2, 1e-2, 3.162e-3, 1e-3\}$, $\{0, 1e-1, 1e1\}$, and $\{2e3, 4e3\}$, respectively.
- For CODASCA, η_ℓ , θ , and K_0 are chosen in the same way as those of CODA+, and η_g is tuned from $\{1.1, 1.0, 0.99\}$ following Yuan et al. (2021).

Table 2 shows the best hyper-parameters for each algorithm on the robust adversarial network training experiment.

Table 2: Best hyper-parameters on the robust adversarial network training experiment.

Algorithm	Best hyper-parameters on MNIST	Best hyper-parameters on Fashion MNIST
CD-MAGE	$\eta = 1e-3, \gamma = 3.162e-1$	$\eta = 1e-3, \gamma = 1e-1$
CD-MA	$\eta = 1e-3, \gamma = 3.162e-2$	$\eta = 1e-3, \gamma = 3.162e-2$
Parallel SGDA	$\eta = 1e-2, \gamma = 1$	$\eta = 1e-2, \gamma = 3.162e-1$
Local SGDA+	$\eta = 1e-3, \gamma = 3.162e-2$	$\eta = 1e-3, \gamma = 3.162e-2$
Extra Step Local SGD	$\eta_\ell = 3.162e-4$	$\eta_\ell = 1e-3$
CD-MAGE+	$c_\eta = 1e-2, c_\gamma = 1, c_\alpha = 5, \rho = 1/3$	$c_\eta = 1e-2, c_\gamma = 1, c_\alpha = 5, \rho = 1/3$
CODA+	$\eta_\ell = 1e-2, \theta = 1e-1, K_0 = 2e3$	$\eta_\ell = 1e-3, \theta = 0, K_0 = 2e3$
Catalyst-Scaffold-S	$\eta_\ell = 1e-3, \theta = 1e1, K_0 = 2e3$	$\eta_\ell = 1e-3, \theta = 1e-1, K_0 = 4e3$
CODASCA	$\eta_\ell = 3.162e-3, \eta_g = 1, \theta = 1e1, K_0 = 2e3$	$\eta_\ell = 3.162e-3, \eta_g = 1.1, \theta = 1e-1, K_0 = 4e3$

Hyper-parameters for GAN Training For the GAN training task, the hyper-parameters are chosen as follows.

- For CD-MAGE, CD-MA, Parallel SGDA, and Local SGDA+, both η and γ are chosen from $\{1e-2, 1e-3, 1e-4\}$.
- The step size η_ℓ of Extra Step Local SGD is tuned from $\{1e-2, 1e-3, 1e-4, 1e-5\}$.
- For CD-MAGE+, both c_η and c_γ are selected from $\{1e-2, 1e-3, 1e-4\}$, $c_\alpha \in \{5, 10\}$, and $\rho \in \{1/5, 1/3\}$.
- The hyper-parameters η_ℓ , θ , and K_0 of CODA+, and Catalyst-Scaffold-S are chosen from $\{1e-2, 1e-3, 1e-4\}$, $\{0, 1e-1, 1e1\}$, and $\{2e3, 4e3\}$, respectively.
- For CODASCA, η_ℓ , θ , and K_0 are chosen in the same way as those of CODA+, and η_g is tuned from $\{1.1, 1.0, 0.99\}$ following Yuan et al. (2021).

Table 3 summarizes the best hyper-parameters for each algorithm on MNIST and Fashion MNIST.

Table 3: Best hyper-parameters for the GAN training experiment.

Algorithm	Best hyper-parameters on MNIST	Best hyper-parameters on Fashion MNIST
CD-MAGE	$\eta = 1e-2, \gamma = 1e-2$	$\eta = 1e-2, \gamma = 1e-3$
CD-MA	$\eta = 1e-3, \gamma = 1e-2$	$\eta = 1e-3, \gamma = 1e-3$
Parallel SGDA	$\eta = 1e-2, \gamma = 1e-2$	$\eta = 1e-2, \gamma = 1e-2$
Local SGDA+	$\eta = 1e-2, \gamma = 1e-3$	$\eta = 1e-3, \gamma = 1e-3$
Extra Step Local SGD	$\eta_\ell = 1e-3$	$\eta_\ell = 1e-3$
CD-MAGE+	$c_\eta = 1e-2, c_\gamma = 1e-2, c_\alpha = 10, \rho = 1/5$	$c_\eta = 1e-2, c_\gamma = 1e-3, c_\alpha = 10, \rho = 1/5$
CODA+	$\eta_\ell = 1e-2, \theta = 0, K_0 = 2e3$	$\eta_\ell = 1e-2, \theta = 1e-1, K_0 = 2e3$
Catalyst-Scaffold-S	$\eta_\ell = 1e-2, \theta = 0, K_0 = 2e3$	$\eta_\ell = 1e-2, \theta = 1e-1, K_0 = 4e3$
CODASCA	$\eta_\ell = 1e-2, \eta_g = 1.0, \theta = 1e-1, K_0 = 4e3$	$\eta_\ell = 1e-2, \eta_g = 1, \theta = 1e-1, K_0 = 4e3$

B.2 The ℓ_2 -relaxed AUC Maximization Problem and its Equivalent Minimax Formulation

Suppose that we are given a dataset $\{\mathbf{w}_i, \ell_i\}_{i=1}^m$ where \mathbf{w}_i denotes a feature vector and $\ell_i \in \{-1, +1\}$ denotes the corresponding label. For a scoring function h_θ of a classification model parameterized by $\theta \in \mathbb{R}^p$, the AUC is defined as

$$\max_{\theta} \frac{1}{m^+ m^-} \sum_{\ell_i=+1, \ell_j=-1} \mathbb{I}_{\{h_\theta(\mathbf{w}_i) \geq h_\theta(\mathbf{w}_j)\}}, \quad (6)$$

where m^+ (m^-) denotes the number of positive (negative) samples and \mathbb{I} denotes the indicator function. Since directly maximizing the AUC is NP hard in general, the indicator function in (6) is usually replaced by a surrogate such as the squared loss in practice:

$$\max_{\theta} \frac{1}{m^+ m^-} \sum_{\ell_i=+1, \ell_j=-1} (1 - h_\theta(\mathbf{w}_i) + h_\theta(\mathbf{w}_j))^2. \quad (7)$$

It has been shown that (7) has the following equivalent minimax formulation (Ying, Wen, and Lyu 2016; Liu et al. 2020a)

$$\min_{(\theta, a, b) \in \mathbb{R}^{p+2}} \max_{\lambda \in \mathbb{R}} f(\theta, a, b, \lambda) := \frac{1}{m} \sum_{i=1}^m \left\{ (1 - \tau)(h_\theta(\mathbf{w}_i) - a)^2 \mathbb{I}_{\{\ell_i=1\}} - \tau(1 - \tau)\lambda^2 + \tau(h_\theta(\mathbf{w}_i) - b)^2 \mathbb{I}_{\{\ell_i=-1\}} \right. \\ \left. + 2(1 + \lambda)\tau h_\theta(\mathbf{w}_i) \mathbb{I}_{\{\ell_i=-1\}} - 2(1 + \lambda)(1 - \tau)h_\theta(\mathbf{w}_i) \mathbb{I}_{\{\ell_i=1\}} \right\},$$

where $\tau := m^+ / (m^+ + m^-)$ is the ratio of positive data. Note that $f(\theta, a, b, \cdot)$ is strongly concave for any $(\theta, a, b) \in \mathbb{R}^{p+2}$ and thus satisfies Assumption 3.

B.3 Additional Results of the AUC maximization and robust adversarial Network training tasks

The test results of the AUC maximization task in Section 5.1 are shown in Figure 4. These results are similar to the training results in Figure 1.

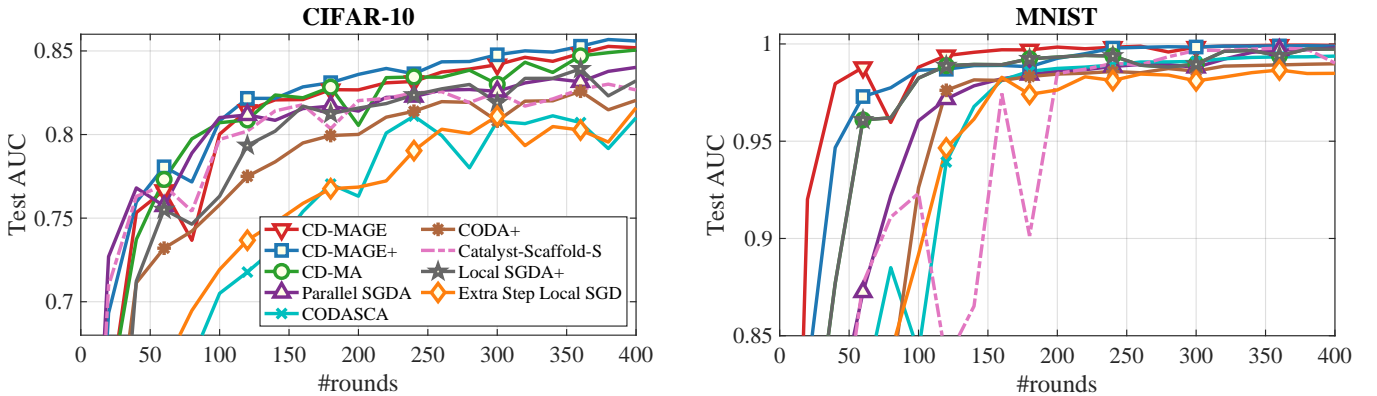


Figure 4: Test results on the AUC maximization task (left: CIFAR-10, right: MNIST).

Figure 5 presents the robust test loss of the robust adversarial network training experiment in Section 5.1. We observe that the test results are basically the same as the training results in Figure 2.

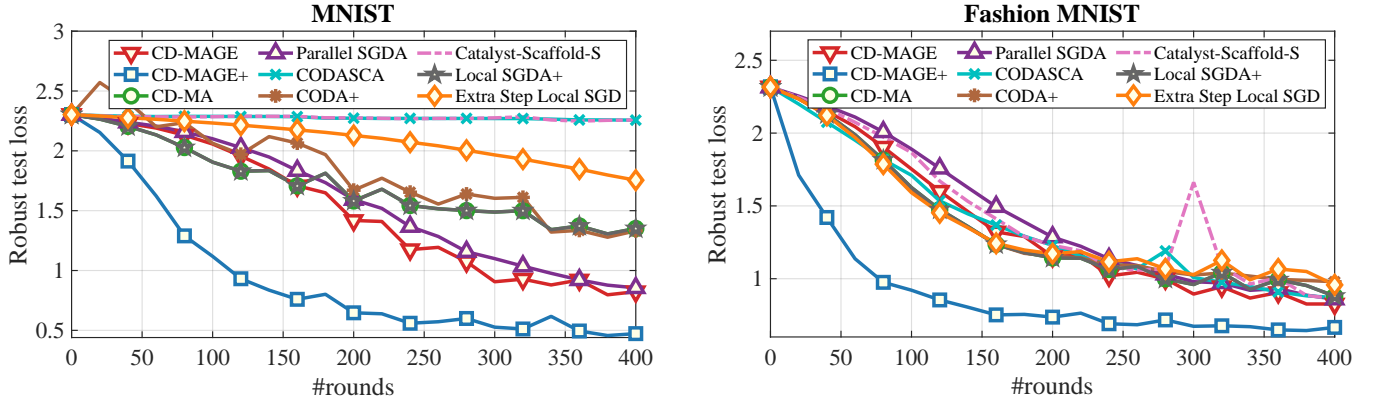


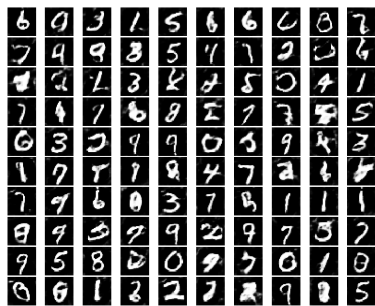
Figure 5: Test results on the robust neural network training task (left: MNIST, right: Fashion MNIST).

B.4 Additional Results of the GAN training task in Section 5.3

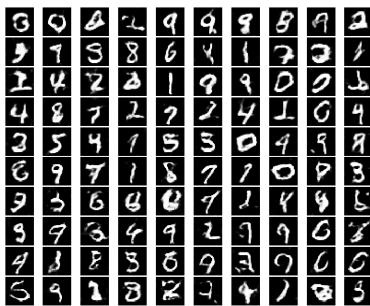
Table 4 shows the final Inception score of each algorithm after 400 (resp., 800) rounds of training on the MNIST (resp., Fashion MNIST) dataset. We note that in the evaluation of the Inception score, we used the Resnet18 network pretrained on MNIST/Fashion MNIST following (Chavdarova et al. 2019), instead of using the original Inception network pretrained on ImageNet. The reason is that both MNIST and Fashion MNIST consist of grayscale images, whereas the ImageNet dataset consists of colored images. We also visualize sample images generated by the algorithms in Figure 6 and Figure 7. We can see that CD-MAGE and CD-MAGE+ generate relatively high-quality images.

Algorithm	IS on MNIST	IS on Fashion MNIST
CD-MAGE	8.58 ± 0.030	8.76 ± 0.012
CD-MAGE+	8.47 ± 0.026	7.93 ± 0.022
CD-MA	7.79 ± 0.061	7.34 ± 0.014
Parallel SGDA	6.08 ± 0.051	6.34 ± 0.038
CODASCA	8.10 ± 0.059	6.31 ± 0.033
CODA+	8.28 ± 0.076	7.34 ± 0.041
Catalyst-Scaffold-S	8.15 ± 0.026	7.67 ± 0.040
Local SGDA+	8.08 ± 0.009	7.39 ± 0.022
Extra Step Local SGD	7.39 ± 0.025	7.46 ± 0.034

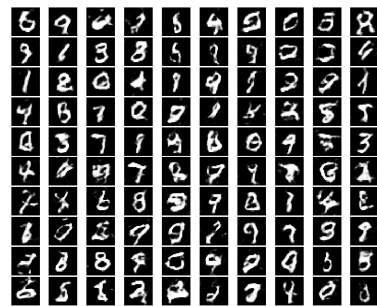
Table 4: The final Inception Score (IS) of the compared algorithms on MNIST and Fashion MNIST.



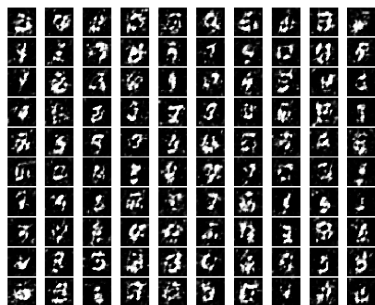
(a) CD-MAGE



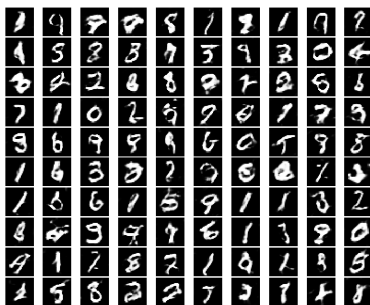
(b) CD-MAGE+



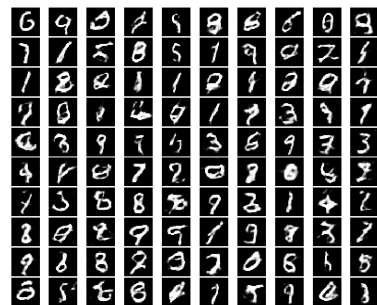
(c) CD-MA



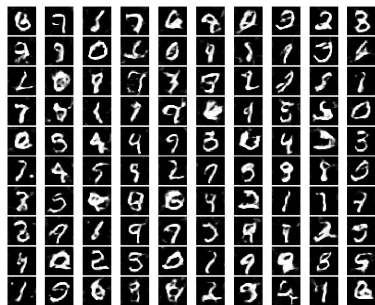
(d) Parallel SGD



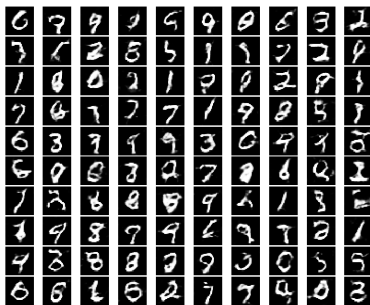
(e) CODASCA



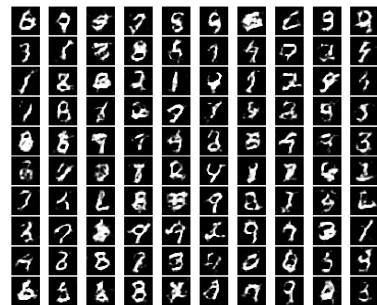
(f) CODA+



(g) Catalyst-Scaffold-S



(h) Local SGD+



(i) Extra Step Local SGD

Figure 6: Generative samples of the compared algorithms after 400 rounds of training on MNIST. The samples are generated using the same set of random noise vectors.



(a) CD-MAGE



(b) CD-MAGE+



(c) CD-MA



(d) Parallel SGDA



(e) CODASCA



(f) CODA+



(g) Catalyst-Scaffold-S



(h) Local SGDA+



(i) Extra Step Local SGD

Figure 7: Generative samples of the compared algorithms after 800 rounds of training on Fashion MNIST. The samples are generated using the same set of random noise vectors.

C Deferred proofs

In our proofs, we denote the pair of primal and dual variables (\mathbf{x}, \mathbf{y}) as \mathbf{z} for ease of notation. For example, $\mathbf{z}_{t,i}^{(k)}$ represents client i 's local iterate $(\mathbf{x}_{t,i}^{(k)}, \mathbf{y}_{t,i}^{(k)})$ at the k -th local iteration in round t .

C.1 Proof of Lemma 1

Proof. Denote $\mathbf{z}_1 := (\mathbf{x}_1, \mathbf{y}_1)$ and $\mathbf{z}_2 := (\mathbf{x}_2, \mathbf{y}_2)$. By Assumption 2, we have

$$\begin{aligned} \|\nabla F_i(\mathbf{z}_1; \zeta) - \nabla F_i(\mathbf{z}_2; \zeta)\|^2 &= \|\nabla_{\mathbf{x}} F_i(\mathbf{x}_1, \mathbf{y}_1; \zeta) - \nabla_{\mathbf{x}} F_i(\mathbf{x}_2, \mathbf{y}_2; \zeta)\|^2 + \|\nabla_{\mathbf{y}} F_i(\mathbf{x}_1, \mathbf{y}_1; \zeta) - \nabla_{\mathbf{y}} F_i(\mathbf{x}_2, \mathbf{y}_2; \zeta)\|^2 \\ &\leq 2\|\nabla_{\mathbf{x}} F_i(\mathbf{x}_1, \mathbf{y}_1; \zeta) - \nabla_{\mathbf{x}} F_i(\mathbf{x}_1, \mathbf{y}_2; \zeta)\|^2 + 2\|\nabla_{\mathbf{x}} F_i(\mathbf{x}_1, \mathbf{y}_2; \zeta) - \nabla_{\mathbf{x}} F_i(\mathbf{x}_2, \mathbf{y}_2; \zeta)\|^2 \\ &\quad + 2\|\nabla_{\mathbf{y}} F_i(\mathbf{x}_1, \mathbf{y}_1; \zeta) - \nabla_{\mathbf{y}} F_i(\mathbf{x}_1, \mathbf{y}_2; \zeta)\|^2 + 2\|\nabla_{\mathbf{y}} F_i(\mathbf{x}_1, \mathbf{y}_2; \zeta) - \nabla_{\mathbf{y}} F_i(\mathbf{x}_2, \mathbf{y}_2; \zeta)\|^2 \\ &\leq 2(L_1^2 + L_{21}^2)\|\mathbf{x}_1 - \mathbf{x}_2\|^2 + 2(L_2^2 + L_{12}^2)\|\mathbf{y}_1 - \mathbf{y}_2\|^2 \\ &\leq \max\{2(L_1^2 + L_{21}^2), 2(L_2^2 + L_{12}^2)\}\|\mathbf{z}_1 - \mathbf{z}_2\|^2 = L_f^2\|\mathbf{z}_1 - \mathbf{z}_2\|^2. \end{aligned}$$

Thus, $F_i(\mathbf{x}, \mathbf{y}, \zeta)$ is L_f -smooth w.r.t. (\mathbf{x}, \mathbf{y}) . Recall that $f_i = \frac{1}{n_i} \sum_{j=1}^{n_i} F_i(\mathbf{x}, \mathbf{y}; \zeta_{i,j})$ and $f(\mathbf{x}, \mathbf{y}) = \mathbb{E}_{i \sim \mathcal{D}}[f_i(\mathbf{x}, \mathbf{y})]$. By Jensen's inequality and the convexity of $\|\cdot\|^2$, both f_i and f are L_f -smooth. \square

C.2 Proofs of the results in Section 4.1

Proof of Lemma 3

Proof. The global primal variable \mathbf{x}_{t+1} can be rewritten as

$$\begin{aligned} \mathbf{x}_{t+1} &= \mathbf{x}_t - \frac{\eta_t}{S} \sum_{i \in \mathcal{S}_t} \sum_{k=0}^{K-1} (\nabla_{\mathbf{x}} F_i(\mathbf{z}_{t,i}^{(k)}; \mathcal{B}_{t,i}^{(k)}) - \nabla_{\mathbf{x}} f_i(\mathbf{z}_t; \mathcal{B}_{t,i}^{(k)}) + \mathbf{u}_t) \\ &= \mathbf{x}_t - \eta_t K \left(\mathbf{u}_t + \frac{1}{SK} \sum_{i \in \mathcal{S}_t} \sum_{k=0}^{K-1} (\nabla_{\mathbf{x}} F_i(\mathbf{z}_{t,i}^{(k)}; \mathcal{B}_{t,i}^{(k)}) - \nabla_{\mathbf{x}} F_i(\mathbf{z}_t; \mathcal{B}_{t,i}^{(k)})) \right) \\ &= \mathbf{x}_t - \eta_t K (\mathbf{u}_t + \mathbf{e}_{\mathbf{x},t}) \end{aligned}$$

Similarly, the global dual variable \mathbf{y}_{t+1} can be rewritten as $\mathbf{y}_{t+1} = \mathbf{y}_t + \gamma_t K (\mathbf{v}_t + \mathbf{e}_{\mathbf{y},t})$. \square

Proof of Lemma 4

Proof. By the smoothness of L_Φ , we have

$$\begin{aligned} \mathbb{E}[\Phi(\mathbf{x}_{t+1}) - \Phi(\mathbf{x}_t)] &\leq \mathbb{E}\left[\langle \nabla \Phi(\mathbf{x}_t), \mathbf{x}_{t+1} - \mathbf{x}_t \rangle + \frac{L_\Phi}{2} \|\mathbf{x}_{t+1} - \mathbf{x}_t\|^2\right] \\ &\stackrel{(a)}{=} -\eta_t K \mathbb{E}[\langle \nabla \Phi(\mathbf{x}_t), \mathbf{u}_t + \mathbf{e}_{\mathbf{x},t} \rangle] + \frac{L_\Phi \eta_t^2 K^2}{2} \mathbb{E}[\|\mathbf{u}_t + \mathbf{e}_{\mathbf{x},t}\|^2] \\ &\stackrel{(b)}{=} -\eta_t K \mathbb{E}[\langle \nabla \Phi(\mathbf{x}_t), \nabla_{\mathbf{x}} f(\mathbf{z}_t) + \mathbf{e}_{\mathbf{x},t} \rangle] + \frac{L_\Phi \eta_t^2 K^2}{2} \mathbb{E}[\|\mathbf{u}_t + \mathbf{e}_{\mathbf{x},t}\|^2] \\ &= \frac{\eta_t K}{2} \mathbb{E}[\|\nabla_{\mathbf{x}} f(\mathbf{z}_t) + \mathbf{e}_{\mathbf{x},t} - \nabla \Phi(\mathbf{x}_t)\|^2] - \frac{\eta_t K}{2} \mathbb{E}[\|\nabla \Phi(\mathbf{x}_t)\|^2] - \frac{\eta_t K}{2} \mathbb{E}[\|\nabla_{\mathbf{x}} f(\mathbf{z}_t) + \mathbf{e}_{\mathbf{x},t}\|^2] \\ &\quad + L_\Phi \eta_t^2 K^2 \mathbb{E}[\|\mathbf{e}_{\mathbf{x},t} + \nabla_{\mathbf{x}} f(\mathbf{z}_t)\|^2 + \|\mathbf{u}_t - \nabla_{\mathbf{x}} f(\mathbf{z}_t)\|^2] \\ &\stackrel{(c)}{\leq} \eta_t K \mathbb{E}[\|\nabla_{\mathbf{x}} f(\mathbf{z}_t) - \nabla \Phi(\mathbf{x}_t)\|^2 + \|\mathbf{e}_{\mathbf{x},t}\|^2] - \frac{\eta_t K}{2} \mathbb{E}[\|\nabla \Phi(\mathbf{x}_t)\|^2] \\ &\quad - \left(\frac{\eta_t K}{2} - L_\Phi \eta_t^2 K^2\right) \mathbb{E}[\|\mathbf{e}_{\mathbf{x},t} + \nabla_{\mathbf{x}} f(\mathbf{z}_t)\|^2] + \frac{L_\Phi \eta_t^2 K^2}{S} \sigma_1^2 \\ &\stackrel{(d)}{\leq} \eta_t K \mathbb{E}[L_{12}^2 \|\mathbf{y}_t - \mathbf{y}^*(\mathbf{x}_t)\|^2 + \|\mathbf{e}_{\mathbf{x},t}\|^2] - \frac{\eta_t K}{2} \mathbb{E}[\|\nabla \Phi(\mathbf{x}_t)\|^2] \\ &\quad + \frac{L_\Phi \eta_t^2 K^2}{S} \sigma_1^2 - \frac{\eta_t K}{8} \mathbb{E}[\|\nabla_{\mathbf{x}} f(\mathbf{z}_t)\|^2] + \frac{\eta_t K}{4} \mathbb{E}[\|\mathbf{e}_{\mathbf{x},t}\|^2], \end{aligned} \tag{8}$$

where (a) follows from Lemma 3, (b) holds because of the unbiasedness of \mathbf{u}_t , (c) follows from Assumption 1, and (d) follows from Assumption 2, the condition $\eta_t \leq 1/(4L_\Phi K)$ and the fact that $\|\mathbf{a} + \mathbf{b}\|^2 \geq \frac{1}{2}\|\mathbf{a}\|^2 - \|\mathbf{b}\|^2$. By (Karimi, Nutini, and Schmidt 2016, Theorem 2), the PL condition (Assumption 3) implies that $\forall (\mathbf{x}, \mathbf{y}) \in \mathbb{R}^{p \times q}$,

$$\Phi(\mathbf{x}) - f(\mathbf{x}, \mathbf{y}) \geq 2\mu \|\mathbf{y} - \mathbf{y}^*(\mathbf{x})\|^2. \tag{9}$$

Combining the above two inequalities leads to the desired result. \square

Proof of Lemma 5 To prove Lemma 5, we provide upper bounds of the error terms $\mathbb{E}[\|\mathbf{e}_{\mathbf{x},t}\|^2]$ and $\mathbb{E}[\Phi(\mathbf{x}_{t+1}) - f(\mathbf{z}_{t+1})]$ in the next two lemmas, respectively.

Lemma 6. Suppose that $\eta_t, \gamma_t \leq \frac{1}{2KL_f}$ in CD-MAGE. Then, both $\mathbb{E}[\|\mathbf{e}_{\mathbf{x},t}\|^2]$ and $\mathbb{E}[\|\mathbf{e}_{\mathbf{y},t}\|^2]$ are bounded from above by $18L_f^2 \left(\eta_t^2 K^2 \mathbb{E}[\|\nabla_{\mathbf{x}} f(\mathbf{z}_t)\|^2] + \gamma_t^2 K^2 \mathbb{E}[\|\nabla_{\mathbf{y}} f(\mathbf{z}_t)\|^2] + \frac{\eta_t^2 K^2}{S} \sigma_1^2 + \frac{\gamma_t^2 K^2}{S} \sigma_2^2 \right)$.

Proof. First, we observe that

$$\begin{aligned} \mathbb{E}[\|\mathbf{e}_{\mathbf{x},t}\|^2] &= \mathbb{E} \left[\left\| \frac{1}{SK} \sum_{i \in \mathcal{S}_t} \sum_{k=0}^{K-1} \left(\nabla_{\mathbf{x}} F_i(\mathbf{z}_{t,i}^{(k)}; \mathcal{B}_{t,i}^{(k)}) - \nabla_{\mathbf{x}} F_i(\mathbf{z}_t; \mathcal{B}_{t,i}^{(k)}) \right) \right\|^2 \right] \\ &\leq \frac{1}{SK} \sum_{i,k} \mathbb{E} \left[\left\| \nabla_{\mathbf{x}} F_i(\mathbf{z}_{t,i}^{(k)}; \mathcal{B}_{t,i}^{(k)}) - \nabla_{\mathbf{x}} F_i(\mathbf{z}_t; \mathcal{B}_{t,i}^{(k)}) \right\|^2 \right] \leq \frac{L_f^2}{SK} \sum_{i,k} \mathbb{E}[\|\mathbf{z}_{t,i}^{(k)} - \mathbf{z}_t\|^2], \end{aligned}$$

where the first inequality follows from Cauchy-Schwarz and the last inequality follows from Lemma 1. Similarly, we have $\mathbb{E}[\|\mathbf{e}_{\mathbf{y},t}\|^2] \leq \frac{L_f^2}{SK} \sum_{i,k} \mathbb{E}[\|\mathbf{z}_{t,i}^{(k)} - \mathbf{z}_t\|^2]$.

If $K = 1$, then $\mathbb{E}[\|\mathbf{z}_{t,i}^{(1)} - \mathbf{z}_t\|^2] = \eta_t^2 \mathbb{E}[\|\mathbf{u}_t\|^2] + \gamma_t^2 \mathbb{E}[\|\mathbf{v}_t\|^2]$. Suppose that $K \geq 2$, then for any $k \in \{0, \dots, K-1\}$,

$$\begin{aligned} \mathbb{E}[\|\mathbf{z}_{t,i}^{(k+1)} - \mathbf{z}_t\|^2] &= \mathbb{E}[\|\mathbf{x}_{t,i}^{(k)} - \mathbf{x}_t - \eta_t (\nabla_{\mathbf{x}} F_i(\mathbf{z}_{t,i}^{(k)}; \mathcal{B}_{t,i}^{(k)}) - \nabla_{\mathbf{x}} F_i(\mathbf{z}_t; \mathcal{B}_{t,i}^{(k)}) + \mathbf{u}_t)\|^2] \\ &\quad + \mathbb{E}[\|\mathbf{y}_{t,i}^{(k)} - \mathbf{y}_t + \gamma_t (\nabla_{\mathbf{y}} F_i(\mathbf{z}_{t,i}^{(k)}; \mathcal{B}_{t,i}^{(k)}) - \nabla_{\mathbf{y}} F_i(\mathbf{z}_t; \mathcal{B}_{t,i}^{(k)}) + \mathbf{v}_t)\|^2] \\ &\leq (1 + \frac{1}{K-1}) \mathbb{E}[\|\mathbf{z}_{t,i}^{(k)} - \mathbf{z}_t\|^2] + K\eta_t^2 \mathbb{E}[\|\nabla_{\mathbf{x}} F_i(\mathbf{z}_{t,i}^{(k)}; \mathcal{B}_{t,i}^{(k)}) - \nabla_{\mathbf{x}} F_i(\mathbf{z}_t; \mathcal{B}_{t,i}^{(k)}) + \mathbf{u}_t\|^2] \\ &\quad + K\gamma_t^2 \mathbb{E}[\|\nabla_{\mathbf{y}} F_i(\mathbf{z}_{t,i}^{(k)}; \mathcal{B}_{t,i}^{(k)}) - \nabla_{\mathbf{y}} F_i(\mathbf{z}_t; \mathcal{B}_{t,i}^{(k)}) + \mathbf{v}_t\|^2] \\ &\leq (1 + \frac{1}{K-1}) \mathbb{E}[\|\mathbf{z}_{t,i}^{(k)} - \mathbf{z}_t\|^2] + \frac{2K}{4K^2 L_f^2} \mathbb{E}[\|\nabla_{\mathbf{x}} F_i(\mathbf{z}_{t,i}^{(k)}; \mathcal{B}_{t,i}^{(k)}) - \nabla_{\mathbf{x}} F_i(\mathbf{z}_t; \mathcal{B}_{t,i}^{(k)})\|^2] \\ &\quad + \frac{2K}{4K^2 L_f^2} \mathbb{E}[\|\nabla_{\mathbf{y}} F_i(\mathbf{z}_{t,i}^{(k)}; \mathcal{B}_{t,i}^{(k)}) - \nabla_{\mathbf{y}} F_i(\mathbf{z}_t; \mathcal{B}_{t,i}^{(k)})\|^2] + 2K\eta_t^2 \mathbb{E}[\|\mathbf{u}_t\|^2] + 2K\gamma_t^2 \mathbb{E}[\|\mathbf{v}_t\|^2] \\ &\leq (1 + \frac{2}{K-1}) \mathbb{E}[\|\mathbf{z}_{t,i}^{(k)} - \mathbf{z}_t\|^2] + 2K\eta_t^2 \mathbb{E}[\|\mathbf{u}_t\|^2] + 2K\gamma_t^2 \mathbb{E}[\|\mathbf{v}_t\|^2], \end{aligned}$$

where the first inequality follows from Young's inequality, the second inequality follows from the condition $\eta_t, \gamma_t \leq 1/(2L_f K)$, and the last inequality follows from Lemma 1. Recursively applying the above inequality yields

$$\begin{aligned} \mathbb{E}[\|\mathbf{z}_{t,i}^{(k)} - \mathbf{z}_t\|^2] &\leq (2K\eta_t^2 \mathbb{E}[\|\mathbf{u}_t\|^2] + 2K\gamma_t^2 \mathbb{E}[\|\mathbf{v}_t\|^2]) \sum_{k'=0}^{k-1} (1 + \frac{2}{K-1})^{k'} \\ &\leq 18\eta_t^2 K^2 \mathbb{E}[\|\mathbf{u}_t\|^2] + 18\gamma_t^2 K^2 \mathbb{E}[\|\mathbf{v}_t\|^2] \\ &\leq 18\eta_t^2 K^2 \mathbb{E}[\|\nabla_{\mathbf{x}} f(\mathbf{z}_t)\|^2] + 18\gamma_t^2 K^2 \mathbb{E}[\|\nabla_{\mathbf{y}} f(\mathbf{z}_t)\|^2] + \frac{18\eta_t^2 K^2}{S} \sigma_1^2 + \frac{18\gamma_t^2 K^2}{S} \sigma_2^2, \end{aligned}$$

where the last inequality follows from Assumption 1. □

Lemma 7. Let $\eta_t \leq \min\{1/(2L_f K), 1/(4L_\Phi K)\}$ and $\gamma_t \leq 1/(4L_f K)$ in CD-MAGE. Then

$$\begin{aligned} \mathbb{E}[\Phi(\mathbf{x}_{t+1}) - f(\mathbf{z}_{t+1})] &\leq (1 - \frac{\mu\gamma_t K}{2} + \frac{\eta_t K L_{12}^2}{2\mu}) \mathbb{E}[\Phi(\mathbf{x}_t) - f(\mathbf{z}_t)] + \frac{\gamma_t K}{2} \mathbb{E}[\|\mathbf{e}_{\mathbf{y},t}\|^2] + (\frac{11\eta_t K}{8} + 2\eta_t^2 K^2 L_f) \mathbb{E}[\|\nabla_{\mathbf{x}} f(\mathbf{z}_t)\|^2] \\ &\quad + \frac{\gamma_t^2 K^2 L_f}{S} \sigma_2^2 + (\frac{7\eta_t K}{4} + 2\eta_t^2 K^2 L_f) \mathbb{E}[\|\mathbf{e}_{\mathbf{x},t}\|^2] + \frac{\eta_t^2 K^2 (L_f + L_\Phi)}{S} \sigma_1^2 \\ &\quad - \frac{\gamma_t t K}{4} \mathbb{E}[\|\nabla_{\mathbf{y}} f(\mathbf{z}_t)\|^2] - \frac{\eta_t K}{2} \mathbb{E}[\|\nabla \Phi(\mathbf{x}_t)\|^2]. \end{aligned}$$

Proof. First, we rewrite $\Phi(\mathbf{x}_{t+1}) - f(\mathbf{z}_{t+1})$ as

$$\Phi(\mathbf{x}_{t+1}) - f(\mathbf{z}_{t+1}) = \Phi(\mathbf{x}_{t+1}) - \Phi(\mathbf{x}_t) + \Phi(\mathbf{x}_t) - f(\mathbf{z}_t) + f(\mathbf{z}_t) - f(\mathbf{z}_{t+1}).$$

By the smoothness of f , we have

$$\begin{aligned}
\mathbb{E}[f(\mathbf{z}_t) - f(\mathbf{z}_{t+1})] &\stackrel{(a)}{\leq} \mathbb{E}\left[\eta_t K \langle \nabla_{\mathbf{x}} f(\mathbf{z}_t), \mathbf{u}_t + \mathbf{e}_{\mathbf{x},t} \rangle - \gamma_t K \langle \nabla_{\mathbf{y}} f(\mathbf{z}_t), \mathbf{v}_t + \mathbf{e}_{\mathbf{y},t} \rangle \right. \\
&\quad \left. + \frac{L_f}{2} (\eta_t^2 K^2 \|\mathbf{u}_t + \mathbf{e}_{\mathbf{x},t}\|^2 + \gamma_t^2 K^2 \|\mathbf{v}_t + \mathbf{e}_{\mathbf{y},t}\|^2) \right] \\
&\stackrel{(b)}{\leq} \mathbb{E}\left[\frac{3\eta_t^2 K^2}{2} \|\nabla_{\mathbf{x}} f(\mathbf{z}_t)\|^2 + \frac{\eta_t K}{2} \|\mathbf{e}_{\mathbf{x},t}\|^2 + \frac{\gamma_t K}{2} \|\mathbf{e}_{\mathbf{y},t}\|^2 - \frac{\gamma_t K}{2} \|\nabla_{\mathbf{y}} f(\mathbf{z}_t)\|^2 - \frac{\gamma_t K}{2} \|\nabla_{\mathbf{y}} f(\mathbf{z}_t) + \mathbf{e}_{\mathbf{y},t}\|^2 \right. \\
&\quad \left. + \frac{L_f}{2} (\eta_t^2 K^2 \|\mathbf{u}_t + \mathbf{e}_{\mathbf{x},t}\|^2 + \gamma_t^2 K^2 \|\mathbf{v}_t + \mathbf{e}_{\mathbf{y},t}\|^2) \right] \\
&\stackrel{(c)}{\leq} \mathbb{E}\left[\left(\frac{3\eta_t^2 K^2}{2} + 2\eta_t^2 K^2 L_f \right) \|\nabla_{\mathbf{x}} f(\mathbf{z}_t)\|^2 + \left(\frac{\eta_t K}{2} + 2\eta_t^2 K^2 L_f \right) \|\mathbf{e}_{\mathbf{x},t}\|^2 + \frac{\gamma_t K}{2} \|\mathbf{e}_{\mathbf{y},t}\|^2 \right. \\
&\quad \left. - \frac{\gamma_t K}{2} \|\nabla_{\mathbf{y}} f(\mathbf{z}_t)\|^2 - \left(\frac{\gamma_t K}{2} - 2\gamma_t^2 K^2 L_f \right) \|\nabla_{\mathbf{y}} f(\mathbf{z}_t) + \mathbf{e}_{\mathbf{y},t}\|^2 \right] + \frac{\eta_t^2 K^2 L_f}{S} \sigma_1^2 + \frac{\gamma_t^2 K^2 L_f}{S} \sigma_2^2 \\
&\stackrel{(d)}{\leq} \mathbb{E}\left[\left(\frac{3\eta_t^2 K^2}{2} + 2\eta_t^2 K^2 L_f \right) \|\nabla_{\mathbf{x}} f(\mathbf{z}_t)\|^2 + \left(\frac{\eta_t K}{2} + 2\eta_t^2 K^2 L_f \right) \|\mathbf{e}_{\mathbf{x},t}\|^2 + \frac{\gamma_t K}{2} \|\mathbf{e}_{\mathbf{y},t}\|^2 \right. \\
&\quad \left. - \frac{\gamma_t K}{2} \|\nabla_{\mathbf{y}} f(\mathbf{z}_t)\|^2 \right] + \frac{\eta_t^2 K^2 L_f}{S} \sigma_1^2 + \frac{\gamma_t^2 K^2 L_f}{S} \sigma_2^2,
\end{aligned}$$

where (a) follows from Lemma 3 and Lemma 1; (b) holds because $\mathbb{E}[\langle \nabla_{\mathbf{x}} f(\mathbf{z}_t), \mathbf{u}_t \rangle] = \mathbb{E}[\|\nabla_{\mathbf{x}} f(\mathbf{z}_t)\|^2]$, $\mathbb{E}[\langle \nabla_{\mathbf{y}} f(\mathbf{z}_t), \mathbf{v}_t \rangle] = \mathbb{E}[\|\nabla_{\mathbf{y}} f(\mathbf{z}_t)\|^2]$; (c) follows from Assumption 1; (d) follows from the condition $\gamma_t \leq 1/(4L_f K)$.

Combining the above inequalities and Lemma 4, we have

$$\begin{aligned}
\mathbb{E}[\Phi(\mathbf{x}_{t+1}) - f(\mathbf{z}_{t+1})] &\leq \left(1 + \frac{\eta_t K L_{12}^2}{2\mu}\right) \mathbb{E}[\Phi(\mathbf{x}_t) - f(\mathbf{z}_t)] + \left(\frac{11\eta_t K}{8} + 2\eta_t^2 K^2 L_f\right) \mathbb{E}[\|\nabla_{\mathbf{x}} f(\mathbf{z}_t)\|^2] \\
&\quad + \left(\frac{7\eta_t K}{4} + 2\eta_t^2 K^2 L_f\right) \mathbb{E}[\|\mathbf{e}_{\mathbf{x},t}\|^2] + \frac{\gamma_t K}{2} \mathbb{E}[\|\mathbf{e}_{\mathbf{y},t}\|^2] + \frac{\eta_t^2 K^2 (L_f + L_\Phi)}{S} \sigma_1^2 + \frac{\gamma_t^2 K^2 L_f}{S} \sigma_2^2 \\
&\quad - \frac{\mu\gamma_t K}{2} \mathbb{E}[\Phi(\mathbf{x}_t) - f(\mathbf{z}_t)] - \frac{\eta_t K}{2} \mathbb{E}[\|\nabla_{\mathbf{x}} \Phi(\mathbf{x}_t)\|^2] - \frac{\gamma_t K}{4} \mathbb{E}[\|\nabla_{\mathbf{y}} f(\mathbf{z}_t)\|^2] \\
&= \left(1 - \frac{\mu\gamma_t K}{2} + \frac{\eta_t K L_{12}^2}{2\mu}\right) \mathbb{E}[\Phi(\mathbf{x}_t) - f(\mathbf{z}_t)] + \left(\frac{11\eta_t K}{8} + 2\eta_t^2 K^2 L_f\right) \mathbb{E}[\|\nabla_{\mathbf{x}} f(\mathbf{z}_t)\|^2] \\
&\quad + \left(\frac{7\eta_t K}{4} + 2\eta_t^2 K^2 L_f\right) \mathbb{E}[\|\mathbf{e}_{\mathbf{x},t}\|^2] + \frac{\eta_t^2 K^2 (L_f + L_\Phi)}{S} \sigma_1^2 + \frac{\gamma_t K}{2} \mathbb{E}[\|\mathbf{e}_{\mathbf{y},t}\|^2] + \frac{\gamma_t^2 K^2 L_f}{S} \sigma_2^2 \\
&\quad - \frac{\gamma_t K}{4} \mathbb{E}[\|\nabla_{\mathbf{y}} f(\mathbf{z}_t)\|^2] - \frac{\eta_t K}{2} \mathbb{E}[\|\nabla \Phi(\mathbf{x}_t)\|^2],
\end{aligned}$$

where the first inequality follows from Assumption 3. □

Now, we are ready to prove Lemma 5.

Proof of Lemma 5. Recall that we define the potential function \mathcal{L}_t as

$$\mathcal{L}_t = \mathbb{E}[\Phi(\mathbf{x}_t) - \Phi(\mathbf{x}^*) + \frac{1}{20} (\Phi(\mathbf{x}_t) - f(\mathbf{x}_t, \mathbf{y}_t))].$$

Combining Lemma 4 and Lemma 7, we have

$$\begin{aligned}
&\mathbb{E}[\Phi(\mathbf{x}_{t+1}) - \Phi(\mathbf{x}^*) + \frac{1}{20} (\Phi(\mathbf{x}_{t+1}) - f(\mathbf{x}_{t+1}, \mathbf{y}_{t+1}))] \\
&\leq \mathbb{E}[\Phi(\mathbf{x}_t) - \Phi(\mathbf{x}^*)] + \left(\frac{1}{20} - \frac{\mu\gamma_t K}{40} + \frac{21\eta_t K L_{12}^2}{40\mu}\right) \mathbb{E}[\Phi(\mathbf{x}_t) - f(\mathbf{x}_t, \mathbf{y}_t)] \\
&\quad - \frac{21\eta_t K}{40} \mathbb{E}[\|\nabla \Phi(\mathbf{x}_t)\|^2] - \left(\frac{\eta_t K}{8} - \frac{1}{20} \left(\frac{11\eta_t K}{8} + 2\eta_t^2 K^2 L_f\right)\right) \mathbb{E}[\|\nabla_{\mathbf{x}} f(\mathbf{z}_t)\|^2] \\
&\quad + \left(\frac{5\eta_t K}{4} + \frac{1}{20} \left(\frac{7\eta_t K}{4} + 2\eta_t^2 K^2 L_f\right)\right) \mathbb{E}[\|\mathbf{e}_{\mathbf{x},t}\|^2] + \frac{\gamma_t K}{40} \mathbb{E}[\|\mathbf{e}_{\mathbf{y},t}\|^2] \\
&\quad + \frac{\eta_t^2 K^2}{S} \left(\frac{21L_\Phi}{20} + \frac{L_f}{20}\right) \sigma_1^2 + \frac{\gamma_t^2 K^2 L_f}{20S} \sigma_2^2 - \frac{\gamma_t K}{80} \mathbb{E}[\|\nabla_{\mathbf{y}} f(\mathbf{z}_t)\|^2]
\end{aligned}$$

$$\begin{aligned}
&\leq \mathbb{E}[\Phi(\mathbf{x}_t) - \Phi(\mathbf{x}^*)] + \left(\frac{1}{20} - \frac{\mu\gamma_t K}{40} + \frac{21\eta_t K L_{12}^2}{40\mu}\right) \mathbb{E}[\Phi(\mathbf{x}_t) - f(\mathbf{x}_t, \mathbf{y}_t)] - \frac{21\eta_t K}{40} \mathbb{E}[\|\nabla\Phi(\mathbf{x}_t)\|^2] \\
&\quad + \left(-\frac{\eta_t K}{8} + \frac{11\eta_t K}{160} + \frac{\eta_t^2 K^2 L_f}{10} + 18\eta_t^2 K^2 L_f^2 \left(\frac{5\eta_t K}{4} + \frac{7\eta_t K}{80} + \frac{\eta_t^2 K^2 L_f}{10}\right) + \frac{9\gamma_t \eta_t^2 K^3 L_f^2}{20}\right) \mathbb{E}[\|\nabla_{\mathbf{x}} f(\mathbf{z}_t)\|^2] \\
&\quad + \left(\frac{\eta_t^2 K^2}{S} \left(\frac{21L_\Phi}{20} + \frac{L_f}{20}\right) + \frac{18\eta_t^2 K^2 L_f^2}{S} \left(\frac{5\eta_t K}{4} + \frac{7\eta_t K}{80} + \frac{\eta_t^2 K^2 L_f}{10}\right) + \frac{9\gamma_t \eta_t^2 K^3 L_f^2}{20S}\right) \sigma_1^2 \\
&\quad + \left(-\frac{\gamma_t K}{80} + 18\gamma_t^2 K^2 L_f^2 \left(\frac{5\eta_t K}{4} + \frac{7\eta_t K}{80} + \frac{\eta_t^2 K^2 L_f}{10}\right) + \frac{9\gamma_t^3 K^3 L_f^2}{20}\right) \mathbb{E}[\|\nabla_{\mathbf{y}} f(\mathbf{z}_t)\|^2] \\
&\quad + \left(\frac{\gamma_t^2 K^2 L_f}{20S} + \frac{18\gamma_t^2 K^2 L_f^2}{S} \left(\frac{5\eta_t K}{4} + \frac{7\eta_t K}{80} + \frac{\eta_t^2 K^2 L_f}{10}\right) + \frac{9\gamma_t^3 K^3 L_f^2}{20S}\right) \sigma_2^2 \\
&\leq \mathbb{E}[\Phi(\mathbf{x}_t) - \Phi(\mathbf{x}^*)] + \frac{1}{20} \mathbb{E}[\Phi(\mathbf{x}_t) - f(\mathbf{x}_t, \mathbf{y}_t)] - \frac{21\eta_t K}{40} \mathbb{E}[\|\nabla\Phi(\mathbf{x}_t)\|^2] \\
&\quad + \frac{\eta_t^2 K^2}{S} (1.05L_\Phi + 0.81L_f) \sigma_1^2 + \frac{3\gamma_t^2 K^2 L_f}{4S} \sigma_2^2, \tag{10}
\end{aligned}$$

where the second inequality follows from Lemma 6 and the last inequality follows from the conditions $\eta_t \leq \min \left\{ \frac{1}{36L_f K}, \frac{1}{4L_\Phi K}, \frac{\mu^2}{21L_{12}^2} \gamma_t \right\}$ and $\gamma_t \leq \frac{1}{87L_f K}$. \square

Proof of Theorem 1

Proof. Denote $\gamma_t = \gamma := \min \left\{ \frac{1}{87L_f K}, \sqrt{\frac{4\mathcal{L}_0 S}{3L_f T K^2 \sigma_2^2}} \right\}$ and $\eta_t = \eta := \min \left\{ \frac{1}{36L_f K}, \frac{1}{4L_\Phi K}, \frac{\mu^2 \gamma}{21L_{12}^2}, \sqrt{\frac{40\mathcal{L}_0 S}{21(L_\Phi + L_f) T K^2 \sigma_1^2}} \right\}$. Recursively applying the inequality in Lemma 5 yields

$$\mathcal{L}_T \leq \mathcal{L}_0 - \frac{21\eta K}{40} \sum_{t=0}^{T-1} \mathbb{E}[\|\nabla\Phi(\mathbf{x})\|^2] + \frac{21T}{20S} \eta^2 K^2 (L_\Phi + L_f) \sigma_1^2 + \frac{3T}{4S} \gamma^2 K^2 L_f \sigma_2^2.$$

Plugging the values of η and γ to the above inequality and rearranging terms, we arrive at

$$\begin{aligned}
&\frac{1}{T} \sum_{t=0}^{T-1} \mathbb{E}[\|\nabla\Phi(\mathbf{x}_t)\|^2] \\
&\leq \frac{40}{21\eta K T} \mathcal{L}_0 + \frac{2\eta K (L_\Phi + L_f)}{S} \sigma_1^2 + \frac{10\gamma^2 K L_f}{7\eta S} \sigma_2^2 \\
&\leq \left(\sqrt{\frac{21(L_\Phi + L_f) T \sigma_1^2 K^2}{40\mathcal{L}_0 S}} + 36L_f K + 4L_\Phi K + \frac{21L_{12}^2}{\mu^2} \left(87L_f K + \sqrt{\frac{3L_f T K^2 \sigma_2^2}{4\mathcal{L}_0 S}} \right) \right) \frac{40\mathcal{L}_0}{21KT} \\
&\quad + \frac{2(L_\Phi + L_f) K \sigma_1^2}{S} \sqrt{\frac{40\mathcal{L}_0 S}{21(L_\Phi + L_f) T K^2 \sigma_1^2}} + \left(\sqrt{\frac{21(L_\Phi + L_f) T \sigma_1^2 K^2}{40\mathcal{L}_0 S}} + 36L_f K + 4L_\Phi K + \frac{21L_{12}^2}{\mu^2 \gamma} \right) \frac{10\gamma^2 K L_f \sigma_2^2}{7S} \\
&\leq 3\sqrt{\frac{40\mathcal{L}_0 (L_\Phi + L_f) \sigma_1^2}{21ST}} + \left(36L_f K + 4L_\Phi K + \frac{1827L_{12}^2 L_f K}{\mu^2} \right) \frac{40\mathcal{L}_0}{21KT} + \frac{20}{7} \sqrt{\frac{\mathcal{L}_0 L_f \sigma_2^2}{3ST}} \\
&\quad + \left(\sqrt{\frac{21(L_\Phi + L_f) T \sigma_1^2 K^2}{40\mathcal{L}_0 S}} + 36L_f K + 4L_\Phi K \right) \frac{10K L_f^2 \sigma_2^2}{7S} \cdot \frac{4\mathcal{L}_0 S}{3L_f T K^2 \sigma_2^2} + \frac{30L_{12}^2 K L_f \sigma_2^2}{7\mu^2 S} \gamma \\
&\leq 4\sqrt{\frac{40\mathcal{L}_0 (L_\Phi + L_f) \sigma_1^2}{21ST}} + \left(\frac{20}{7} + \frac{60L_{12}^2}{\mu^2} \right) \sqrt{\frac{\mathcal{L}_0 L_f \sigma_2^2}{3ST}} + \left(8L_\Phi + \left(\frac{1827L_{12}^2}{\mu^2} + 72 \right) L_f \right) \frac{40\mathcal{L}_0}{21T},
\end{aligned}$$

which is the desired result. \square

C.3 Proofs of the results in Section 4.2

The analysis of CD-MAGE+ is more sophisticated than that of CD-MAGE. For ease of notation, we omit the subscript t, i of the iterates in CD-MAGE+ and denote $\mathbf{x}_{t,i}^{(k)}$ (resp., $\mathbf{y}_{t,i}^{(k)}$) as $\mathbf{x}^{(k)}$ (resp., $\mathbf{y}^{(k)}$). To prove Theorem 2, we first define some auxiliary quantities and establish several lemmas. We denote the error of gradient estimations in CD-MAGE+ as

$$\begin{cases} \varepsilon_{\mathbf{x},t} := \mathbb{E}[\|\mathbf{u}_t - \nabla_{\mathbf{x}} f(\mathbf{x}_t, \mathbf{y}_t)\|^2], \\ \varepsilon_{\mathbf{y},t} := \mathbb{E}[\|\mathbf{v}_t - \nabla_{\mathbf{y}} f(\mathbf{x}_t, \mathbf{y}_t)\|^2], \end{cases}$$

where the expectation is taken over all randomness. These two quantities can be bounded as follows.

Lemma 8. *The gradient estimation errors $\varepsilon_{\mathbf{x},t+1}$ and $\varepsilon_{\mathbf{y},t+1}$ can be bounded by*

$$\begin{cases} \varepsilon_{\mathbf{x},t+1} \leq (1 - \alpha_{t+1})^2 \varepsilon_{\mathbf{x},t} + \frac{2\alpha_{t+1}^2 \sigma_1^2}{S} + \frac{8(1-\alpha_{t+1})^2 L_f^2}{S} \mathbb{E}[\|\mathbf{z}_{t+1} - \mathbf{z}_t\|^2], \\ \varepsilon_{\mathbf{y},t+1} \leq (1 - \alpha_{t+1})^2 \varepsilon_{\mathbf{y},t} + \frac{2\alpha_{t+1}^2 \sigma_2^2}{S} + \frac{8(1-\alpha_{t+1})^2 L_f^2}{S} \mathbb{E}[\|\mathbf{z}_{t+1} - \mathbf{z}_t\|^2]. \end{cases}$$

Proof. By the definition of $\varepsilon_{\mathbf{x},t+1}$, we have

$$\begin{aligned} \varepsilon_{\mathbf{x},t+1} &= \mathbb{E}[\|\mathbf{u}_{t+1} - \nabla_{\mathbf{x}} f(\mathbf{z}_{t+1})\|^2] \\ &= \mathbb{E}\left[\left\| (1 - \alpha_{t+1})(\mathbf{u}_t - \nabla_{\mathbf{x}} f(\mathbf{z}_t)) + \alpha_{t+1} \left(\frac{1}{S} \sum_{i \in \mathcal{S}'_{t+1}} \nabla_{\mathbf{x}} f_i(\mathbf{z}_{t+1}) - \nabla_{\mathbf{x}} f(\mathbf{z}_{t+1}) \right) \right. \right. \\ &\quad \left. \left. + (1 - \alpha_{t+1}) \left(\frac{1}{S} \sum_{i \in \mathcal{S}'_{t+1}} (\nabla_{\mathbf{x}} f_i(\mathbf{z}_{t+1}) - \nabla_{\mathbf{x}} f_i(\mathbf{z}_t)) - \nabla_{\mathbf{x}} f(\mathbf{z}_{t+1}) + \nabla_{\mathbf{x}} f(\mathbf{z}_t) \right) \right\|^2\right] \\ &\stackrel{(a)}{=} (1 - \alpha_{t+1})^2 \varepsilon_{\mathbf{x},t} + \mathbb{E}\left[\left\| \alpha_{t+1} \left(\frac{1}{S} \sum_{i \in \mathcal{S}'_{t+1}} \nabla_{\mathbf{x}} f_i(\mathbf{z}_{t+1}) - \nabla_{\mathbf{x}} f(\mathbf{z}_{t+1}) \right) \right. \right. \\ &\quad \left. \left. + (1 - \alpha_{t+1}) \left(\frac{1}{S} \sum_{i \in \mathcal{S}'_{t+1}} (\nabla_{\mathbf{x}} f_i(\mathbf{z}_{t+1}) - \nabla_{\mathbf{x}} f_i(\mathbf{z}_t)) - \nabla_{\mathbf{x}} f(\mathbf{z}_{t+1}) + \nabla_{\mathbf{x}} f(\mathbf{z}_t) \right) \right\|^2\right] \\ &\leq (1 - \alpha_{t+1})^2 \varepsilon_{\mathbf{x},t} + 2\alpha_{t+1}^2 \mathbb{E}\left[\left\| \left(\frac{1}{S} \sum_{i \in \mathcal{S}'_{t+1}} \nabla_{\mathbf{x}} f_i(\mathbf{z}_{t+1}) - \nabla_{\mathbf{x}} f(\mathbf{z}_{t+1}) \right) \right\|^2\right] \\ &\quad + 2(1 - \alpha_{t+1})^2 \mathbb{E}\left[\left\| \left(\frac{1}{S} \sum_{i \in \mathcal{S}'_{t+1}} (\nabla_{\mathbf{x}} f_i(\mathbf{z}_{t+1}) - \nabla_{\mathbf{x}} f_i(\mathbf{z}_t)) - \nabla_{\mathbf{x}} f(\mathbf{z}_{t+1}) + \nabla_{\mathbf{x}} f(\mathbf{z}_t) \right) \right\|^2\right] \\ &\stackrel{(b)}{\leq} (1 - \alpha_{t+1})^2 \varepsilon_{\mathbf{x},t} + \frac{8(1 - \alpha_{t+1})^2 L_f^2}{S} \mathbb{E}[\|\mathbf{z}_{t+1} - \mathbf{z}_t\|^2] + \frac{2\alpha_{t+1}^2 \sigma_1^2}{S}, \end{aligned}$$

where (a) holds because $\mathbb{E}_{\mathcal{S}'_{t+1}}[\frac{1}{|\mathcal{S}'_{t+1}|} \sum_{i \in \mathcal{S}'_{t+1}} f_i(\mathbf{z})] = f(\mathbf{z})$ and \mathcal{S}'_{t+1} is independent of $\varepsilon_{\mathbf{x},t}$; (b) follows from Assumption 1 and Lemma 1. This completes the first part of Lemma 8. The second part of the lemma follows from the same argument. \square

The following lemma relates the approximation error of $\mathbf{d}_{\mathbf{x}}^{(k)}$ (resp., $\mathbf{d}_{\mathbf{y}}^{(k)}$) defined in (4) to $\varepsilon_{\mathbf{x},t}$ (resp., $\varepsilon_{\mathbf{y},t}$).

Lemma 9. *Consider CD-MAGE+. Under Assumptions 2-3, we have*

$$\begin{cases} \mathbb{E}[\|\mathbf{d}_{\mathbf{x}}^{(k)} - \nabla \Phi(\mathbf{x}^{(k)})\|^2] \leq \frac{3L_{12}^2}{2\mu} \mathbb{E}[\Phi(\mathbf{x}^{(k)}) - f(\mathbf{z}^{(k)})] + 12L_f^2 \mathbb{E}[\|\mathbf{z}^{(k)} - \mathbf{z}_t\|^2] + 3\varepsilon_{\mathbf{x},t}, \\ \mathbb{E}[\|\mathbf{d}_{\mathbf{x}}^{(k)} - \nabla_{\mathbf{x}} f(\mathbf{z}^{(k)})\|^2] \leq 8L_f^2 \mathbb{E}[\|\mathbf{z}^{(k)} - \mathbf{z}_t\|^2] + 2\varepsilon_{\mathbf{x},t}, \\ \mathbb{E}[\|\mathbf{d}_{\mathbf{y}}^{(k)} - \nabla_{\mathbf{y}} f(\mathbf{z}^{(k)})\|^2] \leq 8L_f^2 \mathbb{E}[\|\mathbf{z}^{(k)} - \mathbf{z}_t\|^2] + 2\varepsilon_{\mathbf{y},t}. \end{cases}$$

Proof. By Lemma 1, both $F_i(\cdot, \cdot; \mathcal{B}^{(k)})$ and $f(\cdot, \cdot)$ are L_f -smooth. Thus, we can bound

$$\begin{aligned} &\mathbb{E}[\|\nabla_{\mathbf{x}} F_i(\mathbf{z}^{(k)}; \mathcal{B}^{(k)}) - \nabla_{\mathbf{x}} F_i(\mathbf{z}_t; \mathcal{B}^{(k)}) + \mathbf{u}_t - \nabla \Phi(\mathbf{x}^{(k)})\|^2] \\ &= \mathbb{E}[\|\nabla_{\mathbf{x}} F_i(\mathbf{z}^{(k)}; \mathcal{B}^{(k)}) - \nabla_{\mathbf{x}} F_i(\mathbf{z}_t; \mathcal{B}^{(k)}) - \nabla_{\mathbf{x}} f(\mathbf{z}^{(k)}) + \nabla_{\mathbf{x}} f(\mathbf{z}_t) - \nabla_{\mathbf{x}} f(\mathbf{z}_t) + \mathbf{u}_t + \nabla_{\mathbf{x}} f(\mathbf{z}^{(k)}) - \nabla \Phi(\mathbf{x}^{(k)})\|^2] \\ &\leq 3\mathbb{E}[\|\nabla_{\mathbf{x}} F_i(\mathbf{z}^{(k)}; \mathcal{B}^{(k)}) - \nabla_{\mathbf{x}} F_i(\mathbf{z}_t; \mathcal{B}^{(k)}) - (\nabla_{\mathbf{x}} f(\mathbf{z}^{(k)}) - \nabla_{\mathbf{x}} f(\mathbf{z}_t))\|^2] + 3\varepsilon_{\mathbf{x},t} + 3\mathbb{E}[\|\nabla_{\mathbf{x}} f(\mathbf{z}^{(k)}) - \nabla \Phi(\mathbf{x}^{(k)})\|^2] \\ &\leq 6\mathbb{E}[\|\nabla_{\mathbf{x}} F_i(\mathbf{z}^{(k)}; \mathcal{B}^{(k)}) - \nabla_{\mathbf{x}} F_i(\mathbf{z}_t; \mathcal{B}^{(k)})\|^2] + \|\nabla_{\mathbf{x}} f(\mathbf{z}^{(k)}) - \nabla_{\mathbf{x}} f(\mathbf{z}_t)\|^2 + 3\varepsilon_{\mathbf{x},t} + 3\mathbb{E}[\|\nabla_{\mathbf{x}} f(\mathbf{z}^{(k)}) - \nabla \Phi(\mathbf{x}^{(k)})\|^2] \\ &\stackrel{(a)}{\leq} 12L_f^2 \mathbb{E}[\|\mathbf{z}^{(k)} - \mathbf{z}_t\|^2] + 3\varepsilon_{\mathbf{x},t} + 3\mathbb{E}[\|\nabla_{\mathbf{x}} f(\mathbf{z}^{(k)}) - \nabla \Phi(\mathbf{x}^{(k)})\|^2] \\ &\stackrel{(b)}{\leq} 12L_f^2 \mathbb{E}[\|\mathbf{z}^{(k)} - \mathbf{z}_t\|^2] + 3\varepsilon_{\mathbf{x},t} + 3L_{12}^2 \mathbb{E}[\|\mathbf{y}^{(k)} - \mathbf{y}^*(\mathbf{x}^{(k)})\|^2] \\ &\stackrel{(c)}{\leq} 12L_f^2 \mathbb{E}[\|\mathbf{z}^{(k)} - \mathbf{z}_t\|^2] + 3\varepsilon_{\mathbf{x},t} + \frac{3L_{12}^2}{2\mu} \mathbb{E}[\Phi(\mathbf{x}^{(k)}) - f(\mathbf{z}^{(k)})], \end{aligned}$$

where (a) follows from Lemma 1, (b) follows from Assumption 2, and (c) follows from (9). This proves the first inequality of Lemma 9. Similarly, we can bound

$$\begin{aligned}\mathbb{E}[\|\mathbf{d}_{\mathbf{x}}^{(k)} - \nabla_{\mathbf{x}} f(\mathbf{z}^{(k)})\|^2] &= \mathbb{E}[\|\nabla_{\mathbf{x}} F_i(\mathbf{z}^{(k)}; \mathcal{B}^{(k)}) - \nabla_{\mathbf{x}} F_i(\mathbf{z}_t; \mathcal{B}^{(k)}) - \nabla_{\mathbf{x}} f(\mathbf{z}^{(k)}) + \nabla_{\mathbf{x}} f(\mathbf{z}_t) + \mathbf{u}_t - \nabla_{\mathbf{x}} f(\mathbf{z}_t)\|^2] \\ &\leq 8L_f^2 \mathbb{E}[\|\mathbf{z}^{(k)} - \mathbf{z}_t\|^2] + 2\varepsilon_{\mathbf{x},t}, \\ \mathbb{E}[\|\mathbf{d}_{\mathbf{y}}^{(k)} - \nabla_{\mathbf{y}} f(\mathbf{z}^{(k)})\|^2] &= \mathbb{E}[\|\nabla_{\mathbf{y}} F_i(\mathbf{z}^{(k)}; \mathcal{B}^{(k)}) - \nabla_{\mathbf{y}} F_i(\mathbf{z}_t; \mathcal{B}^{(k)}) - \nabla_{\mathbf{y}} f(\mathbf{z}^{(k)}) + \nabla_{\mathbf{y}} f(\mathbf{z}_t) + \mathbf{v}_t - \nabla_{\mathbf{y}} f(\mathbf{z}_t)\|^2] \\ &\leq 8L_f^2 \mathbb{E}[\|\mathbf{z}^{(k)} - \mathbf{z}_t\|^2] + 2\varepsilon_{\mathbf{y},t}.\end{aligned}$$

□

The next lemma shows that the expected loss value $\mathbb{E}[\Phi(\mathbf{x}^{(k)})]$ decreases as k increases as long as the errors $\mathbb{E}[\Phi(\mathbf{x}^{(k)}) - f(\mathbf{z}^{(k)})]$, $\mathbb{E}[\|\mathbf{z}^{(k)} - \mathbf{z}_t\|^2]$, and $\varepsilon_{\mathbf{x},t}$ are controlled in a desirable level.

Lemma 10 (One-iteration descent). *Suppose that $\eta_t \leq \frac{1}{2L_{\Phi}}$. Under Assumptions 1-3, $\forall k \in \{0, \dots, K-1\}$, we have*

$$\begin{aligned}\mathbb{E}[\Phi(\mathbf{x}^{(k+1)}) - \Phi(\mathbf{x}^{(k)})] &\leq -\frac{\eta_t}{2} \mathbb{E}[\|\nabla \Phi(\mathbf{x}^{(k)})\|^2] + \frac{3L_{12}^2}{4\mu} \eta_t \mathbb{E}[\Phi(\mathbf{x}^{(k)}) - f(\mathbf{z}^{(k)})] \\ &\quad + 7L_f^2 \eta_t \mathbb{E}[\|\mathbf{z}^{(k)} - \mathbf{z}_t\|^2] + \frac{7\eta_t}{4} \varepsilon_{\mathbf{x},t} - \frac{\eta_t}{16} \mathbb{E}[\|\nabla_{\mathbf{x}} f(\mathbf{z}^{(k)})\|^2] - \frac{\eta_t}{8} \mathbb{E}[\|\mathbf{d}_{\mathbf{x}}^{(k)}\|^2].\end{aligned}$$

Proof. By Lemma 2, we have

$$\begin{aligned}\mathbb{E}[\Phi(\mathbf{x}^{(k+1)}) - \Phi(\mathbf{x}^{(k)})] &\leq \mathbb{E}[\langle \nabla \Phi(\mathbf{x}^{(k)}), \mathbf{x}^{(k+1)} - \mathbf{x}^{(k)} \rangle + \frac{L_{\Phi}}{2} \|\mathbf{x}^{(k+1)} - \mathbf{x}^{(k)}\|^2] \\ &= -\eta_t \mathbb{E}[\langle \nabla \Phi(\mathbf{x}^{(k)}), \mathbf{d}_{\mathbf{x}}^{(k)} \rangle] + \frac{L_{\Phi} \eta_t^2}{2} \mathbb{E}[\|\mathbf{d}_{\mathbf{x}}^{(k)}\|^2] \\ &= \frac{\eta_t}{2} \mathbb{E}[\|\mathbf{d}_{\mathbf{x}}^{(k)} - \nabla \Phi(\mathbf{x}^{(k)})\|^2] - \frac{\eta_t}{2} \mathbb{E}[\|\nabla \Phi(\mathbf{x}^{(k)})\|^2] - \left(\frac{\eta_t}{2} - \frac{L_{\Phi} \eta_t^2}{2}\right) \mathbb{E}[\|\mathbf{d}_{\mathbf{x}}^{(k)}\|^2] \\ &\leq \frac{\eta_t}{2} \mathbb{E}[\|\mathbf{d}_{\mathbf{x}}^{(k)} - \nabla \Phi(\mathbf{x}^{(k)})\|^2] - \frac{\eta_t}{2} \mathbb{E}[\|\nabla \Phi(\mathbf{x}^{(k)})\|^2] - \frac{\eta_t}{4} \mathbb{E}[\|\mathbf{d}_{\mathbf{x}}^{(k)}\|^2] \\ &\leq \frac{\eta_t}{2} \mathbb{E}[\|\mathbf{d}_{\mathbf{x}}^{(k)} - \nabla \Phi(\mathbf{x}^{(k)})\|^2] - \frac{\eta_t}{2} \mathbb{E}[\|\nabla \Phi(\mathbf{x}^{(k)})\|^2] - \frac{\eta_t}{8} \mathbb{E}[\|\mathbf{d}_{\mathbf{x}}^{(k)}\|^2] \\ &\quad - \frac{\eta_t}{16} \mathbb{E}[\|\nabla_{\mathbf{x}} f(\mathbf{x}^{(k)}, \mathbf{y}^{(k)})\|^2] + \frac{\eta_t}{8} \mathbb{E}[\|\mathbf{d}_{\mathbf{x}}^{(k)} - \nabla_{\mathbf{x}} f(\mathbf{x}^{(k)}, \mathbf{y}^{(k)})\|^2],\end{aligned}\tag{11}$$

where the first equality follows from the update rule $\mathbf{x}^{(k+1)} = \mathbf{x}^{(k)} - \eta_t \mathbf{d}_{\mathbf{x}}^{(k)}$ and the second equality follows from the fact that $-2\langle \mathbf{a}, \mathbf{b} \rangle = \|\mathbf{a} - \mathbf{b}\|^2 - \|\mathbf{a}\|^2 - \|\mathbf{b}\|^2$. Combining (11) and Lemma 9 completes the proof. □

We provide upper bounds of the error terms $\mathbb{E}[\|\mathbf{z}^{(k)} - \mathbf{z}_t\|^2]$ and $\mathbb{E}[\Phi(\mathbf{x}^{(k)}) - f(\mathbf{z}^{(k)})]$ in the next two lemmas.

Lemma 11. *Under Assumptions 1-3, for any $k \in \{0, \dots, K-1\}$, we have*

$$\begin{cases} \mathbb{E}[\|\mathbf{x}^{(k+1)} - \mathbf{x}_t\|^2] \leq (1 + \frac{1}{K}) \mathbb{E}[\|\mathbf{x}^{(k)} - \mathbf{x}_t\|^2] + (1 + K) \eta_t^2 \mathbb{E}[\|\mathbf{d}_{\mathbf{x}}^{(k)}\|^2], \\ \mathbb{E}[\|\mathbf{y}^{(k+1)} - \mathbf{y}_t\|^2] \leq (1 + \frac{1}{K}) \mathbb{E}[\|\mathbf{y}^{(k)} - \mathbf{y}_t\|^2] + (1 + K) \gamma_t^2 \mathbb{E}[\|\mathbf{d}_{\mathbf{y}}^{(k)}\|^2]. \end{cases}$$

Proof. First, we bound $\mathbb{E}[\|\mathbf{x}^{(k+1)} - \mathbf{x}_t\|^2]$ as follows

$$\mathbb{E}[\|\mathbf{x}^{(k+1)} - \mathbf{x}_t\|^2] = \mathbb{E}[\|\mathbf{x}^{(k)} - \eta_t \mathbf{d}_{\mathbf{x}}^{(k)} - \mathbf{x}_t\|^2] \leq (1 + \frac{1}{K}) \mathbb{E}[\|\mathbf{x}^{(k)} - \mathbf{x}_t\|^2] + (1 + K) \eta_t^2 \mathbb{E}[\|\mathbf{d}_{\mathbf{x}}^{(k)}\|^2],$$

where the inequality follows from Young's inequality. Similarly, $\mathbb{E}[\|\mathbf{y}^{(k+1)} - \mathbf{y}_t\|^2]$ can be bounded by

$$\mathbb{E}[\|\mathbf{y}^{(k+1)} - \mathbf{y}_t\|^2] \leq (1 + \frac{1}{K}) \mathbb{E}[\|\mathbf{y}^{(k)} - \mathbf{y}_t\|^2] + (1 + K) \gamma_t^2 \mathbb{E}[\|\mathbf{d}_{\mathbf{y}}^{(k)}\|^2].$$

□

Lemma 12. *Suppose that $\eta_t \leq \min\{\frac{1}{2L_f}, \frac{1}{2L_{\Phi}}\}$ and $\gamma_t \leq \frac{1}{2L_f}$. Under Assumptions 1-3, for any $k \in \{0, \dots, K-1\}$, we have*

$$\begin{aligned}\mathbb{E}[\Phi(\mathbf{x}^{(k+1)}) - f(\mathbf{z}^{(k+1)})] &\leq (1 - \frac{\mu \gamma_t}{2} + \frac{3L_{12}^2}{4\mu} \eta_t) \mathbb{E}[\Phi(\mathbf{x}^{(k)}) - f(\mathbf{z}^{(k)})] - \frac{\eta_t}{2} \mathbb{E}[\|\nabla \Phi(\mathbf{x}^{(k)})\|^2] \\ &\quad + (7\eta_t + 4\gamma_t) L_f^2 \mathbb{E}[\|\mathbf{z}^{(k)} - \mathbf{z}_t\|^2] + \frac{7\eta_t}{16} \mathbb{E}[\|\nabla_{\mathbf{x}} f(\mathbf{z}^{(k)})\|^2] + \frac{5\eta_t}{8} \mathbb{E}[\|\mathbf{d}_{\mathbf{x}}^{(k)}\|^2] + \frac{7\eta_t}{4} \varepsilon_{\mathbf{x},t} \\ &\quad + \gamma_t \varepsilon_{\mathbf{y},t} - \frac{\gamma_t}{4} \mathbb{E}[\|\mathbf{d}_{\mathbf{y}}^{(k)}\|^2] - \frac{\gamma_t}{4} \mathbb{E}[\|\nabla_{\mathbf{y}} f(\mathbf{z}^{(k)})\|^2].\end{aligned}$$

Proof. First, we notice that

$$\mathbb{E}[\Phi(\mathbf{x}^{(k+1)}) - f(\mathbf{z}^{(k+1)})] = \mathbb{E}[\Phi(\mathbf{x}^{(k+1)}) - \Phi(\mathbf{x}^{(k)}) + \Phi(\mathbf{x}^{(k)}) - f(\mathbf{z}^{(k)}) + f(\mathbf{z}^{(k)}) - f(\mathbf{z}^{(k+1)})].$$

In what follows, we bound $\mathbb{E}[f(\mathbf{z}^{(k)}) - f(\mathbf{z}^{(k+1)})]$.

$$\begin{aligned} & \mathbb{E}[f(\mathbf{z}^{(k)}) - f(\mathbf{z}^{(k+1)})] \\ & \leq \mathbb{E}\left[\langle \nabla_{\mathbf{x}} f(\mathbf{z}^{(k)}), \mathbf{x}^{(k)} - \mathbf{x}^{(k+1)} \rangle + \langle \nabla_{\mathbf{y}} f(\mathbf{z}^{(k)}), \mathbf{y}^{(k)} - \mathbf{y}^{(k+1)} \rangle + \frac{L_f}{2} (\|\mathbf{x}^{(k)} - \mathbf{x}^{(k+1)}\|^2 + \|\mathbf{y}^{(k)} - \mathbf{y}^{(k+1)}\|^2)\right] \\ & = \mathbb{E}\left[\eta_t \langle \nabla_{\mathbf{x}} f(\mathbf{z}^{(k)}), \mathbf{d}_{\mathbf{x}}^{(k)} \rangle - \gamma_t \langle \nabla_{\mathbf{y}} f(\mathbf{z}^{(k)}), \mathbf{d}_{\mathbf{y}}^{(k)} \rangle + \frac{L_f \eta_t^2}{2} \|\mathbf{d}_{\mathbf{x}}^{(k)}\|^2 + \frac{L_f \gamma_t^2}{2} \|\mathbf{d}_{\mathbf{y}}^{(k)}\|^2\right] \\ & \leq \mathbb{E}\left[\frac{\eta_t}{2} \|\nabla_{\mathbf{x}} f(\mathbf{z}^{(k)})\|^2 + \frac{\eta_t(1 + \eta_t L_f)}{2} \|\mathbf{d}_{\mathbf{x}}^{(k)}\|^2 - \frac{\gamma_t}{2} \|\nabla_{\mathbf{y}} f(\mathbf{z}^{(k)})\|^2 - \left(\frac{\gamma_t}{2} - \frac{L_f \gamma_t^2}{2}\right) \|\mathbf{d}_{\mathbf{y}}^{(k)}\|^2 + \frac{\gamma_t}{2} \|\mathbf{d}_{\mathbf{y}}^{(k)} - \nabla_{\mathbf{y}} f(\mathbf{z}^{(k)})\|^2\right] \\ & \leq \mathbb{E}\left[\frac{\eta_t}{2} \|\nabla_{\mathbf{x}} f(\mathbf{z}^{(k)})\|^2 + \frac{\eta_t(1 + \eta_t L_f)}{2} \|\mathbf{d}_{\mathbf{x}}^{(k)}\|^2 - \frac{\gamma_t}{2} \|\nabla_{\mathbf{y}} f(\mathbf{z}^{(k)})\|^2 - \frac{\gamma_t}{4} \|\mathbf{d}_{\mathbf{y}}^{(k)}\|^2 + 4\gamma_t L_f^2 \mathbb{E}[\|\mathbf{z}^{(k)} - \mathbf{z}_t\|^2] + \gamma_t \varepsilon_{\mathbf{y},t}\right], \end{aligned}$$

where the last inequality follows from the condition $\gamma_t \leq 1/(2L_f)$ and Lemma 9. Combining the above two inequalities and Lemma 10, we obtain

$$\begin{aligned} & \mathbb{E}[\Phi(\mathbf{x}^{(k+1)}) - f(\mathbf{z}^{(k+1)})] \\ & \leq \left(1 + \frac{3L_{12}^2}{4\mu} \eta_t\right) \mathbb{E}[\Phi(\mathbf{x}^{(k)}) - f(\mathbf{z}^{(k)})] - \frac{\eta_t}{2} \mathbb{E}[\|\nabla \Phi(\mathbf{x}^{(k)})\|^2] \\ & \quad + 7L_f^2 \eta_t \mathbb{E}[\|\mathbf{z}^{(k)} - \mathbf{z}_t\|^2] + \frac{7\eta_t}{4} \varepsilon_{\mathbf{x},t} - \frac{\eta_t}{16} \mathbb{E}[\|\nabla_{\mathbf{x}} f(\mathbf{z}^{(k)})\|^2] - \frac{\eta_t}{8} \mathbb{E}[\|\mathbf{d}_{\mathbf{x}}^{(k)}\|^2] \\ & \quad + \mathbb{E}\left[\frac{\eta_t}{2} \|\nabla_{\mathbf{x}} f(\mathbf{z}^{(k)})\|^2 + \frac{\eta_t(1 + \eta_t L_f)}{2} \|\mathbf{d}_{\mathbf{x}}^{(k)}\|^2 - \frac{\gamma_t}{2} \|\nabla_{\mathbf{y}} f(\mathbf{z}^{(k)})\|^2 - \frac{\gamma_t}{4} \|\mathbf{d}_{\mathbf{y}}^{(k)}\|^2 + 4\gamma_t L_f^2 \mathbb{E}[\|\mathbf{z}^{(k)} - \mathbf{z}_t\|^2] + \gamma_t \varepsilon_{\mathbf{y},t}\right] \\ & \leq \left(1 - \frac{\mu\gamma_t}{2} + \frac{3L_{12}^2}{4\mu} \eta_t\right) \mathbb{E}[\Phi(\mathbf{x}^{(k)}) - f(\mathbf{z}^{(k)})] - \frac{\eta_t}{2} \mathbb{E}[\|\nabla \Phi(\mathbf{x}^{(k)})\|^2] + (7\eta_t + 4\gamma_t) L_f^2 \mathbb{E}[\|\mathbf{z}^{(k)} - \mathbf{z}_t\|^2] \\ & \quad + \frac{7\eta_t}{16} \mathbb{E}[\|\nabla_{\mathbf{x}} f(\mathbf{z}^{(k)})\|^2] + \frac{5\eta_t}{8} \mathbb{E}[\|\mathbf{d}_{\mathbf{x}}^{(k)}\|^2] + \frac{7\eta_t}{4} \varepsilon_{\mathbf{x},t} + \gamma_t \varepsilon_{\mathbf{y},t} - \frac{\gamma_t}{4} \mathbb{E}[\|\mathbf{d}_{\mathbf{y}}^{(k)}\|^2] - \frac{\gamma_t}{4} \mathbb{E}[\|\nabla_{\mathbf{y}} f(\mathbf{z}^{(k)})\|^2], \end{aligned}$$

where the last inequality follows from the condition $\eta_t \leq 1/(2L_f)$ and Assumption 3. This completes the proof. \square

Proof of Theorem 2

Proof. First, we define the following potential function

$$\begin{aligned} \mathcal{L}^{(k)} &:= \mathbb{E}[\Phi(\mathbf{x}^{(k)}) - \Phi(\mathbf{x}^*)] + \frac{1}{10} \mathbb{E}[\Phi(\mathbf{x}^{(k)}) - f(\mathbf{z}^{(k)})] \\ & \quad + \frac{64(1.1L_\Phi + 0.1L_f)\gamma_t}{\alpha_t} \left(1 + \frac{2}{K}\right)^{K-k} \mathbb{E}[\|\mathbf{x}^{(k)} - \mathbf{x}_t\|^2] + \frac{6.4L_f K \gamma_t}{\alpha_t} \left(1 + \frac{2}{K}\right)^{K-k} \mathbb{E}[\|\mathbf{y}^{(k)} - \mathbf{y}_t\|^2]. \end{aligned}$$

Combining Lemma 10, 11, 12, and 8, we can bound

$$\begin{aligned} & \mathcal{L}^{(k+1)} + \frac{4\eta_{t+1}}{\alpha_{t+1}} \varepsilon_{\mathbf{x},t+1} + \frac{2\gamma_{t+1}}{5\alpha_{t+1}} \varepsilon_{\mathbf{y},t+1} \\ & \leq \mathbb{E}[\Phi(\mathbf{x}^{(k)}) - \Phi(\mathbf{x}^*)] + c_1 \mathbb{E}[\Phi(\mathbf{x}^{(k)}) - f(\mathbf{z}^{(k)})] - \frac{11\eta_t}{20} \mathbb{E}[\|\nabla_{\mathbf{x}} \Phi(\mathbf{x}^{(k)})\|^2] + c_2 \mathbb{E}[\|\mathbf{x}^{(k)} - \mathbf{x}_t\|^2] \\ & \quad + c_3 \mathbb{E}[\|\mathbf{y}^{(k)} - \mathbf{x}_t\|^2] + c_4 \varepsilon_{\mathbf{x},t} + c_5 \varepsilon_{\mathbf{y},t} - \frac{3}{160} \mathbb{E}[\|\nabla_{\mathbf{x}} f(\mathbf{z}^{(k)})\|^2] - \frac{\gamma_t}{40} \mathbb{E}[\|\nabla_{\mathbf{y}} f(\mathbf{z}^{(k)})\|^2] + c_6 \mathbb{E}[\|\mathbf{d}_{\mathbf{x}}^{(k)}\|^2] \\ & \quad + c_7 \mathbb{E}[\|\mathbf{d}_{\mathbf{y}}^{(k)}\|^2] + c_8 \mathbb{E}[\|\mathbf{z}_{t+1} - \mathbf{z}_t\|^2] + \frac{8\eta_{t+1}\alpha_{t+1}}{S} \sigma_1^2 + \frac{4\gamma_{t+1}\alpha_{t+1}}{5S} \sigma_2^2, \end{aligned} \tag{12}$$

where c_1, \dots, c_8 are given by

$$\begin{aligned} c_1 &:= \frac{1}{10} \left(1 - \frac{\mu\gamma_t}{2} + \frac{3L_{12}^2}{4\mu} \eta_t\right), \\ c_2 &:= 7L_f^2 \eta_t + 0.1(7\eta_t + 4\gamma_t) L_f^2 + \frac{64(1.1L_\Phi + 0.1L_f)^2 K \gamma_t}{\alpha_t} \left(1 + \frac{2}{K}\right)^{K-k+1} \left(1 + \frac{1}{K}\right), \end{aligned}$$

$$\begin{aligned}
c_3 &:= 7L_f^2\eta_t + 0.1(7\eta_t + 4\gamma_t)L_f^2 + \frac{6.4L_f^2K\gamma_t}{\alpha_t} \left(1 + \frac{2}{K}\right)^{K-k+1} \left(1 + \frac{1}{K}\right), \\
c_4 &:= \frac{77\eta_t}{40} + \frac{4\eta_{t+1}}{\alpha_{t+1}}(1 - \alpha_{t+1})^2, \\
c_5 &:= 0.1\gamma_t + \frac{2\eta_{t+1}}{5\alpha_{t+1}}(1 - \alpha_{t+1})^2, \\
c_6 &:= -\frac{\eta_t}{8} + \frac{5\eta_t}{80} + \frac{(1.1L_\Phi + 0.1L_f)^2K\gamma_t}{10\alpha_t} \left(1 + \frac{2}{K}\right)^{K-k+1} (1 + K)\eta_t^2, \\
c_7 &:= -\frac{\gamma_t}{40} + \frac{6.4L_f^2K\gamma_t}{\alpha_t} \left(1 + \frac{2}{K}\right)^{K-k+1} (1 + K)\gamma_t^2, \\
c_8 &:= \frac{32\eta_{t+1}(1 - \alpha_{t+1})^2L_f^2}{S\alpha_{t+1}} + \frac{16\gamma_{t+1}(1 - \alpha_{t+1})^2L_f^2}{5S\alpha_{t+1}}.
\end{aligned}$$

Notice that $1 \leq (1 + \frac{2}{K})^{K-k} \leq 8$, $\eta_t/2 \leq \eta_{t+1} \leq \eta_t$, and $\gamma_t/2 \leq \gamma_{t+1} \leq \gamma_t$. Applying our choice of $(\eta_t, \gamma_t, \alpha_t, \alpha_t)$, we have

$$\begin{aligned}
c_1 &\leq 0.1, \quad c_2 \leq \frac{64(1.1L_\Phi + 0.1L_f)K\gamma_t}{\alpha_t} \left(1 + \frac{2}{K}\right)^{K-k}, \quad c_3 \leq \frac{2L_fK\gamma_t}{\alpha_t} \left(1 + \frac{2}{K}\right)^{K-k}, \\
c_4 &\leq \frac{4\eta_t}{\alpha_t}, \quad c_5 \leq \frac{2\gamma_t}{5\alpha_t}, \quad c_6 \leq 0, \quad c_7 \leq 0, \quad c_8 \leq \frac{64(1.1L_\Phi + 0.1L_f)^2K\gamma_t}{S\alpha_t} + \frac{2L_f^2K\gamma_t}{5S\alpha_t}.
\end{aligned}$$

Plugging the bounds of c_1, \dots, c_8 into (12), we get

$$\begin{aligned}
\tilde{\mathcal{L}}^{(k+1)} + \frac{4\eta_{t+1}}{\alpha_{t+1}}\varepsilon_{\mathbf{x},t+1} + \frac{2\gamma_{t+1}}{5\alpha_{t+1}}\varepsilon_{\mathbf{y},t+1} &\leq \tilde{\mathcal{L}}^{(k)} - \frac{\eta_t}{2}\mathbb{E}[\|\nabla_{\mathbf{x}}\Phi(\mathbf{x}^{(k)})\|^2] + \frac{4\eta_t}{\alpha_t}\varepsilon_{\mathbf{x},t} + \frac{2\gamma_t}{5\alpha_t}\varepsilon_{\mathbf{y},t} + \frac{8\eta_{t+1}\alpha_{t+1}}{S}\sigma_1^2 \\
&\quad + \left(\frac{64(1.1L_\Phi + 0.1L_f)^2K\gamma_t}{S\alpha_t} + \frac{2L_f^2K\gamma_t}{5S\alpha_t}\right)\mathbb{E}[\|\mathbf{z}_{t+1} - \mathbf{z}_t\|^2] + \frac{4\gamma_{t+1}\alpha_{t+1}}{5S}\sigma_2^2.
\end{aligned} \tag{13}$$

Recall that $f(\mathbf{x}, \mathbf{y})$ is L_f -smooth w.r.t. (\mathbf{x}, \mathbf{y}) and $\Phi(\mathbf{x})$ is L_Φ -smooth w.r.t. \mathbf{x} . Besides, by our choice of $(\alpha_t, \alpha_t, \gamma_t)$, we have $\frac{64(1.1L_\Phi + 0.1L_f)^2K\gamma_t}{\alpha_t} \geq \frac{1.1L_\Phi + 0.1L_f}{2}$ and $\frac{2L_f^2K\gamma_t}{5\alpha_t} \geq \frac{L_f}{20}$. Therefore, the function $\Phi(\mathbf{x}) - \Phi(\mathbf{x}^*) + 0.1(\Phi(\mathbf{x}) - f(\mathbf{x}, \mathbf{y})) + \frac{64(1.1L_\Phi + 0.1L_f)^2K\gamma_t}{\alpha_t}\|\mathbf{x} - \mathbf{x}_t\|^2 + \frac{2L_f^2K\gamma_t}{5\alpha_t}\|\mathbf{y} - \mathbf{y}_t\|^2$ is convex w.r.t. (\mathbf{x}, \mathbf{y}) , which implies that

$$\begin{aligned}
&\frac{1}{S} \sum_{i \in \mathcal{S}_t} \left(\Phi(\mathbf{x}^{(K)}) - \Phi(\mathbf{x}^*) + 0.1(\Phi(\mathbf{x}^{(K)}) - f(\mathbf{z}^{(K)})) + \frac{64(1.1L_\Phi + 0.1L_f)^2K\gamma_t}{\alpha_t}\|\mathbf{x}^{(K)} - \mathbf{x}_t\|^2 + \frac{2L_f^2K\gamma_t}{5\alpha_t}\|\mathbf{y}^{(K)} - \mathbf{y}_t\|^2 \right) \\
&\geq \Phi(\mathbf{x}_{t+1}) - \Phi(\mathbf{x}^*) + 0.1(\Phi(\mathbf{x}_{t+1}) - f(\mathbf{z}_{t+1})) + \frac{64(1.1L_\Phi + 0.1L_f)^2K\gamma_t}{\alpha_t}\|\mathbf{x}_{t+1} - \mathbf{x}_t\|^2 + \frac{2L_f^2K\gamma_t}{5\alpha_t}\|\mathbf{y}_{t+1} - \mathbf{y}_t\|^2.
\end{aligned} \tag{14}$$

Combining (13) and (14) yields

$$\begin{aligned}
&\frac{\eta_t}{2SK} \sum_{i \in \mathcal{S}_t} \sum_{k=0}^{K-1} \mathbb{E}[\|\nabla_{\mathbf{x}}\Phi(\mathbf{x}_{t,i}^{(k)})\|^2] \\
&\leq \left(\frac{1}{K}\mathbb{E}[\Phi(\mathbf{x}_t) - \Phi(\mathbf{x}^*)] + \frac{1}{10K}\mathbb{E}[\Phi(\mathbf{x}_t) - f(\mathbf{z}_t)] + \frac{4\eta_t}{\alpha_t}\varepsilon_{\mathbf{x},t} + \frac{2\gamma_t}{5\alpha_t}\varepsilon_{\mathbf{y},t} \right) + \frac{8\eta_{t+1}\alpha_{t+1}}{S}\sigma_1^2 + \frac{4\gamma_{t+1}\alpha_{t+1}}{5S}\sigma_2^2 \\
&\quad - \left(\frac{1}{K}\mathbb{E}[\Phi(\mathbf{x}_{t+1}) - \Phi(\mathbf{x}^*)] + \frac{1}{10K}\mathbb{E}[\Phi(\mathbf{x}_{t+1}) - f(\mathbf{z}_{t+1})] + \frac{4\eta_{t+1}}{\alpha_{t+1}}\varepsilon_{\mathbf{x},t+1} + \frac{2\gamma_{t+1}}{5\alpha_{t+1}}\varepsilon_{\mathbf{y},t+1} \right).
\end{aligned}$$

Telescoping the above inequality yields

$$\begin{aligned}
& \frac{1}{SKT} \sum_{t=0}^{T-1} \sum_{k=0}^{K-1} \sum_{i \in \mathcal{S}_t} \mathbb{E}[\|\nabla \Phi(\mathbf{x}_{t,i}^{(k)})\|^2] \\
& \leq \frac{2\tilde{\mathcal{L}}_0}{KT\eta_{T-1}} + \frac{8\eta_0\sigma_1^2}{S\alpha_0T\eta_{T-1}} + \frac{4\gamma_0\sigma_2^2}{5S\alpha_0T\eta_{T-1}} + \frac{16\sigma_1^2}{ST\eta_{T-1}} \sum_{t=0}^{T-1} \eta_{t+1}\alpha_{t+1} + \frac{8\sigma_2^2}{5ST\eta_{T-1}} \sum_{t=0}^{T-1} \gamma_{t+1}\alpha_{t+1} \\
& \leq \mathcal{O}\left(\left(\frac{L_\Phi}{T} + \frac{L_{12}^2}{\mu^2}\left(\frac{L_f K}{T} + \frac{L_f K}{S^{1/3}T^{2/3}}\right)\right) \times \left(\frac{\tilde{\mathcal{L}}_0}{K} + (\sigma_1^2 + \sigma_2^2)\frac{\log(T+1)}{L_f K}\right)\right) \\
& = \mathcal{O}\left(\left(\frac{L_\Phi}{TK} + \frac{L_{12}^2 L_f}{\mu^2}\left(\frac{1}{T} + \frac{1}{S^{1/3}T^{2/3}}\right)\right) \times \left(\tilde{\mathcal{L}}_0 + (\sigma_1^2 + \sigma_2^2)\frac{\log(T+1)}{L_f}\right)\right),
\end{aligned}$$

which is the desired result. \square

C.4 Proofs of the results in Section 4.3

The analysis is similar to that of CD-MAGE. Before we prove Theorem 3, we first present and prove some useful lemmas.

Lemma 13. *The update rule of CD-MA can be written as*

$$\begin{cases} \mathbf{x}_{t+1} = \mathbf{x}_t - \eta_t K \left(\frac{1}{S} \sum_{i \in \mathcal{S}_t} \nabla_{\mathbf{x}} f_i(\mathbf{z}_t) + \mathbf{e}'_{\mathbf{x},t} \right), \\ \mathbf{y}_{t+1} = \mathbf{y}_t + \eta_t K \left(\frac{1}{S} \sum_{i \in \mathcal{S}_t} \nabla_{\mathbf{y}} f_i(\mathbf{z}_t) + \mathbf{e}'_{\mathbf{y},t} \right), \end{cases}$$

where $\mathbf{e}'_{\mathbf{x},t}$ and $\mathbf{e}'_{\mathbf{y},t}$ are defined as

$$\begin{cases} \mathbf{e}'_{\mathbf{x},t} = \frac{1}{SK} \sum_{i \in \mathcal{S}_t} \sum_{k=0}^{K-1} (\nabla_{\mathbf{x}} F_i(\mathbf{z}_{t,i}^{(k)}; \mathcal{B}_{t,i}^{(k)}) - \frac{1}{S} \sum_{i \in \mathcal{S}_t} \nabla_{\mathbf{x}} f_i(\mathbf{z}_t)), \\ \mathbf{e}'_{\mathbf{y},t} = \frac{1}{SK} \sum_{i \in \mathcal{S}_t} \sum_{k=0}^{K-1} (\nabla_{\mathbf{y}} F_i(\mathbf{z}_{t,i}^{(k)}; \mathcal{B}_{t,i}^{(k)}) - \frac{1}{S} \sum_{i \in \mathcal{S}_t} \nabla_{\mathbf{y}} f_i(\mathbf{z}_t)). \end{cases}$$

Proof. The primal global variable \mathbf{x}_{t+1} can be written as

$$\begin{aligned}
\mathbf{x}_{t+1} &= \mathbf{x}_t - \frac{\eta_t}{S} \sum_{i \in \mathcal{S}_t} \sum_{k=0}^{K-1} \nabla_{\mathbf{x}} F_i(\mathbf{z}_{t,i}^{(k)}; \mathcal{B}_{t,i}^{(k)}) \\
&= \mathbf{x}_t - \eta_t K \left(\frac{1}{S} \sum_{i \in \mathcal{S}_t} \nabla_{\mathbf{x}} f_i(\mathbf{z}_t) - \frac{1}{S} \sum_{i \in \mathcal{S}_t} \nabla_{\mathbf{x}} f_i(\mathbf{z}_t) + \frac{1}{SK} \sum_{i \in \mathcal{S}_t} \sum_{k=0}^{K-1} \nabla_{\mathbf{x}} F_i(\mathbf{z}_{t,i}^{(k)}; \mathcal{B}_{t,i}^{(k)}) \right) \\
&= \mathbf{x}_t - \eta_t K \left(\frac{1}{S} \sum_{i \in \mathcal{S}_t} \nabla_{\mathbf{x}} f_i(\mathbf{z}_t) + \mathbf{e}'_{\mathbf{x},t} \right).
\end{aligned}$$

Similarly, $\mathbf{y}_{t+1} = \mathbf{y}_t + \eta_t K \left(\frac{1}{S} \sum_{i \in \mathcal{S}_t} \nabla_{\mathbf{y}} f_i(\mathbf{z}_t) + \mathbf{e}'_{\mathbf{y},t} \right)$. \square

Lemma 14. *Suppose that $\eta_t, \gamma_t \leq \frac{1}{2KL_f}$ in CD-MA. If the minibatches $\mathcal{B}_{t,i}^{(0)}, \dots, \mathcal{B}_{t,i}^{(K-1)}$ in CD-MA are drawn in a random reshuffling manner and K is an integral multiple of the epoch length, then both $\mathbb{E}[\|\mathbf{e}'_{\mathbf{x},t}\|^2]$ and $\mathbb{E}[\|\mathbf{e}'_{\mathbf{y},t}\|^2]$ are bounded from above by $\frac{4L_f^2}{3}\eta_t^2 K^2 (\mathbb{E}[\|\nabla_{\mathbf{x}} f(\mathbf{z}_t)\|^2] + \sigma_1^2 + G_1^2) + \frac{4L_f^2}{3}\gamma_t^2 K^2 (\mathbb{E}[\|\nabla_{\mathbf{y}} f(\mathbf{z}_t)\|^2] + \sigma_2^2 + G_2^2)$.*

Proof. By the definition of $\mathbf{e}'_{\mathbf{x},t}$, we have

$$\begin{aligned}
\mathbb{E}[\|\mathbf{e}'_{\mathbf{x},t}\|^2] &= \mathbb{E}\left[\left\| \frac{1}{SK} \sum_{i,k} \left(\nabla_{\mathbf{x}} F_i(\mathbf{z}_{t,i}^{(k)}; \mathcal{B}_{t,i}^{(k)}) - \nabla_{\mathbf{x}} f_i(\mathbf{z}_t; \mathcal{B}_{t,i}^{(k)}) \right) + \frac{1}{S} \sum_{i \in \mathcal{S}_t} \left(\frac{1}{K} \sum_{k=0}^{K-1} \nabla_{\mathbf{x}} F_i(\mathbf{z}_t; \mathcal{B}_{t,i}^{(k)}) - \nabla_{\mathbf{x}} f_i(\mathbf{z}_t) \right) \right\|^2 \right] \\
&= \mathbb{E}\left[\left\| \frac{1}{SK} \sum_{i,k} \left(\nabla_{\mathbf{x}} F_i(\mathbf{z}_{t,i}^{(k)}; \mathcal{B}_{t,i}^{(k)}) - \nabla_{\mathbf{x}} f_i(\mathbf{z}_t; \mathcal{B}_{t,i}^{(k)}) \right) \right\|^2 \right] \\
&\leq \frac{1}{SK} \sum_{i,k} \mathbb{E}\left[\left\| \nabla_{\mathbf{x}} F_i(\mathbf{z}_{t,i}^{(k)}; \mathcal{B}_{t,i}^{(k)}) - \nabla_{\mathbf{x}} f_i(\mathbf{z}_t; \mathcal{B}_{t,i}^{(k)}) \right\|^2\right] \leq \frac{L_f^2}{SK} \sum_{i,k} \mathbb{E}[\|\mathbf{z}_{t,i}^{(k)} - \mathbf{z}_t\|^2],
\end{aligned}$$

where the second equality follows from the condition that the minibatches $\mathcal{B}_{t,i}^{(1)}, \dots, \mathcal{B}_{t,i}^{(K-1)}$ in CD-MA are drawn in a random reshuffling manner and K is an integral multiple of the epoch length. Similarly, we have $\mathbb{E}[\|\mathbf{e}_{\mathbf{y},t}\|^2] \leq \frac{L_f^2}{SK} \sum_{i,k} \mathbb{E}[\|\mathbf{z}_{t,i}^{(k)} - \mathbf{z}_t\|^2]$.

If $k \geq 1$, then

$$\mathbb{E}[\|\mathbf{z}_{t,i}^{(k)} - \mathbf{z}_t\|^2] = \eta_t^2 \mathbb{E} \left[\left\| \sum_{k'=0}^{k-1} \nabla_{\mathbf{x}} F_i(\mathbf{z}_{t,i}^{(k)}; \mathcal{B}_{t,i}^{(k')}) \right\|^2 \right] + \gamma_t^2 \mathbb{E} \left[\left\| \sum_{k'=0}^{k-1} \nabla_{\mathbf{y}} F_i(\mathbf{z}_{t,i}^{(k)}; \mathcal{B}_{t,i}^{(k')}) \right\|^2 \right]. \quad (15)$$

The first term on the RHS of (15) can be bounded by

$$\begin{aligned} & \mathbb{E} \left[\left\| \sum_{k'=0}^{k-1} \nabla_{\mathbf{x}} F_i(\mathbf{z}_{t,i}^{(k)}; \mathcal{B}_{t,i}^{(k')}) \right\|^2 \right] \\ & \leq 2\mathbb{E} \left[\left\| \sum_{k'=0}^{k-1} \left(\nabla_{\mathbf{x}} F_i(\mathbf{z}_{t,i}^{(k)}; \mathcal{B}_{t,i}^{(k')}) - \nabla_{\mathbf{x}} F_i(\mathbf{z}_t; \mathcal{B}_{t,i}^{(k')}) \right) \right\|^2 \right] + 2\mathbb{E} \left[\left\| \sum_{k'=0}^{k-1} \nabla_{\mathbf{x}} F_i(\mathbf{z}_t; \mathcal{B}_{t,i}^{(k')}) \right\|^2 \right] \\ & \leq 2kL_f^2 \sum_{k'=0}^{k-1} \mathbb{E}[\|\mathbf{z}_{t,i}^{(k')} - \mathbf{z}_t\|^2] + 2\mathbb{E} \left[\left\| \sum_{k'=0}^{k-1} \nabla_{\mathbf{x}} F_i(\mathbf{z}_t; \mathcal{B}_{t,i}^{(k')}) \right\|^2 \right] \\ & \leq 2kL_f^2 \sum_{k'=0}^{k-1} \mathbb{E}[\|\mathbf{z}_{t,i}^{(k')} - \mathbf{z}_t\|^2] + 2k^2 \mathbb{E}[\|\nabla_{\mathbf{x}} f_i(\mathbf{z}_t)\|^2] + 2k^2 \mathbb{E} \left[\left\| \frac{1}{k} \sum_{k'=0}^{k-1} \nabla_{\mathbf{x}} F_i(\mathbf{z}_t; \mathcal{B}_{t,i}^{(k')}) - \nabla_{\mathbf{x}} f_i(\mathbf{z}_t) \right\|^2 \right], \end{aligned} \quad (16)$$

where the last inequality follows the fact that $\mathbb{E}[\nabla_{\mathbf{x}} F_i(\mathbf{z}_t; \mathcal{B}_{t,i}^{(k')})] = \mathbb{E}[\nabla_{\mathbf{x}} f_i(\mathbf{z}_t)]$. Let us denote the minibatch size $|\mathcal{B}_{t,i}^{(k')}| = B$. Recall that $\nabla_{\mathbf{x}} F_i(\mathbf{z}_t; \mathcal{B}_{t,i}^{(k')}) = \frac{1}{B} \sum_{\zeta \in \mathcal{B}_{t,i}^{(k')}} \nabla_{\mathbf{x}} F_i(\mathbf{z}_t; \zeta)$ and the minibatches $\mathcal{B}_{t,i}^{(0)}, \dots, \mathcal{B}_{t,i}^{(K-1)}$ are drawn in a random reshuffling manner. By Assumption 4 and (Mishchenko, Khaled Ragab Bayoumi, and Richtárik 2020, Lemma 1), we can bound

$$\mathbb{E} \left[\left\| \frac{1}{k} \sum_{k'=0}^{k-1} \nabla_{\mathbf{x}} F_i(\mathbf{z}_t; \mathcal{B}_{t,i}^{(k')}) - \nabla_{\mathbf{x}} f_i(\mathbf{z}_t) \right\|^2 \right] \leq \frac{n_i - 1 - \text{mod}(kB - 1, n_i)}{(\text{mod}(kB - 1, n_i) + 1)(n_i - 1)} G_1^2 \leq G_1^2.$$

Plugging the above inequality into (16) yields

$$\begin{aligned} \mathbb{E} \left[\left\| \sum_{k'=0}^{k-1} \nabla_{\mathbf{x}} F_i(\mathbf{z}_{t,i}^{(k)}; \mathcal{B}_{t,i}^{(k')}) \right\|^2 \right] & \leq 2kL_f^2 \sum_{k'=0}^{k-1} \mathbb{E}[\|\mathbf{z}_{t,i}^{(k')} - \mathbf{z}_t\|^2] + 2k^2 \mathbb{E}[\|\nabla_{\mathbf{x}} f_i(\mathbf{z}_t)\|^2] + 2k^2 G_1^2 \\ & \leq 2kL_f^2 \sum_{k'=0}^{k-1} \mathbb{E}[\|\mathbf{z}_{t,i}^{(k')} - \mathbf{z}_t\|^2] + 2k^2 \mathbb{E}[\|\nabla_{\mathbf{x}} f(\mathbf{z}_t)\|^2] + \|\nabla_{\mathbf{x}} f_i(\mathbf{z}_t) - f(\mathbf{z}_t)\|^2] + 2k^2 G_1^2 \\ & \leq 2kL_f^2 \sum_{k'=0}^{k-1} \mathbb{E}[\|\mathbf{z}_{t,i}^{(k')} - \mathbf{z}_t\|^2] + 2k^2 \mathbb{E}[\|\nabla_{\mathbf{x}} f(\mathbf{z}_t)\|^2] + 2k^2 (\sigma_1^2 + G_1^2), \end{aligned}$$

where the last inequality follows from Assumption 1. Similarly, we can show that

$$\mathbb{E} \left[\left\| \sum_{k'=0}^{k-1} \nabla_{\mathbf{y}} F_i(\mathbf{z}_{t,i}^{(k)}; \mathcal{B}_{t,i}^{(k')}) \right\|^2 \right] \leq 2kL_f^2 \sum_{k'=0}^{k-1} \mathbb{E}[\|\mathbf{z}_{t,i}^{(k')} - \mathbf{z}_t\|^2] + 2k^2 \mathbb{E}[\|\nabla_{\mathbf{y}} f(\mathbf{z}_t)\|^2] + 2k^2 (\sigma_2^2 + G_2^2).$$

Combining the above two inequalities, we have

$$\begin{aligned} \mathbb{E}[\|\mathbf{z}_{t,i}^{(k)} - \mathbf{z}_t\|^2] & \leq 2kL_f^2 (\eta_t^2 + \gamma_t^2) \sum_{k'=0}^{k-1} \mathbb{E}[\|\mathbf{z}_{t,i}^{(k')} - \mathbf{z}_t\|^2] + 2\eta_t^2 k^2 \mathbb{E}[\|\nabla_{\mathbf{x}} f(\mathbf{z}_t)\|^2] + 2\gamma_t^2 k^2 \mathbb{E}[\|\nabla_{\mathbf{y}} f(\mathbf{z}_t)\|^2] \\ & \quad + 2\eta_t^2 k^2 (\sigma_1^2 + G_1^2) + 2\gamma_t^2 k^2 (\sigma_2^2 + G_2^2). \end{aligned}$$

Summing the above inequality from $k = 1$ to $k = K - 1$ yields

$$\begin{aligned} \sum_{k=0}^{K-1} \mathbb{E}[\|\mathbf{z}_{t,i}^{(k)} - \mathbf{z}_t\|^2] & \leq L_f^2 K(K-1) (\eta_t^2 + \gamma_t^2) \sum_{k=0}^{K-1} \mathbb{E}[\|\mathbf{z}_{t,i}^{(k)} - \mathbf{z}_t\|^2] + \frac{\eta_t^2}{3} (K-1)K(2K-1) (\mathbb{E}[\|\nabla_{\mathbf{x}} f(\mathbf{z}_t)\|^2] + \sigma_1^2 + G_1^2) \\ & \quad + \frac{\gamma_t^2}{3} (K-1)K(2K-1) (\mathbb{E}[\|\nabla_{\mathbf{y}} f(\mathbf{z}_t)\|^2] + \sigma_2^2 + G_2^2). \end{aligned}$$

Plugging the condition $\eta_t, \gamma_t \leq 1/(2L_f K)$ into the above inequality and rearranging terms, we obtain

$$\frac{1}{K} \sum_{k=0}^{K-1} \mathbb{E}[\|\mathbf{z}_{t,i}^{(k)} - \mathbf{z}_t\|^2] \leq \frac{4}{3} \eta_t^2 K^2 (\mathbb{E}[\|\nabla_{\mathbf{x}} f(\mathbf{z}_t)\|^2] + \sigma_1^2 + G_1^2) + \frac{4}{3} \gamma_t^2 K^2 (\mathbb{E}[\|\nabla_{\mathbf{y}} f(\mathbf{z}_t)\|^2] + \sigma_2^2 + G_2^2).$$

Summing the above inequality for $i \in \mathcal{S}_t$ leads to the desired result. \square

Proof of Theorem 3

Proof. The proof is similar to that of Theorem 1. Denote $\gamma_t = \gamma := \min \left\{ \sqrt{\frac{20\mathcal{L}_0 S}{L_f T K^2 \sigma_2^2}}, \left(\frac{30\mathcal{L}_0}{L_f^2 (\sigma_2^2 + G_2^2) T K^3} \right)^{1/3}, \frac{1}{87L_f K} \right\}$ and $\eta_t = \eta := \min \left\{ \sqrt{\frac{20\mathcal{L}_0 S}{7(L_\Phi + L_f) T K^2 \sigma_1^2}}, \left(\frac{3\mathcal{L}_0}{L_f^2 (\sigma_1^2 + G_1^2) T K^3} \right)^{1/3}, \frac{1}{36L_f K}, \frac{1}{4L_\Phi K}, \frac{1}{21L_{12}^2} \right\}$. We note that Lemma 4 and Lemma 7 also apply to CD-MA with $\mathbf{e}_{\mathbf{x},t}$ and $\mathbf{e}_{\mathbf{y},t}$ replaced by $\mathbf{e}'_{\mathbf{x},t}$ and $\mathbf{e}'_{\mathbf{y},t}$, respectively. Following the same argument as (10), we have

$$\begin{aligned} & \mathbb{E}[\Phi(\mathbf{x}_{t+1}) - \Phi(\mathbf{x}^*) + \frac{1}{20}(\Phi(\mathbf{x}_{t+1}) - f(\mathbf{x}_{t+1}, \mathbf{y}_{t+1}))] \\ & \leq \mathbb{E}[\Phi(\mathbf{x}_t) - \Phi(\mathbf{x}^*)] + \left(\frac{1}{20} - \frac{\mu\gamma_t K}{40} + \frac{21\eta_t K L_{12}^2}{40\mu} \right) \mathbb{E}[\Phi(\mathbf{x}_t) - f(\mathbf{x}_t, \mathbf{y}_t)] \\ & \quad - \frac{21\eta_t K}{40} \mathbb{E}[\|\nabla \Phi(\mathbf{x}_t)\|^2] - \left(\frac{\eta_t K}{8} - \frac{1}{20} \left(\frac{11\eta_t K}{8} + 2\eta_t^2 K^2 L_f \right) \right) \mathbb{E}[\|\nabla_{\mathbf{x}} f(\mathbf{z}_t)\|^2] \\ & \quad + \left(\frac{5\eta_t K}{4} + \frac{1}{20} \left(\frac{7\eta_t K}{4} + 2\eta_t^2 K^2 L_f \right) \right) \mathbb{E}[\|\mathbf{e}'_{\mathbf{x},t}\|^2] + \frac{\gamma_t K}{40} \mathbb{E}[\|\mathbf{e}'_{\mathbf{y},t}\|^2] \\ & \quad + \frac{\eta_t^2 K^2}{S} \left(\frac{21L_\Phi}{20} + \frac{L_f}{20} \right) \sigma_1^2 + \frac{\gamma_t^2 K^2 L_f}{20S} \sigma_2^2 - \frac{\gamma_t K}{80} \mathbb{E}[\|\nabla_{\mathbf{y}} f(\mathbf{z}_t)\|^2] \\ & \leq \mathbb{E}[\Phi(\mathbf{x}_t) - \Phi(\mathbf{x}^*)] + \left(\frac{1}{20} - \frac{\mu\gamma_t K}{40} + \frac{21\eta_t K L_{12}^2}{40\mu} \right) \mathbb{E}[\Phi(\mathbf{x}_t) - f(\mathbf{x}_t, \mathbf{y}_t)] - \frac{21\eta_t K}{40} \mathbb{E}[\|\nabla \Phi(\mathbf{x}_t)\|^2] \\ & \quad + \left(-\frac{\eta_t K}{8} + \frac{11\eta_t K}{160} + \frac{\eta_t^2 K^2 L_f}{10} + \frac{4\eta_t^2 K^2 L_f^2}{3} \left(\frac{5\eta_t K}{4} + \frac{7\eta_t K}{80} + \frac{\eta_t^2 K^2 L_f}{10} \right) + \frac{\gamma_t \eta_t^2 K^3 L_f^2}{30} \right) \mathbb{E}[\|\nabla_{\mathbf{x}} f(\mathbf{z}_t)\|^2] \\ & \quad + \left(\frac{\eta_t^2 K^2}{S} \left(\frac{21L_\Phi}{20} + \frac{L_f}{20} \right) + \frac{4\eta_t^2 K^2 L_f^2}{3} \left(\frac{5\eta_t K}{4} + \frac{7\eta_t K}{80} + \frac{\eta_t^2 K^2 L_f}{10} \right) + \frac{\gamma_t \eta_t^2 K^3 L_f^2}{30S} \right) \sigma_1^2 \\ & \quad + \left(-\frac{\gamma_t K}{80} + \frac{4\gamma_t^2 K^2 L_f^2}{3} \left(\frac{5\eta_t K}{4} + \frac{7\eta_t K}{80} + \frac{\eta_t^2 K^2 L_f}{10} \right) + \frac{\gamma_t^3 K^3 L_f^2}{30} \right) \mathbb{E}[\|\nabla_{\mathbf{y}} f(\mathbf{z}_t)\|^2] \\ & \quad + \left(\frac{\gamma_t^2 K^2 L_f}{20S} + \frac{4\gamma_t^2 K^2 L_f^2}{3} \left(\frac{5\eta_t K}{4} + \frac{7\eta_t K}{80} + \frac{\eta_t^2 K^2 L_f}{10} \right) + \frac{\gamma_t^3 K^3 L_f^2}{30} \right) \sigma_2^2 \\ & \quad + \left(\frac{4\eta_t^2 K^2 L_f^2}{3} \left(\frac{5\eta_t K}{4} + \frac{7\eta_t K}{80} + \frac{\eta_t^2 K^2 L_f}{10} \right) + \frac{\gamma_t \eta_t^2 K^3 L_f^2}{30S} \right) G_1^2 \\ & \quad + \left(\frac{4\gamma_t^2 K^2 L_f^2}{3} \left(\frac{5\eta_t K}{4} + \frac{7\eta_t K}{80} + \frac{\eta_t^2 K^2 L_f}{10} \right) + \frac{\gamma_t^3 K^3 L_f^2}{30} \right) G_2^2 \\ & \leq \mathbb{E}[\Phi(\mathbf{x}_t) - \Phi(\mathbf{x}^*)] + \frac{1}{20} \mathbb{E}[\Phi(\mathbf{x}_t) - f(\mathbf{x}_t, \mathbf{y}_t)] - \frac{21\eta_t K}{40} \mathbb{E}[\|\nabla \Phi(\mathbf{x}_t)\|^2] \\ & \quad + \frac{21\eta_t^2 K^2}{20S} (L_\Phi + L_f) \sigma_1^2 + \left(\eta_t^3 K^3 L_f^2 + \frac{\gamma_t \eta_t^2 K^3 L_f^2}{30} \right) (\sigma_1^2 + G_1^2) \\ & \quad + \frac{\gamma_t^2 K^2 L_f}{20S} \sigma_2^2 + \left(\eta_t \gamma_t^2 K^3 L_f^2 + \frac{\gamma_t^3 K^3 L_f^2}{30} \right) (\sigma_2^2 + G_2^2), \tag{17} \end{aligned}$$

where the second inequality follows from Lemma 6 and the last inequality follows from the conditions $\eta_t \leq \min \left\{ \frac{1}{36L_f K}, \frac{1}{4L_\Phi K}, \frac{\mu^2}{21L_{12}^2} \gamma_t \right\}$ and $\gamma_t \leq \frac{1}{87L_f K}$. Recursively applying the above inequality yields

$$\begin{aligned} \mathbb{E}[\Phi(\mathbf{x}_T) - \Phi(\mathbf{x}^*)] + \frac{1}{20} \mathbb{E}[\Phi(\mathbf{x}_T) - f(\mathbf{x}_T)] & \leq \mathcal{L}_0 - \frac{21\eta K}{40} \sum_{t=0}^{T-1} \mathbb{E}[\|\nabla \Phi(\mathbf{x}_t)\|^2] \\ & \quad + \frac{21\eta^2 K^2 T}{20S} (L_\Phi + L_f) \sigma_1^2 + \left(\eta^3 K^3 L_f^2 + \frac{\gamma \eta^2 K^3 L_f^2}{30} \right) (\sigma_1^2 + G_1^2) T \\ & \quad + \frac{\gamma^2 K^2 L_f T}{20S} \sigma_2^2 + \left(\eta \gamma^2 K^3 L_f^2 + \frac{\gamma^3 K^3 L_f^2}{30} \right) (\sigma_2^2 + G_2^2) T. \end{aligned}$$

Plugging the values of η and γ to the above inequality and rearranging terms, we arrive at

$$\begin{aligned}
& \frac{1}{T} \sum_{t=0}^{T-1} \mathbb{E}[\|\nabla \Phi(\mathbf{x}_t)\|^2] \\
& \leq \frac{40}{21\eta KT} \mathcal{L}_0 + \frac{2\eta K(L_\Phi + L_f)}{S} \sigma_1^2 + \frac{2\gamma^2 K L_f}{21\eta S} \sigma_2^2 + \left(\frac{40\eta^2 K^2 L_f^2}{21} + \frac{4\gamma\eta K^2 L_f^2}{63} \right) (\sigma_1^2 + G_1^2) \\
& \quad + \left(\frac{40\gamma^2 K^2 L_f^2}{21} + \frac{4\gamma^3 K^2 L_f^2}{63\eta} \right) (\sigma_2^2 + G_2^2) \\
& \leq (36L_f + 4L_\Phi + \frac{21L_{12}^2}{\mu^2\gamma K}) \left(\frac{40\mathcal{L}_0}{21} + \frac{2\gamma^2 K^2 L_f \sigma_2^2}{21S} + \frac{4L_f^2}{63} (\sigma_1^2 + \sigma_2^2) \gamma^3 K^3 \right) + 2\sqrt{\frac{80\mathcal{L}_0(L_f + L_\Phi)\sigma_1^2}{7ST}} \\
& \quad + \frac{4}{63} \left(\frac{90\mathcal{L}_0^2(\sigma_1^2 + G_1^2)^2 L_f^2}{(\sigma_2^2 + G_2^2)T^2} \right)^{1/3} + \frac{80L_f^2}{21} \left(\frac{3\mathcal{L}_0}{L_f^2(\sigma_1^2 + G_1^2)T} \right)^{2/3} (\sigma_1^2 + G_1^2) + \frac{40L_f^2}{21} \left(\frac{30\mathcal{L}_0}{L_f^2(\sigma_2^2 + G_2^2)T} \right)^{2/3} (\sigma_2^2 + G_2^2) \\
& \leq (36L_f + 4L_\Phi) \frac{40\mathcal{L}_0}{7T} + \frac{2L_{12}^2 L_f \sigma_2^2}{\mu^2 S} \gamma K + \frac{4L_{12}^2 L_f^2}{3\mu^2} (\sigma_2^2 + G_2^2) \gamma^2 K^2 + 8\sqrt{\frac{5\mathcal{L}_0(L_f + L_\Phi)\sigma_1^2}{7ST}} \\
& \quad + \frac{3}{10} \left(\frac{\mathcal{L}_0 L_f (\sigma_1^2 + G_1^2)}{(\sigma_2^2 + G_2^2)^{1/2} T} \right)^{2/3} + 8 \left(\frac{\mathcal{L}_0 L_f (\sigma_1^2 + G_1^2)^{1/2}}{T} \right)^{2/3} + 37 \left(\frac{\mathcal{L}_0 L_f (\sigma_2^2 + G_2^2)^{1/2}}{T} \right)^{2/3} \\
& \leq \frac{160(9L_f + L_\Phi)\mathcal{L}_0}{7T} + 7\sigma_1 \sqrt{\frac{\mathcal{L}_0(L_f + L_\Phi)}{ST}} + \frac{9L_{12}^2 \sigma_2^2}{\mu^2} \sqrt{\frac{\mathcal{L}_0 L_f}{ST}} \\
& \quad + \left(8(\sigma_1^2 + G_1^2)^{1/3} + \frac{3(\sigma_1^2 + G_1^2)^{2/3}}{10(\sigma_2^2 + G_2^2)^{1/3}} + \left(37 + \frac{13L_{12}^2}{\mu^2} \right) (\sigma_1^2 + G_1^2)^{1/3} \right) \left(\frac{\mathcal{L}_0 L_f}{T} \right)^{2/3},
\end{aligned}$$

which is the desired result. \square